Authors' Response to the Reviewers

Authors appreciate thoughtful and constructive comments and suggestions given by anonymous referee #1 and Isobel R. Lawrence. By resolving the issues raised by the referee, the authors believe that the logical flow of this study was strengthened, especially by counting the radar freeboard.

Please find the following point-by-point responses to the referee's comments below. A marked-up version of the revised manuscript regarding the changes is attached at the end of this authors' response.

Response to anonymous referee #1

1. Major Points

1.1. Difference between radar freeboard and scattering horizon height

L22: The statement "altimeters . . . measure sea ice freeboard" is only approximately correct in the case of radar altimeters. The instrument on board CS2 measures a time of flight, which can be related to the height of some radar scattering horizon only where no snow lies in between the scattering horizon and the instrument. When snow is in between and fully penetrated by the radar, the radar range to the scattering surface is overestimated due to slower pulse propagation in the overlying snow. Correcting for this and estimating the height of the ice-snow interface requires knowledge of the overlying snow (Mallett et al., 2020).

This issue surfaces again when the authors identify the radar freeboard as the height from the sea surface to the radar scattering horizon in L28. This is only the case for bare ice. Where overlying snow is present and fully penetrated, the radar freeboard is a finite distance below the ice freeboard (the assumed scattering surface). In the freeboard product used in this manuscript (Kurtz et al., 2014) this displacement is $\underline{h_s}(1 - c_s/c)$.

This is relevant to Fig. 1, where h_{rf} *is depicted as being above the ice freeboard. While it may be true that the radar scattering horizon is above the snow-ice interface, in products that assume full radar penetration of the snowpack the radar freeboard is lower than the ice freeboard. Theoretically for total radar penetration and a freeboard depressed to near the water by snow, the radar freeboard can be below the waterline (while the ice freeboard and scattering horizon are above).*

We became aware of that the definition of 'radar freeboard' used in the manuscript was not consistent with the one used in CS2 data-related references (e.g., Kurtz et al., 2014), which is difference in the radar ranging between the sea surface and the radar scattering horizon. Therefore, Fig. 1 in the manuscript was modified, by following your suggestion on using different notations for clarity.

Now, the system includes correction terms regarding the wave propagation speed change in the snow layer (F_c), and the displacement of the scattering horizon from the ice surface (F_p) following Kwok and Cunningham (2015) and Armitage and Ridout (2015).

$$F_i = F_r + \left(F_c - F_p\right) \quad \text{(AR1)}$$

$$F_c = (\eta_s - 1)\, f h_s \quad \text{(AR2)}$$

$$F_p = (1 - f) h_s \quad \text{(AR3)}$$

Here, η_s denotes the refractive index of snow layer ($\eta_s = c/c_s$) and f denotes the radar penetration

factor, which is the depth of the radar scattering horizon relative to the snow depth (e.g. $f = 1$ if the radar scattering horizon is at snow–ice interface and $f = 0$ if the radar scattering horizon is at air-snow interface), respectively. Combining three equations yields the following relationship.

$$F_i = F_r + (f\eta_s - 1)h_s \quad \text{(AR4)}$$

In the revision, new formulae are introduced for simultaneously solving snow depth and ice thickness even for radar-based freeboard measurements. These changes can be found in introduction, Sect. 2.3 and Fig. 1 in the revised manuscript.

1.2 The freeboard product used by the authors has been created with mW99

In the final sentence of the abstract, the authors state:

> *"In conclusion, the developed α-based method has the capacity to derive ice thickness and snow depth, without relying on the snow depth information as input to the buoyancy equation for converting freeboard to ice thickness."*

However, the method presented here works directly from ice freeboard data which can only be derived by relying on snow depth information (Sect. 5.1 & Eq. 15 of Kurtz et al., 2014).

I feel that what the authors would like to present is a way to convert radar freeboards to ice thickness without relying on snow depth data, and this should be done before publication. I think it is possible for the authors to adapt their processing chain to deal with this, although it may complicate things.

Thanks for the suggestion which in fact led us to deeper understanding of radar altimeter remote sensing. Luckily, we were able to include this issue in the retrieval, by modifying Eqs. (5) and (7) of the first version of manuscript (see below for Eqs. (5) and (7) written with new notation), using Eq. (AR4).

Eq. (5): $H_i = \left(\frac{\rho_w}{\rho_w - \rho_i}\right) F_i + \left(\frac{\rho_s}{\rho_w - \rho_i}\right) h_s$

Eq. (7): $H_i = \frac{\rho_w}{\rho_w - \rho_i - \alpha\rho_s} F_i$

It was possible because Eq. (AR4) does not include additional unknowns, for given parameterization and assumption on the radar penetration. We assumed $f = 0.84$ for CS2 (Armitage and Ridout, 2015). η_s can be parameterized as a function of the snow density, i.e., $\eta_s = (1+0.51\rho_s)^{1.5}$ (Ulaby et al., 1986). Here we present how the equations were solved.

First, the traditional method for the ice thickness retrieval with the snow depth as input can be written in the following equation by substituting F_i with F_r using Eq. (AR4).

$$H_i = \frac{\rho_w}{\rho_w - \rho_i} F_r + \frac{(f\eta_s - 1)\rho_w + \rho_s}{\rho_w - \rho_i} h_s \quad \text{(AR5)}$$

Then, substituting h_s with αH_i and rearranging the equation yield the equation for H_i as a function of radar freeboard and α, without snow depth information.

$$H_i = \frac{\rho_w}{\rho_w - \rho_i - \alpha\{(f\eta_s - 1)\rho_w + \rho_s\}} F_r \quad \text{(AR6)}$$

Note that Eq. (AR6) becomes equivalent to the equation for the total freeboard if $f = 0$ (no wave penetration into snow layer).

This new setup requires the data processing chain to be modified as well. Here we describe what changes were made (in Sect. 3.3 and 3.4 of the revised manuscript). First, CS2-like radar freeboard was derived from OIB total freeboard (F_t^{OIB}) and snow depth (h_s^{OIB}). From Eq. (AR4) and the relationship $F_i = F_t - h_s$, the radar freeboard can be expressed as follows.

$$F_r^{OIB} = F_t^{OIB} - h_s^{OIB} - (f\eta_s - 1)h_s^{OIB} \quad \text{(AR7)}$$

Because the main objective of using OIB data is to evaluate the relative performance of the simultaneous retrieval method when the method is applied to CS2 data, the radar penetration factor (f) for OIB data processing was also set to be 0.84 (Artimage and Ridout, 2015). In the data processing chain, h_s^{OIB} was removed if it is smaller than the given uncertainty level of the dataset (~5.7 cm) or it is larger than the total freeboard F_t^{OIB}.

The CS2 radar freeboard (F_r^{CS2}) was obtained from CS2 ice freeboard dataset. The CS2 ice freeboard data (F_i^{CS2}) distributed by NSIDC (Kurtz et al. 2017) assume that radar scattering horizon locates at snow–ice interface and applies a wave propagation speed correction. However, the correction was made using the MW99 snow depth (h_s^{MW99}) climatology with an erroneous correction form of $h_c = (1 - \eta_s^{-1})\, h_s$, instead of the correct correction form of $h_c = (\eta_s - 1)\, h_s$ (Mallet et al. 2020). Thus, at this point, it is straightforward to derive the CS2 radar freeboard by removing the correction term as in the following equation.

$$F_r^{CS2} = F_i^{CS2} - (1 - \eta_s^{-1})h_s^{MW99} \quad \text{(AR8)}$$

Finally, analyses in the first version of the manuscript were conducted again using the radar freeboard rather than using the ice freeboard. This time SIC criteria for α calculation was set to be 95% (original: 98%) for a wider coverage. Figs. 6–9 in the revised manuscript are the reprocessed results. Despite of these changes, we find little changes in the conclusions we made in the first version of the manuscript. In addition, for more comprehensive information, snow depth comparison results are provided in Fig. 9.

The changes for method and data can be found in Sect. 2.3 and in Sect. 3.3–3.4, respectively. The corresponding results can be found in Sect. 4.2 and 4.3 and Figs. 6–9.

1.3 Uncertainty Analysis

The authors state in their Discussion and Conclusions section:

> *Overall, the developed α-based method yields ice thickness and snow depth, without relying on a priori 'uncertain' snow depth information, which results in uncertainty in the ice thickness retrieval.*

They are of course correct to identify that uncertainty in snow depth leads to uncertainty in the ice thickness retrieval. To avoid having to quantify snow depth, they instead rely on a parameter equal to h/H, which they empirically derive from the temperature of the air-snow and ice-snow interfaces.

Clearly there is significant uncertainty in the value of α, and the authors should try to quantify how this propagates through into uncertainty in ice thickness. It's possible that their α parameter is more uncertain than other published data for h, and if so this method will deliver lower quality estimates of H than the traditional method.

It seems (looking at Fig. 1 of this review) that a given error in α would have a more serious impact on H than the same error in h, because the gradients of the lines are much more similar in on the left panel of Fig. 1 than on the right. This issue scales with the alpha parameter (i.e. as the freeboard goes down), and at high α very small uncertainties in alpha will lead to large uncertainties in H.

As alpha becomes so large that the freeboard tends to zero (not that uncommon in the Atlantic sector of the Arctic), the method seems to lose its usefulness, whereas the traditional method continues to function. That is to say in the case of near-zero freeboard, the traditional method still provides an estimate of H, but that proposed by the authors does not (see Eq. 7 as $h_f \rightarrow 0$).

This is addressed in L161/162, where a critical value is given for alpha, and it is explained that for alpha above this value data are not produced. How often does this occur? And what is the effect on H of small errors in alpha just below this critical threshold?

To identify the uncertainty of simultaneous method, snow depth error (Δh_s) equivalent to α error ($\Delta\alpha$) was calculated for chosen three typical sea ice conditions (thicker / moderate / thinner). The simultaneous method showed a small sensitivity to $\Delta\alpha = 0.03$, which is RMSE value of the regression equation when total freeboard was used. On the other hand, sensitivity was greater when radar freeboard was used, especially for thinner ice where α is close to α_{crit}. In case of ice thickness error (ΔH_i), gap of sensitivity between total freeboard and radar freeboard methods was reduced because ΔH_i is more sensitive to Δh_s when the total freeboard is used. This characteristic of sensitivity is consistent with results from OIB analysis.

Majority of data used in this study belong to moderate or thicker ice and retrieved α rarely exceeds α_{crit}. Therefore, there would not be many cases having great uncertainty that might be expected from thinner ice condition. As a matter of fact, it seems that retrieved α shows reasonable values upon presumed thermodynamic condition. Areas where thermodynamic condition is not met are located at around the marginal ice zones and in the east of Greenland. Details can be found in Appendix B in the revised manuscript. In addition, we clarify that "a priori 'uncertain' snow depth in formation' is MW99 snow depth climatology.

2. Minor Points

2.1. General

• L21: The authors should consider directing the reader to Laxon et al. (2003) when illustrating that thickness has been estimated for nearly two decades.

Laxon et al. (2003) is now included in the revised manuscript.

• When discussing studies indicating the height difference between the scattering horizon and the snow-ice interface, the authors should consider directing the reader to Nandan et al. (2017) and Willatt et al. (2010, 2011).

Nandan et al. (2017) and Willatt et al. (2011) are now referred in the revised manuscript. Because characteristic of sea ice is different between Arctic and Antarctic, study on Antarctic sea ice by Willatt et al. (2010) is not included.

• L62 & 64: Define RTM before using the acronym

The acronym 'RTM' stands for 'Radiative Transfer Model'. It is now defined in the revised manuscript.

• The font sizes of some annotations to Figure 3 should be increased so as to be legible and comparable to the (a), (b), (c) lettering.

Annotations are now increased to be legible (see Fig. 3 in the revised manuscript).

• In Fig. 2, the box that reads 'Find temperature discontinuity point'. It is my understanding that the temperature is continuous (but not a smooth function), and therefore it has no discontinuities (but its gradient does). Should this box then read 'Find temperature gradient discontinuity point'?

Yes, what discontinuous is temperature gradient, not temperature. The text now reads 'Find temperature gradient discontinuity point' (see Fig. 2 in the revised manuscript).

• I think the notation of H and h in combination with h_f, h_{rf} and h_{tf} is confusing to the casual reader. For instance, the fact that h and h_f look so similar but are in fact unrelated confused me initially. Even changing $H \rightarrow H_{ice}$ and $h \rightarrow h_{snow}$ would clarify this.

Following your comment, we have changed our notations throughout the revised manuscript (See Fig. 1 in the revised manuscript).

2.2. Validation of H against OIB Data

The authors are able to create two products from freeboard data obtained by OIB and CryoSat-2, one for snow depth (h), and one for ice thickness (H). They then rightly try to assess the quality of these data products against other datasets, namely the OIB snow depth and ice thickness data. There are at least five algorithms published to process the raw OIB radar returns into along-track snow depth data, and they produce a spread in the mean snow depth (Kwok et al., 2017). 'Validation' of a model or data implies comparison to true or certain values, and it is unclear which OIB snow depth product (if any) represents the truth. This limits the strength of the validation exercise. Nonetheless, I understand that OIB snow depth values have historically been taken as the truth in published work so this is a perhaps not a big issue. It might also be argued that the spread of different

OIB data is sufficiently small relative to other methods of snow depth estimation to allow OIB to approximate the truth for validation purposes.

I feel that there is however a more significant issue with the authors' claims to have 'validated' their ice thickness data against OIB ice thickness data (H_{OIB}). OIB aircraft instruments do not measure thickness (H_{true}) directly, but instead estimate it based on freeboard, snow depth, snow density and ice density values. As such, OIB thickness data (while likely to be the most accurate data on H_{true} outside of in-situ measurement), undoubtedly suffer from biases involving snow depth, snow density and ice density, and therefore should not be mistaken for H_{true}.

The technique for determining H_{OIB} is very similar to that presented in this manuscript: the authors use identical freeboard, snow density and ice density values to estimate thickness with the hydrostatic equilibrium assumption. Given these similarities, comparing the thickness estimates in this paper with OIB thickness estimates doesn't really qualify as independent validation.

It seems more like the exercise of comparing H estimates is in fact comparing the novel snow depth estimates with OIB snow depths (Fig 7 top row; a valuable analysis), and then investigating how that singular difference propagates into sea ice thickness estimates. I suspect that the strong agreement between the two datasets presented in the middle row of Fig. 7. is largely a result of the identical radar freeboards and geophysical parameters used in each processing chain.

After all, much of sea ice thickness is determined by radar freeboard information, independent of snow data. The fact that the 'simultaneous' method matches H_{OIB} data more closely than MW99 is therefore evidence that the snow depth product produced by the 'simultaneous' method is closer to OIB snow depths than MW99 (because everything else is equal).

I think it is perfectly reasonable (and in fact expected) to compare H estimates from the new method with H_{OIB}. However, I think this should be presented as a 'comparison with' or 'evaluation against' OIB data, rather that implying that the new data are being validated against some true value. It is also an understandable bit of reasoning to say that values which are closer to H_{OIB} are likely to be closer to H_{true}, but if this assumption is made it should be stated explicitly.

We agree upon your notion that snow depth and ice thickness comparisons are the same problem. To address your comment, we first clarified how H_i^{OIB} is calculated in Sect 3.3. Then, we changed the subtitle of Sect 4.2 from '*Validation* against OIB estimates' to '*Evaluation* against OIB estimates'. Finally, *validation* on ice thickness contents were modified in the direction to address that the estimated snow depth showing a more consistency with h_s^{OIB} implies improved ice thickness. Accordingly, the snow depth comparisons between $h_s(\alpha^{sat}, F_r^{OIB})$ vs. h_s^{MW99} and $h_s(\alpha^{sat}, F_r^{CS2})$ vs. h_s^{MW99} are included in Fig. 9 in the revised manuscript.

2.3. Limitations of Other Data

L66 - 69: Other approaches worth mentioning are snow depth retrieval using dual-frequency altimetry (Guerreiro et al., 2016; Lawrence et al., 2018, Kwok and Markus, 2018), snow on sea ice model accumulating snowfall from reanalysis (Petty et al., 2018), multilinear regression (Kilic et al., 2019), and the neural network approach (Braakmann-Folgmann and Donlon, 2019). However, these methods do not satisfactorily meet the criteria required for freeboard to ice conversion over the entire Arctic Ocean basin scale or multi-year time

scale.

The approach of Guerreiro et al. (2016) and Lawrence et al. (2018) are limited latitudinally by the AltiKa orbital inclination and Lawrence et al. (2018) additionally through calibration with OIB which only operates in Spring. As the authors identify, they are limited in spatial or temporal extent. While there are limitations to the data products of Petty et al. (2018), Kilic et al. (2019) and Braakmann-Folgmann and Donlon (2019), it's not obvious that these can be characterized by failure to cover the entire basin on a multiyear timescale. As such, the statement on L69 that they do not satisfactorily meet these criteria should be clarified.

The purpose of this paragraph was to introduce recent researches to readers. Therefore, the last sentence describing limitations of other data, which is not necessary, was removed. In case of Petty et al. (2018), we decided to not include it in the text to keep manuscript's focus on remote sensing, as characteristic of their product seems to be closer to model than remote sensing.

2.4. Rainbow Color Schemes

Where possible, authors should avoid presenting continuous data with 'rainbow' color schemes as in Figures 6 & 8. This is because (among other reasons) the scheme tends to imply sharp transitions in the data where they do not exist (Borland and Taylor, 2007). Alternatives for geoscientists are given by Light and Bartlein (2004), Stauffer et al. (2015) and Thyng et al. (2016).

Thanks for valuable comment. We changed our color scheme to generate figures from 'jet (rainbow)' from 'viridis', which is perceptually uniform colormap, available in matplotlib/python. Figs. 6, 8, and A1 in the revised manuscript are new plots with the new color scheme.

Response to Isobel R. Lawrence

1. Major comments

In order to use this methodology with satellite data from CryoSat-2, ice freeboard (the elevation of the snow/ice interface above the ocean surface) is required. However, it is impossible to retrieve ice freeboard from CryoSat-2 without a-priori knowledge of the snow layer. Since the radar pulse slows down as it travels through the snow, snow depth is required in order to correct for the slower speed of propagation and estimate sea ice freeboard.

To compound the issue, the equation to convert radar freeboard into ice freeboard is incorrectly reported in a number of studies, including that of Kurtz et al. (2014, eq. 16) which describes the CS2 ice freeboard dataset you use in your analysis.

Please see Mallett et al. (2020) for the correct derivation of the equation and details of its misreporting in the literature. The correct equation for sea ice thickness from radar altimetry (assuming full snow penetration) is:

$$H = \left(f_r + h\left(\frac{c}{c_s} - 1\right)\right)\left(\frac{\rho_w}{\rho_w - \rho_i}\right) + h\left(\frac{\rho_s}{\rho_w - \rho_i}\right),$$

where f_r is radar freeboard, as estimated from radar altimeters like CryoSat-2. If this equation cannot be solved by the proposed methodology (I do not believe it can be), then the paper should be restructured to focus on the

laser case. The methodology remains valid for use with snow freeboards, and these are available from ICESat and now ICESat-2, so perhaps section 4.3 could be changed to an application to ICESat data. I appreciate that this will require a substantial amount of work, which is why I consider this revision major. However I find this methodology novel and valuable and the results in section 4.2 are encouraging; I would like to reiterate therefore that I think the paper deserves publication subject to this alteration and the following minor revisions:

Thanks for the comment on the fact that the radar algorithm depends on the snow depth, even before retrieving the snow depth. As a matter of fact, another reviewer raised the similar concern, and thus following responses are nearly same.

Recognizing the problems related to the radar altimetry, we modified equations for the model system to handle the radar freeboard as well. The modified model system is delineated in Fig. 1 (with slightly changed notations).

Now, the system includes correction terms regarding the wave propagation speed change in the snow layer (F_c), and the displacement of the scattering horizon from the ice surface (F_p) following Kwok and Cunningham (2015) and Armitage and Ridout (2015).

$$F_i = F_r + \left(F_c - F_p\right) \quad \text{(AR1)}$$

$$F_c = (\eta_s - 1)\, f h_s \quad \text{(AR2)}$$

$$F_p = (1 - f) h_s \quad \text{(AR3)}$$

Here, η_s denotes the refractive index of snow layer ($\eta_s = c/c_s$) and f denotes the radar penetration factor, which is the depth of the radar scattering horizon relative to the snow depth (e.g. $f = 1$ if the radar scattering horizon is at snow–ice interface and $f = 0$ if the radar scattering horizon is at air-snow interface), respectively. Combining three equations yields the following relationship.

$$F_i = F_r + (f\eta_s - 1) h_s \quad \text{(AR4)}$$

Luckily, we were able to include this issue in the retrieval, by modifying Eqs. (5) and (7) of the first version of manuscript (see below for Eqs. (5) and (7) written with new notation), using Eq. (AR4).

Eq. (5): $H_i = \left(\frac{\rho_w}{\rho_w - \rho_i}\right) F_i + \left(\frac{\rho_s}{\rho_w - \rho_i}\right) h_s$

Eq. (7): $H_i = \frac{\rho_w}{\rho_w - \rho_i - \alpha\rho_s} F_i$

It is because Eq. (AR4) does not include additional unknowns, for given parameterization and assumption on the radar penetration. We assumed $f = 0.84$ for CS2 (Armitage and Ridout, 2015). η_s can be parameterized as a function of the snow density, i.e., $\eta_s = (1+0.51\rho_s)^{1.5}$ (Ulaby et al., 1986). Here we present how the equations were solved.

First, the traditional method for the ice thickness retrieval with the snow depth as input can be written in the following equation by substituting F_i with F_r using Eq. (AR4).

$$H_i = \frac{\rho_w}{\rho_w - \rho_i} F_r + \frac{(f\eta_s - 1)\rho_w + \rho_s}{\rho_w - \rho_i} h_s \quad \text{(AR5)}$$

Please note that this equation is equivalent to the equation assuming full snow penetration which

you presented. Then, substituting h_s with αH_i and rearranging the equation yield the equation for H_i as a function of radar freeboard and α, without snow depth information.

$$H_i = \frac{\rho_w}{\rho_w - \rho_i - \alpha\{(f\eta_s - 1)\rho_w + \rho_s\}} F_r \quad \text{(AR6)}$$

Also note that Eq. (AR6) becomes equivalent to the equation for the total freeboard if $f = 0$ (no wave penetration into snow layer).

This new setup requires the data processing chain to be modified as well. Here we describe what changes were made (in Sect. 3.3 and 3.4 of the revised manuscript). First, CS2-like radar freeboard was derived from OIB total freeboard (F_t^{OIB}) and snow depth (h_s^{OIB}). From Eq. (AR4) and the relationship $F_i = F_t - h_s$, the radar freeboard can be expressed as follows.

$$F_r^{OIB} = F_t^{OIB} - h_s^{OIB} - (f\eta_s - 1)h_s^{OIB} \quad \text{(AR7)}$$

Because the main objective of using OIB data is to evaluate the relative performance of the simultaneous retrieval method when the method is applied to CS2 data, the radar penetration factor (f) for OIB data processing was also set to be 0.84 (Artimage and Ridout, 2015). In the data processing chain, h_s^{OIB} was removed if it is smaller than the given uncertainty level of the dataset (~5.7 cm) or it is larger than the total freeboard F_t^{OIB}.

The CS2 radar freeboard (F_r^{CS2}) was obtained from CS2 ice freeboard dataset. The CS2 ice freeboard data (F_i^{CS2}) distributed by NSIDC (Kurtz et al. 2017) assume that radar scattering horizon locates at snow–ice interface and applies a wave propagation speed correction. However, the correction was made using the MW99 snow depth (h_s^{MW99}) climatology with an erroneous correction form of $h_c = (1 - \eta_s^{-1})\, h_s$, instead of the correct correction form of $h_c = (\eta_s - 1)\, h_s$ (Mallet et al. 2020). Thus, at this point, it is straightforward to derive the CS2 radar freeboard by removing the correction term as in the following equation.

$$F_r^{CS2} = F_i^{CS2} - (1 - \eta_s^{-1})h_s^{MW99} \quad \text{(AR8)}$$

Finally, analyses in the first version of the manuscript were conducted again using the radar freeboard rather than using the ice freeboard. This time SIC criteria for α calculation was set to be 95% (original: 98%) for a wider coverage. Figs. 6–9 in the revised manuscript are the reprocessed results. Despite of these changes, we find little changes in the conclusions we made in the first version of the manuscript. In addition, for more comprehensive information, snow depth comparison results are provided in Fig. 9.

The changes for the definition of radar freeboard can be found in introduction (the second paragraph) and Fig. 1 in the revised manuscript. The changes for method and data can be found in Sect. 2.3 and in Sect. 3.3–3.4, respectively. The corresponding results can be found in Sect. 4.2 and 4.3 and Figs. 6–9.

2. Minor comments

• I think you need to include an uncertainty budget for your sea ice thickness and snow depth estimates.

Sensitivity test for our method was conducted and the result is included as Appendix B in the revised manuscript. In Appendix B, snow depth error caused by α error is presented for different cases of α and freeboard.

• L30: "However, the radar scattering horizon is often treated as the snow–ice interface". Include Hendricks et al. (2016), Guerreiro et al. (2017), Tilling et al. (2018) as refs here since AWI, LEGOS and CPOM CryoSat-2 ice thickness products all make the same assumption.

Hendricks et al. (2016), Guerreiro et al. (2017) and Tilling et al. (2018) are now referred in the revised manuscript.

• L72: ..."for given densities and freeboard" – (and assuming no snow penetration for laser and full snow penetration for radar)

We rewrote the sentence as follow:

"… for given densities, freeboard, and assumptions on radar penetration of the snow layer".

• L138: Could you say how many are discarded based on this criterion, and out of how many total.

By examining the outputs from the program, we found no outputs discarded by this criterion, therefore, we removed this sentence from the revised manuscript.

Here we provide total number of buoy data obtained from different averaging periods for your information (Table AR1, will not be included in the text).

• L159: Can you provide a reference for the OIB data processing document where the densities are given?

We now referred Kurtz et al. (2013) in the revised manuscript.

• L160: I understand that you keep ice density constant in order to compare with OIB data, but later when comparing with satellite-derived ice thickness should you not then use the densities used in those products for a fair comparison?

As you mentioned, '*CS2 H*' in Fig 9 of the manuscript should not be same as the CS2 product available from NSIDC. Instead, CS2 ice thickness was reproduced with the same densities and MW99 snow depth for the fair comparison. New figure is given in Fig. 9 in the revised manuscript. We also clarified this data processing in the comparison section.

• *L198: "It was reported…" – By who?*

It was reported by Lee et al. (2018). We clarified this in the revised manuscript.

• *L200: Where does T_{si} for March come from if the Lee et al. (2018) dataset is only December-February?*

We produced T_{si} for March by applying the same algorithm. We clarified this in the revised manuscript.

• *L201: "…if data frequency is over 20". Do you mean if 20 days out of the month contain data? Or are you referring to a number of points per grid cell?*

Monthly mean temperature was calculated by gird cell by grid cell and the average was done only for the grid cells where there are more than 20 data available during a month. We clarified this in the revised manuscript.

• *L205: Please could you provide the details and a reference for which OIB dataset you used and where it is available from? i.e. L2, L4, Quicklook?*

We utilized L4 dataset for 2011-2013 period, and Quick look dataset for 2014-2015 period. Details on OIB data are now provided in the revised manuscript. Reference and accessibility information were already included in 'Data availability' section.

• *Figure 4: Why do you choose to show us the 7-day averaged plot in Fig.4 when Figure 3 was showing 15-day averaged temperature profiles?*

We intended to show results from various averaging period to readers. The results for different averaging period can be found in Figs. 5 and 6 in the text. For your information, same figures for different averaging periods are presented in Fig. AR1 (will not be included in the text).

• *L235: At the end of this sentence you could refer the reader to the appendix.*

Appendix A is now referred at the end of the sentence.

• *L244: bias is not near-zero in Fig 4b, it is zero.*

Yes, it is zero. The comment is now applied in the revised manuscript.

• *L269: Did you calculate a different alpha for each year, and apply the different alpha to each year of OIB*

data? Or did you just average all the years together? Please clarify this in the text.

We calculated and applied a different α for each year. It is now clarified in the revised manuscript.

• L295: Do you get the MW99 for input into Eqs. (4) and (5) from the CS2 data? If so is it monthly grid-averaged? How do you assign each OIB point a snow depth?

Yes, MW99 was obtained from the CS2 dataset. OIB data were reformatted in a 25 km polar stereographic grid by method described in Sect. 3.3 in the manuscript. As OIB data is reformatted into the grid format, it is straightforward to assign the OIB snow depth to the MW99.

One possible concern is that the monthly mean of daily MW99 might differ significantly from the daily MW99, because the MW99 depends on the sea ice type. However, it may not be a critical issue when following points are considered: 1) W99 is already a monthly climatology, 2) ice type distribution would not be changed significantly by the sea ice drift in March because the Arctic Ocean is nearly filled with sea ice and thus the sea ice mobility is reduced.

• L301: "Therefore, if there are decreasing trends in both ice thickness and snow depth, the decreasing trend of ice thickness estimated from the constant snow depth will be diminished in radar, while being amplified in lidar" – This sentence seems overcomplicated. To me, all that the bottom two plots of Figure 7 demonstrate is that MW99 snow depth is larger than OIB snow depth. For the laser case, this means that using W99 causes ice thickness to be underestimated compared to H(OIB), and for the radar case using W99 results in ice thicknesses that are too thick compared to OIB. Perhaps you could plot MW99 against h(OIB) to clarify this? The retrieval of sea ice thickness from ICESat has not traditionally used the Warren climatology- see Kwok and Cunningham (2008) and Petty et al. (2020). Therefore I don't think it's justified to call this 'ICESat-like thickness' since you are not using the same snow depth product that they do.

Yes, what you mentioned is the appropriate interpretation of Fig. 7; MW99 is larger than OIB snow depth. This can be verified by Fig. S1 (included as a supplementary figure). However, we attempted to address a possible unintended result of 'diverging direction in errors in ice thickness retrieval, when the same snow depth error is applied to two different satellite altimetry measurements'. We modified this paragraph to deliver such message.

Regarding the naming issue, we are not referring existing products when we call ICESat-like and CS2-like thickness. Those are explicitly defined in the revised manuscript text. Besides, there is an ice thickness dataset from ICESat total freeboard distributed by NSIDC (Yi and Zwally, 2009; doi: 10.5067/SXJVJ3A2XIZT) which uses MW99. However, we think that the expression "current practices of retrieving sea ice thickness" might confuse readers. Therefore, we replaced such expression with "MW99 method" for clarity.

3. Typos / Grammar

• L128: "Therefore, the interface searching algorithm…" -> "Therefore, an interface searching algorithm…"

• L165: "Sea ice thicknesses converted from MW99 using Eqs. (4) and (5) are also compared to examine how simultaneous retrievals…" -> "Sea ice thicknesses are also calculated from Eqs. (4) and (5), using MW99 as snow depth, to examine how simultaneous retrievals…"

• L194: "This reformatted AASTI-v2 data are called…" -> "This reformatted AASTI-v2 dataset is called…"

• L293: "Examining how the current practices of retrieving the sea ice thickness through ICESat and CS2 measurements are compared with the simultaneous retrievals is of interest" -> "We now examine how the current practises of retrieving sea ice thickness from ICESat and CS2 measurements compare with our method."

• L294: "In doing so, OIB-measured…" -> "To do so, OIB-measured…"

• L297: "Apparently, ICESat-like thickness tends…." -> "According to our analysis, ICESat-like thickness tends…."

• L416: "…which are hard to be quantified explicitly." -> "…which are hard to quantify explicitly."

All comments were applied in the manuscript and some other grammatical errors were also corrected in the revised manuscript.

References

Armitage, T. W. K., and Ridout, A. L.: Arctic sea ice freeboard from AltiKa and comparison with CryoSat-2 and Operation IceBridge, Geophys. Res. Lett., 42, 6724–6731, doi: 10.1002/2015GL064823, 2015.

Braakmann-Folgmann, A., and Donlon, C.: Estimating snow depth on Arctic sea ice using satellite microwave radiometry and a neural network, Cryosphere, 13, 2421–2438, doi: 10.5194/tc-13-2421-2019, 2019.

Guerreiro, K., Fleury, S., Zakharova, E., Rémy, F., and Kouraev, A.: Potential for estimation of snow depth on Arctic sea ice from CryoSat-2 and SARAL/AltiKa missions, Remote Sens. Environ., 186, 339–349, doi: 10.1016/j.rse.2016.07.013, 2016.

Guerreiro, K., Fleury, S., Zakharova, E., Kouraev, A., Rémy, F., and Maisongrande, P.: Comparison of CryoSat-2 and ENVISAT radar freeboard over Arctic sea ice: toward an improved Envisat freeboard retrieval, Cryosphere, 11, 2059–2073, doi: 10.5194/tc-11-2059-2017, 2017.

Hendricks, S., Ricker, R., and Helm, V.: User Guide – AWI CryoSat-2 sea Ice thickness data product (v1.2), doi: 10013/epic.48201, 2016.

Kilic, L., Tonboe, R. T., Prigent, C., and Heygster, G.: Estimating the snow depth, the snow-ice interface temperature, and the effective temperature of Arctic sea ice using Advanced Microwave Scanning Radiometer 2 and ice mass balance buoy data, Cryosphere, 13, 1283–1296, doi: 10.5194/tc-13-1283-2019, 2019.

Kurtz, N. T., Farrell, S. L., Studinger, M., Galin, N., Harbeck, J. P., Lindsay, R., Onana, V. D., Panzer, B., and Sonntag, J. G.: Sea ice thickness, freeboard, and snow depth products from Operation IceBridge airborne data, Cryosphere, 7, 1035–1056., doi: 10.5194/tc-7-1035-2013, 2013.

Kurtz, N. T., Galin, N., and Studinger, M.: An improved CryoSat-2 sea ice freeboard retrieval algorithm through the use of waveform fitting, Cryosphere, 8, 1217–1237, doi: 10.5194/tc-8-1217-2014, 2014.

Kurtz, N. and Harbeck, J.: CryoSat-2 Level-4 Sea Ice Elevation, Freeboard, and Thickness, Version 1, National Snow and Ice Data Center, doi: 10.5067/96JO0KIFDAS8, 2017.

Kwok, R., and Cunningham, G. F.: Variability of Arctic sea ice thickness and volume from CryoSat-2, Phil. Trans. R. Soc. A, 373(2045), 20140157, doi: 10.1098/rsta.2014.0157, 2015.

Kwok, R., and Markus, T.: Potential basin-scale estimates of Arctic snow depth with sea ice freeboards from CryoSat-2 and ICESat-2: An exploratory analysis, Adv. Space Res., 62(6), 1243–1250, doi: 10.1016/j.asr.2017.09.007, 2018.

Lawrence, I. R., Tsamados, M. C., Stroeve, J. C., Armitage, T. W. K., and Ridout, A. L.: Estimating snow depth over Arctic sea ice from calibrated dual-frequency radar freeboards, Cryosphere, 12, 3551–3564, doi:10.5194/tc-12-3551-2018, 2018.

Laxon, S., Peacock, N., and Smith, D.: High interannual variablility of sea ice thickness in the Arctic region, Nature, 425, 947–950, doi: 10.1038/nature02050, 2003.

Lee, S.-M., Sohn, B.-J., and Kummerow, C. D.: Long-term Arctic snow/ice interface temperature from special sensor for Microwave imager measurements, Remote Sens., 10(11), 1795, doi: 10.3390/rs10111795, 2018.

Mallett, R. D. C., Lawrence, I. R., Stroeve, J. C., Landy, J. C., and Tsamados, M.: Brief communication: Conventional assumptions involving the speed of radar waves in snow introduce systematic underestimates to sea ice thickness and seasonal growth rate estimates, The Cryosphere, 14, 251-260, doi: 10.5194/tc-14-251-2020, 2020.

Nandan, V., Geldsetzer, T., Yackel, J., Mahmud, M., Scharien, R., Howell, S., King, J., Ricker, R., and Else, B.: Effect of Snow Salinity on CryoSat-2 Arctic First-Year Sea Ice Freeboard Measurements, Geophys. Res. Lett., 44(20), 10,419–10,426, doi:10.1002/2017GL074506, 2017.

Petty, A. A., Webster, M., Boisvert, L., and Markus, T.: The NASA Eulerian Snow On Sea Ice Model (NESOSIM) v1.0: initial model development and analysis, Geosci. Model Dev., 11(11), 4577–4602, doi: 10.5194/gmd-11-4577-2018, 2018.

Tilling, R. L., Ridout, A., and Shepherd, A.: Estimating Arctic sea ice thickness and volume using CryoSat-2 radar altimeter data, Adv. Space Res., 62, 1203–1225, doi: 10.1016/j.asr.2017.10.051, 2018.

Ulaby, F. T., Moore, R. K., and Fung, A. K.: Microwave remotesensing: Active and passive, Volume 3-From theory to applications, 1986.

Willatt, R. C., Giles, K. A., Laxon, S. W., Stone-Drake, L., and Worby, A. P.: Field inves-tigations of Ku-band radar penetration into snow cover on antarctic sea ice, IEEE Transactions on Geoscience and Remote Sensing, 48, 365-372, doi: 10.1109/TGRS.2009.2028237, 2010.

Willatt, R., Laxon, S., Giles, K., Cullen, R., Haas, C., and Helm, V.: Ku-band radar penetration into snow cover on Arctic sea ice using airborne data, Annals of Glaciology, 52, 197–205, doi: 10.3189/172756411795931589, 2011.

Yi, D., and H. J. Zwally: Arctic Sea Ice Freeboard and Thickness, Version 1, National Snow and Ice Data Center, doi: 10.5067/SXJVJ3A2XIZ, 2009.

Table AR1. Number of outputs obtained from the interface searching algorithm

Averaging period	# of obtained outputs
1 day	542
7 days	97
15 days	59
30 days	36

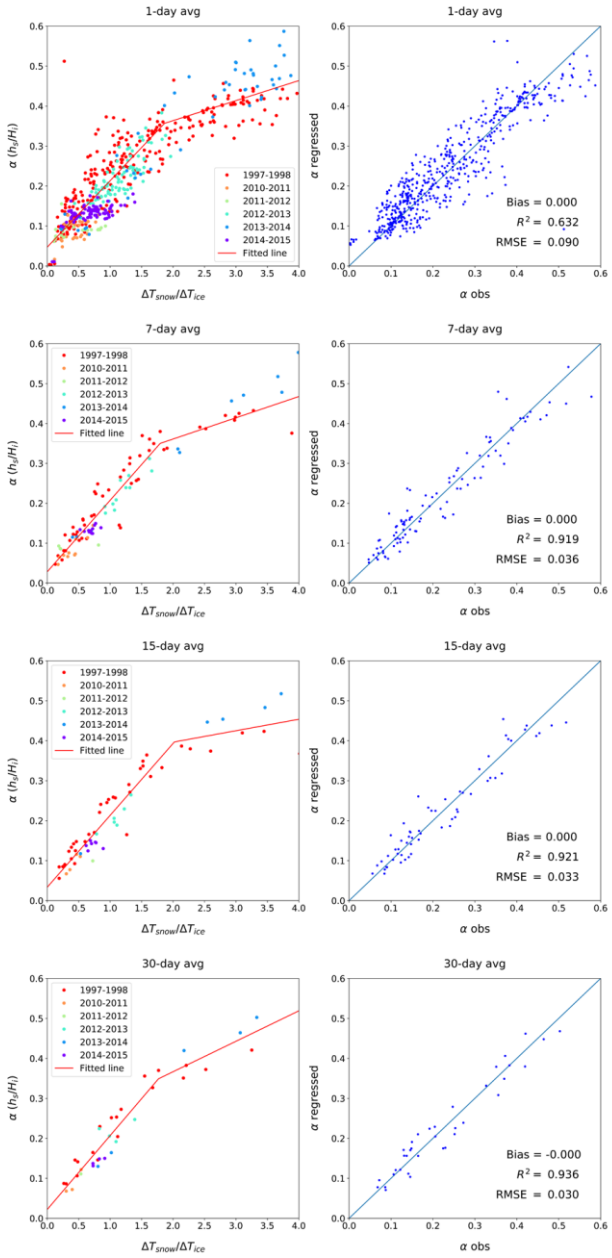

Figure AR1. (Left column) Scatterplots of the temperature difference ratio of the snow and ice layer ($\Delta T_{snow}/\Delta T_{ice}$) and the snow–ice thickness ratio (α) for averaging period of 1,7,15 and 30 days. Color denotes collected year of buoy data. The red lines are the regression lines (defined in Eq. (15) in the text). (Right column) The corresponding scatter plot of observed and regressed α.

Simultaneous estimation of wintertime sea ice thickness and snow depth from space-borne freeboard measurements

Hoyeon Shi[1], Byung-Ju Sohn[1], Gorm Dybkjær[2], Rasmus Tage Tonboe[2], Sang-Moo Lee[1,3,4]

[1]School of Earth and Environmental Sciences, Seoul National University, Seoul, Republic of Korea
[2]Danish Meteorological Institute, Copenhagen, Denmark
[3]Center for Environmental Technology, ECEE, University of Colorado-Boulder, Boulder, Colorado, USA
[4]National Snow and Ice Data Center, CIRES, University of Colorado-Boulder, Boulder, Colorado, USA

Correspondence to: Byung-Ju Sohn (sohn@snu.ac.kr)

Abstract. A method of simultaneously estimating snow depth and sea ice thickness using satellite-based freeboard measurements over the Arctic Ocean during winter was proposed. The ratio of snow depth to ice thickness (referred to as α) was defined and used in constraining the conversion from the freeboard to ice thickness in satellite altimetry~~.~~ without prior knowledge of snow depth. Then, α was empirically determined using the ratio of temperature difference of the snow layer to the difference of the ice layer, to allow the determination of α from satellite-derived snow surface temperature and snow–ice interface temperature. The proposed method was ~~validated~~evaluated against NASA's Operation IceBridge measurements, and ~~comparison~~ results indicated that the algorithm adequately retrieves snow depth and ice thickness simultaneously: retrieved ice thickness was found to be better than the ~~current satellite retrieval~~ methods relying on the use of snow depth climatology as input, in terms of mean bias and RMSE. The application of the proposed method to CryoSat-2 ~~ice~~radar freeboard measurements yields similar results. In conclusion, the developed α-based method has the capacity to derive ice thickness and snow depth, without relying on the snow depth information as input to the buoyancy equation and radar penetration correction for converting freeboard to ice thickness.

1 Introduction

Satellite altimeters have been used to estimate sea ice thickness for nearly two decades (Laxon et al., 2003; Kwok et al., 2009; Laxon et al., 2013). The altimeters do not measure sea ice thickness directly but measure the sea ice freeboard which is then converted to sea ice thickness with assumptions, for example, regarding the snow depth, snow/ice densities, and radar penetration (Ricker et al., 2014). We hereafter refer to this procedure as 'freeboard to thickness conversion'.

Generally ~~used~~, there are two types of satellite altimeters ~~measure~~measuring different sea ice freeboards~~.~~: 1) Lidar altimeters such as NASA's ICESat (Zwally et al., 2002) and ICESat-2 (Markus et al., 2017) missions measure the total freeboard ($~~h_{ff}~~F_t$): the height from the sea surface in cracks and leads to the snow surface. ~~On the other hand, radar~~2) Radar altimeters such as ESA's CryoSat-2 (CS2) (Wingham et al., 2006) measure the radar freeboard ($~~h_{ff}~~F_r$): difference in the radar ranging between the sea surface and the radar scattering horizon. By applying two corrections terms regarding the wave propagation speed

change in the snow layer (F_c) and displacement of the scattering horizon from the ice surface (F_p), the radar freeboard is converted to the ice freeboard (F_i): the height from the sea surface to ~~radar scattering horizon.~~the snow–ice interface (F_i). Several studies indicate that the radar scattering horizon is at or above the snow–ice interface depending on ice type and snow/ice conditions (Nandan et al., 2017; Armitage and Ridout, 2015; Willatt et al., 2011; Tonboe et al. 2010). However, the radar scattering horizon is often treated as the snow–ice interface (Kurtz et al., 2014; Kwok and Cunningham, 2015~~). The height from the sea surface to the snow–ice interface is called ice freeboard (h_f).~~; Hendricks et al., 2016; Guerreiro et al., 2017, Tilling et al., 2018). The three different freeboards are indicated in Fig. 1.

For both lidar and radar altimeters, snow depth (~~h~~h_s) is required as an input to constrain the freeboard to thickness conversion; thus, the conversion results are highly dependent on snow depth (Ricker et al., 2014; Zygmuntowska et al., 2014; Kern et al. 2015). The buoyancy equation used in the freeboard to thickness conversion describes the balance between buoyancy and the weight of snow and ice. For a given freeboard ~~and~~, snow/ice densities, and assumptions on radar penetration of the snow layer, sea ice thickness (~~H~~H_i) is a function of ~~h~~h_s. According to Zygmuntowska et al. (2014), up to 70% of uncertainty in the freeboard to thickness conversion stems from the poorly constrained snow depth. However, mapping the Arctic scale snow depth distribution is challenging. The most commonly used snow depth information necessary for the freeboard to thickness conversion is the modified version of the snow depth climatology by Warren et al. (1999) (hereafter W99). W99 is based on in-situ measurements at Soviet drifting stations (1954–1991) mostly on multi-year ice (MYI). Kurtz and Farrell (2011) compared W99 with Operation IceBridge (OIB) snow depth measurements in 2009 and claimed that W99 was still valid ~~on~~in the MYI region and significantly differed from OIB snow depth on first-year ice (FYI). Based on that study, Modified W99 (hereafter MW99) was developed, which halves W99 snow depth in regions covered by FYI. MW99 is often used in CS2 ice thickness products available at CPOM-UCL (Laxon et al., 2013), AWI (Ricker et al., 2014), and NSIDC (Kurtz et al., 2017). However, the use of MW99 for the freeboard to thickness conversion understandably yields a substantial error, considering that W99 is ~~a~~ climatology and not actual snow depth. This is because the actual snow depth distribution is subject to the year-to-year variation of snow–ice system, thus the climatology based on the 37-year measurements of snow depth would deviate significantly from the actual distribution (Webster et al., 2014). Accordingly, such deviation causes errors in the estimation of ice thickness. Thus, additional snow observations covering both MYI and FYI on the Arctic basin ~~–~~scale would be ideal as a replacement of MW99.

There have been various approaches aimed at obtaining the snow depth distribution over the Arctic scale using satellite observations. Markus and Cavalieri (1998) developed an algorithm based on the Brightness Temperatures (TBs) of Special Sensor Microwave/Imager (SSM/I) based on the negative correlation of the snow depth with the spectral gradient ratio between 18 and 37 GHz of vertically polarized TB's on the Antarctic FYI. Comiso et al. (2003) have updated the coefficients of this algorithm for the Advanced Microwave Scanning Radiometer for EOS (AMSR-E). However, snow depth retrieval using this algorithm is relatively less accurate when the MYI fraction within the grid cell is significant (Brucker and Markus, 2013). Recently, Rostosky et al. (2018) suggested a new method: using the lower frequency pair of 7 and 19 GHz to overcome ~~the~~this limitation. Nonetheless, estimating the basin-scale snow depth distribution seems to be a difficult task.

There are other approaches involving the use of the lower frequency measurements at L-band. Using Soil Moisture Ocean Salinity (SMOS) measurements, Maaß et al. (2013) found that 1.4 GHz TB depends on the snow depth through the insulation effect of snow layer, and they determined snow depth by matching ~~RTM~~Radiative Transfer Model (RTM) simulated TBs with SMOS-measured TBs. Zhou et al. (2018) simultaneously estimated the sea ice thickness and snow depth by adding additional laser altimeter freeboard information, improving the Maaß et al. (2013) approach. However, both of these RTM-based approaches require a priori information on ice properties (e.g. temperature and salinity profiles).

Other satellite remote sensing approaches ~~worth mentioning are~~include the snow depth retrieval using dual-frequency altimetry (Guerreiro et al., 2016; Lawrence et al., 2018, Kwok and Markus, 2018), ~~snow on sea ice model accumulating snowfall from reanalysis (Petty et al., 2018),~~ multilinear regression (Kilic et al., 2019), and ~~the~~a neural network approach (Braakmann-Folgmann and Donlon, 2019). ~~However, these methods do not satisfactorily meet the criteria required for freeboard to ice conversion over the entire Arctic Ocean basin scale or multi year time scale.~~

~~In this situation~~Here, let us switch our point of view to solving the buoyancy equation instead of retrieving snow depth directly. Remember that there ~~is one buoyancy equation with~~are two unknowns (snow depth and ice thickness) in the buoyancy equation for given snow/ice densities ~~and~~, freeboard, and assumptions on radar penetration of the snow layer. The attempt so far has been to add one constraint (snow depth information) to the buoyancy equation for solving ice thickness. However, if a particular relationship between two unknowns is available, it can be used to constrain the equation yielding both ice thickness and snow depth~~.~~ simultaneously.

To identify such a relationship, this study examines the vertical thermal structure within the snow/ice layers observed by drifting buoys. The vertical thermal structure of a snow–ice system in winter is rather simple; the temperature profile of the snow–ice system can be assumed to be piecewise linear, as illustrated in Fig. 1. Therefore, the temperatures at three interfaces can represent the thermal state of the snow–ice system fairly well; they are (1) air–snow interface temperature (T_{as}), (2) snow–ice interface temperature (T_{si}), and (3) ice–water interface temperature (T_{iw}). T_{iw} is assumed to be ~~almost~~nearly constant at the freezing temperature of seawater (Maaß et al., 2013), implying that two other interface temperatures (T_{as} and T_{si}) are sufficient to describe the thermal structure of the system.

Based on this thermal structure, there ~~may exist~~is a constraint relating the snow depth and ice thickness. In identifying ~~a~~this constraint, conductive heat flux is assumed to be continuous through the snow–ice interface (Maykut and Untersteiner, 1971), implying that conductive heat fluxes within the snow and ice layers are same under the steady-state assumed in the given thermal structure. As the conductive heat flux is proportional to the bulk temperature difference of the layer divided by its thickness, it is possible to deduce the relationship between snow depth and ice thickness from the given thermal structure.

Once the relationship is obtained, then it is possible to apply it to the Arctic Ocean basin–scale because the thermal structure can be resolved from satellites, as shown in the recently available basin-scale and long-term satellite-derived interface temperatures (Dybkjær et al., 2020; Lee et al., 2018). In determining the snow depth along with the ice thickness, instead of using the snow depth as an input to solve for the ice thickness, we intend to (1) examine the relationship between the vertical thermal structure of a snow–ice system (T_{as} and T_{si}) and the thicknesses of the snow and ice layer (~~h~~h_s and ~~H~~H_i) using buoy

measurements, (2) retrieve the sea ice thickness and the snow depth simultaneously by applying their relationship to the freeboard to thickness conversion as a constraint, thus replacing the snow depth information. The result may reduce uncertainty in the freeboard to ice thickness conversion by replacing the currently used snow depth ~~information~~climatology.

2 Method

Here, we provide the theoretical background of how the snow–ice thickness ratio (α = ~~h / H~~h_s / H_i) can be related to T_{as} and T_{si}. Then, after empirically determining the relationship of α to T_{as} and T_{si} from buoy measured temperature profiles, α obtained from satellite-observed T_{as} and T_{si} is then used to constrain the conversion from freeboard to ice thickness over the Arctic Ocean during winter.

2.1 Theoretical background

We intend to find a relationship between snow depth and ice thickness in terms of the vertical thermal structure of ~~a~~the snow–ice system. Because the temperature ~~gradient~~gradients within the snow and ice ~~layer is~~layers are linked to both temperature and thickness, we focus on the temperature gradient. Owing to the physical reasoning that the conductive heat flux is continuous across the snow–ice interface (Maykut and Untersteiner, 1971), the following relationship is valid at the snow–ice interface:

$$k_{snow} \frac{\partial T_{snow}}{\partial z}\bigg|_{z=0} = k_{ice} \frac{\partial T_{ice}}{\partial z}\bigg|_{z=0} \quad (1)$$

In Eq. (1), the subscripts *snow* and *ice* denote their respective layers while T, k, and z denote temperature, thermal conductivity, and depth, respectively. The snow–ice interface is defined as z = 0. Assuming a piecewise linear temperature profile within the snow–ice layer, Eq. (1) can be rewritten as follows:

$$k_{snow} \frac{T_{as}-T_{si}}{h} \frac{T_{as}-T_{si}}{h_s} = k_{ice} \frac{T_{si}-T_{iw}}{H} \frac{T_{si}-T_{iw}}{H_i} \quad (2)$$

where subscripts *as*, *si*, and *iw* denote the air–snow, snow–ice, and ice–water interface, respectively, and ~~H~~H_i and ~~h~~h_s denote the sea ice thickness and snow depth as in Fig. 1. Introducing a variable α, which is the snow–ice thickness ratio, Eq. (2) becomes:

$$\alpha = \frac{h}{H} \frac{h_s}{H_i} = \frac{k_{snow}}{k_{ice}} \frac{\Delta T_{snow}}{\Delta T_{ice}} \quad (3)$$

Here, ΔT denotes the temperature difference between the top and bottom of each of the snow ~~or~~and ice ~~layer~~layers (i.e. ΔT_{snow} = T_{as} - T_{si}, ΔT_{ice} = T_{si} - T_{iw}). As explained in detail in Sect. 2.3, α can be used to constrain the freeboard to thickness conversion. Thus, once α is known, both snow depth and ice thickness can be simultaneously estimated from altimeter-measured freeboard, instead of using snow depth data for ice thickness retrieval.

2.2 Empirical determination of 'α-prediction equation' from buoy measurements

To obtain α, the conductivity ratio (k_{snow}/k_{ice}) should be known even if the temperature difference ratio ($\Delta T_{snow}/\Delta T_{ice}$) is given. In this study, instead of using the conventional conductivity ratio found in literature, it is empirically determined using buoy-measured α and $\Delta T_{snow}/\Delta T_{ice}$. Thus, the interface should be defined and determined from buoy-measured temperature profiles, which show a piecewise linear temperature profile as shown in Fig. 1.

The buoy-measured temperature profiles in the vertical resolution of 10 cm are used in this study (Sect. 3.1). Although the instrument initially sets the zero-depth reference position to be approximately at the snow–ice interface, the reference position can deviate from the initial location if the ice deforms, or if the snow refreezes after the temporary melt~~.~~ into snow-ice. In addition, the interfaces (air–snow, snow–ice, and ice–water) may be located in between measurement levels in a 10 cm spacing. Therefore, ~~the~~an interface searching algorithm is developed to determine three interfaces (y_{as}, y_{si}, y_{iw}) and their respective temperatures (T_{as}, T_{si}, T_{iw}) by extrapolating each piecewise linear temperature profile iteratively.

The interface searching algorithm iterates three processes to find the location and temperature of each interface: it (1) divides temperature profile into four layers using the most recently available locations of the three interfaces, (2) finds a linear regression line of the temperature profile at each layer, and (3) updates the location and temperature of each interface by finding an intersection between two adjacent regression lines. The algorithm fails if the temperature profile is far from linear, or the thickness of a certain layer is too thin to have less than two data points. More detailed procedures for determining the interface are provided in Fig. 2, as a flow chart. The outputs are T_{as}, T_{si}, T_{iw}, ~~H~~H_i (= y_{as} - y_{si}), and ~~h~~h_s (= y_{si} - y_{iw}). Examples of the interface searching results for 15-day averaged temperature profiles are shown in Fig. 3. The algorithm works adequately for both CRREL-IMB (Fig. 3a–c) and SHEBA ~~buoys (Fig. 3d–f). For the analysis, temperature profiles are used only if T_{as} is colder than T_{si}. As the analysis period is winter, there are very few discarded profiles when this criterion is applied.~~buoy data (Fig. 3d–f).

~~As~~Since T_{as}, T_{si}, T_{iw}, ~~H~~H_i, and ~~h~~h_s can be obtained from the previous interface determination with buoy data, the calculation of $\Delta T_{snow}/\Delta T_{ice}$ and α ~~becomes straight forward.~~is straightforward. Then, an empirical relationship can be obtained by relating α to $\Delta T_{snow}/\Delta T_{ice}$ by running a regression model, and details are given in Sect. 4. However, for the time being, we assume that the regression equation (referred to as an 'α-prediction equation' that will be discussed in Sect. 4) is used to predict α from $\Delta T_{snow}/\Delta T_{ice}$.

2.3 Simultaneous estimation of ice thickness and snow depth from satellite-based freeboard using α

In this section, we describe how α can be used to constrain the freeboard to thickness conversion. Based on the assumed hydrostatic balance, ice thickness can be obtained from satellite-borne total freeboard or ice freeboard as follows:

$$\text{~~}H = h_{fi}\left(\frac{\rho_{water}}{\rho_{water}-\rho_{ice}}\right) - h\left(\frac{\rho_{water}-\rho_{snow}}{\rho_{water}-\rho_{ice}}\right)\text{~~} \quad H_i = \frac{\rho_w}{\rho_w-\rho_i}F_t - \frac{\rho_w-\rho_s}{\rho_w-\rho_i}h_s \tag{4}$$

~~$H = h_f\left(\frac{\rho_{water}}{\rho_{water}-\rho_{ice}}\right) + h\left(\frac{\rho_{snow}}{\rho_{water}-\rho_{ice}}\right)$~~ $H_i = \frac{\rho_w}{\rho_w-\rho_i}F_i + \frac{\rho_s}{\rho_w-\rho_i}h_s$

(5)

~~h_{if} and h_f are the total freeboard and ice freeboard, and ρ denotes the density.~~Here, ρ_w, ρ_i, and ρ_s denote the bulk densities of water, ice, and snow layer, respectively. Ice freeboard is obtained from radar freeboard by applying two correction terms regarding the change of the wave propagation speed in snow layer (F_c) and the displacement of the scattering horizon from the ice surface (F_p) (Kwok and Cunningham, 2015).

$F_i = F_r + (F_c - F_p)$ ~~With the use of α, defined in Eq. (3), Eqs. (4) and (5) become~~

~~$H = h_{if}\frac{\rho_{water}}{\rho_{water}-\rho_{ice}+\alpha(\rho_{water}-\rho_{snow})}$~~ (6)

~~$H = h_f\frac{\rho_{water}}{\rho_{water}-\rho_{ice}-\alpha\rho_{snow}}$~~The correction terms are expressed in the following equations (Armitage and Ridout, 2015; Kwok and Markus, 2018).

$F_c = (\eta_s - 1)f h_s$ (7)

$F_p = (1-f)h_s$ (8)

Here, η_s denotes the refractive index of the snow layer and f denotes the radar penetration factor (Armitage and Ridout, 2015), which is the depth of the radar scattering horizon relative to the snow depth (e.g. $f = 1$ if the radar scattering horizon is at snow–ice interface and $f = 0$ if the radar scattering horizon is at air-snow interface), respectively. Combination of Eqs. (6)–(8) yields the following relationship.

$F_i = F_r + (f\eta_s - 1)h_s$ (9)

Ice freeboard in Eq. (5) can be substituted by radar freeboard and snow depth using Eq. (9), i.e.:

$H_i = \frac{\rho_w}{\rho_w-\rho_i}F_r + \frac{(f\eta_s-1)\rho_w+\rho_s}{\rho_w-\rho_i}h_s$ (10)

According to Eq. (10), the ice thickness can be estimated from the radar freeboard and the snow depth. Note that Eq. (10) becomes equivalent to the equation for the total freeboard (Eq. (4)) if $f = 0$ (i.e. if there is no radar penetration into snow layer). With the use of α, defined in Eq. (3), Eqs. (4) and (10) become

$H_i = \frac{\rho_w}{\rho_w-\rho_i+\alpha(\rho_w-\rho_s)}F_t$ (11)

$H_i = \frac{\rho_w}{\rho_w-\rho_i-\alpha\{(f\eta_s-1)\rho_w+\rho_s\}}F_r$ (12)

From Eqs. (3~~) (7)~~, (11) and (12), it is evident that the snow depth and ice thickness can be simultaneously estimated from the freeboards once ~~α~~ α, ρ, f and ~~ρ~~ η_s are known.

In order to obtain α from satellite measurements of T_{as} and T_{si}, we need to calculate the temperature difference ratio ($\Delta T_{snow}/\Delta T_{ice}$). For the calculation, T_{iw} is set to be -1.5 °C. The freezing temperature of seawater is often assumed to be -1.8 °C; however, the value of -1.5 °C is chosen, based on the buoy observations. ~~Nevertheless, a~~A sensitivity test indicated that the influence of a 0.3 °C difference in the freezing temperature on α was negligible. α values are calculated only at the pixel whose monthly sea ice concentration (SIC) is greater than ~~98~~95% and rejected if T_{as} is warmer than T_{si}. The densities are prescribed with those used for OIB data processing: ~~ρ_{snow}, ρ_{ices},~~ ρ_i, and ~~ρ_{waterw}~~ are 0.320 ~~kg m~~g cm^{-3}, 0.915 ~~kg m~~g cm^{-3}, and ~~1024 kg m~~1.024 g cm^{-3}, respectively~~.~~ (Kurtz et al., 2013). Although ~~ρ_{snows}~~ varies seasonally (Warren et al., 1999) and ~~ρ_{icei}~~ is greater ~~in~~for MYI than~~ in~~ FYI (Alexandrov et al., 2010), we use the same densities as those of OIB data because we intend to compare outputs against OIB data. In solving Eq. (~~7~~12), cases showing negative ice thickness (α ~~>~~≥ α_{crit} = 0.~~341~~291 for the given densities and radar penetration factor) are rejected. Radar penetration factor f is set to be 0.84 for CS2 (Armitage and Ridout, 2015) and η_s is parameterized as a function of the snow density, i.e., $\eta_s = (1+0.51\rho_s)^{1.5}$ (Ulaby et al., 1986).

Before the Arctic basin-scale retrieval, ice thickness is estimated from OIB total freeboard measurement using Eq. (~~6~~11), and from OIB-derived ~~ice freeboard~~radar freeboards (Sect. 3.3) using Eq. (~~7~~12), using satellite-derived α as a constraint. At the same time, the corresponding snow depth is derived by multiplying the obtained sea ice thickness and α. Sea ice thicknesses ~~converted~~are also calculated from ~~MW99 using~~ Eqs. (4) and (~~5) are also compared~~10), using MW99 as snow depth, to examine how simultaneous retrievals ~~might be compared~~compare with ~~ICESat and CS2 retrieval of~~ ice thickness estimation using MW99. To differentiate various outputs, obtained snow depth and ice thickness are expressed with nomenclature such as '~~[~~(constraint~~ +~~, freeboard source~~]~~)'. For example, the snow depth estimated from satellite-derived α and OIB total freeboard is referred to as '~~h [α + h_{if} (OIB)]~~h_s (α^{sat}, F_t^{OIB})', and sea ice thickness from the MW99 ~~snow depth~~ and OIB ~~ice~~radar freeboard is referred to as '~~H [h (MW99) + h_f (OIB)]'.~~H_i (h_s^{MW99}, F_r^{OIB})'. Finally, ice thickness and snow depth are estimated from CS2 ~~ice~~radar freeboard (Sect. 3.4) over the Arctic Ocean.

3 Data

Here, we provide detailed information on the data sets used for the development of the retrieval algorithm, ~~validation~~evaluation, and application to the Arctic ocean basin scale.

3.1 CRREL and SHEBA buoy data

To determine the empirical relationship between α and $\Delta T_{snow}/\Delta T_{ice}$ using Eq. (3), we need information regarding h, H, T_{as}, T_{si}, and T_{iw} (as depicted in Fig. 1). These are sourced from temperature profiles observed by buoys deployed over the Arctic, as parts of the Surface Heat Energy Budget of the Arctic (SHEBA) campaign (Perovich et al., 2007) and the Cold Regions Research and Engineering Laboratory Ice Mass Balance (CRREL-IMB) buoy program (Perovich et al., 2019). Those buoy observations are stored for further analysis if there ~~is~~are no missing ~~value~~records over the entire period ranging from November

to March of the following year. Detailed information regarding ice ~~types~~type and initial snow/ice ~~thicknesses~~thickness at deployment locations are given in Table 1.

Time averages of temperature profiles are ~~considered~~used as ~~inputs~~input to the interface searching algorithm (described in Sect. 2.2) to meet the required near-equilibrium states (e.g. linear temperature profile). However, because of the possibility ~~of~~that the results are depending on the averaging period, we examine the results ~~by giving~~using various averaging periods from one to 30 days.

3.2 Satellite-derived skin and interface temperatures

For applying the buoy-based α-prediction equation in retrieving the snow/ice thicknesses over the Arctic Ocean, satellite-derived T_{as} and T_{si} data are necessary. In this study, T_{as} is obtained from Arctic and Antarctic ice Surface Temperatures from thermal Infrared satellites sensors – version 2 (AASTI-v2) data (Dybkjær et al., 2020), and the monthly mean for the 1982–2015 period is obtained from daily products. AASTI T_{as} is derived from CM SAF cLoud, Albedo and surface Radiation dataset from AVHRR data - Edition 2 (CLARA-A2) dataset (Karlsson et al., 2017), based on the algorithm described in Dybkjær et al. (2018). Information on the validation of this product is found in Dybkjær and Eastwood (2016). It is available in a 0.25° grid format, however, because other satellite data sets such as SIC are available in a 25 km Polar Stereographic SSM/I Grid, AASTI-v2 data are re-gridded in the same 25 km grid format. This reformatted AASTI-v2 ~~data are~~dataset is called 'satellite skin temperature'.

T_{si} is obtained from Snow/Ice Interface Temperature (SIIT) produced by Lee et al. (2018) over 30 years (1988–2017) of wintertime (December to February) using SSM/I and Special Sensor Microwave Imager/Sounder (SSMIS ~~Fundamental Climate Data Record of~~) homogenized TBs (Berg et al., 2018). The daily data are in the 25 km grid format. ~~It was~~Lee et al. (2018) reported that the satellite-derived T_{si} is consistent with snow–ice interface temperatures observed by CRREL-IMB buoys, with the correlation coefficient, bias, and RMSE of 0.95, 0.15 K and 1.48 K, respectively. In this study, we also ~~include~~produced T_{si} for March using the same algorithm of Lee et al. (2018) for ~~validating~~evaluating results against OIB data which are mostly collected during spring. Monthly composites are constructed by averaging daily data ~~if~~for grid cells where the data frequency is over 20 days. This product is called 'satellite interface temperature'.

3.3 OIB ~~snow depth, total freeboard, and ice freeboard~~data

In this study, OIB snow depth (h_s^{OIB}) and total freeboard (F_t^{OIB}) are used as a reference in the ~~validation~~evaluation of snow depth and ice thickness retrieved from the developed algorithm. NASA's OIB is an aircraft mission and it measures snow depth and total freeboard over the Arctic using the snow radar, Digital Mapping System (DMS), and Airborne Topographic Mapper (ATM) (Kurtz et al., 2013). ~~Ice~~OIB ice thickness is derived from measured snow depth and total freeboard, for the given snow and ice densities~~.~~ using Eq. (4). In this study, ~~ice~~the OIB radar freeboard (F_r^{OIB}) is derived ~~by subtracting the snow depth~~ from F_t^{OIB} and h_s^{OIB} using the ~~total freeboard.~~combined relationship of $F_i = F_t - h_s$ and Eq. (9) as follows:

~~The OIB data are available during the two months of March–April over the 2011–2015 period (Kurtz et al., 2015).~~ $F_r^{OIB} = F_t^{OIB} - h_s^{OIB} - (f\eta_s - 1)h_s^{OIB}$ (13)

Because the main objective of using OIB data is to evaluate the relative performance of the simultaneous retrieval method when the method is applied to CS2 data, the radar penetration factor (f) for OIB data processing is also set to be 0.84. In the data processing chain, h_s^{OIB} is removed if it is smaller than the given uncertainty level of the dataset (~5.7 cm) or it is larger than the total freeboard F_t^{OIB}.

Five years of OIB data during 2011-2015 period are utilized in this study. The level 4 dataset (Kurtz et al., 2015) during 2011-2013 period and Quick look dataset (https://doi.org/10.5067/7Q8HCCWS4I0R, last access: 20 May 2020) during 2014-2015 period are obtained from the NSIDC website. Because we use the November–March period for the buoy analysis, only March OIB data are considered for the ~~validation~~evaluation. The OIB data are also reformatted into the 25 km grid format for comparison. If the location of one OIB individual data point falls within a certain 25 km grid area, then the point data is binned in a corresponding grid. After completing the grid assignment, grid value is determined by calculating a simple arithmetic mean of all data within that grid area.

3.4 CS2 data

For examining the Arctic Ocean basin distribution of ice thickness and snow depth, CS2 freeboard measurement summary data are used (Kurtz et al., 2017). They are monthly mean composites of CS2 ice freeboard data in the 25 km Polar Stereographic SSM/I Grid format, covering the entire Arctic, and available from September 2010. Detailed descriptions of the retracker algorithm used in this dataset are found in the study by Kurtz et al. (2014). The ~~data set~~dataset also includes ~~the sea ice thickness estimated from the use of~~ MW99 (h_s^{MW99}) and W99 snow ~~depth as input to the conversion equation. Those ice thickness estimations and MW99 snow depth values are~~density climatology used for ~~purposes of comparison~~producing the ice freeboard.

The CS2 ice freeboard data (F_i^{CS2}) distributed by NSIDC (Kurtz et al. 2017) assumed that the radar scattering horizon is at the snow–ice interface and applied a wave propagation speed correction. However, the correction was made using h_s^{MW99} and W99 snow density climatology with an erroneous form of $h_c = (1 - \eta_s^{-1})\, h_s$, instead of the proper form of $h_c = (\eta_s - 1)\, h_s$ (Mallett et al., 2020). In this dataset, η_s was parameterized as a function of the snow density, i.e., $\eta_s = (1 + 1.7\rho_s + 0.7\rho_s^2)^{0.5}$ (Tiuri et al., 1984). Thus, at this point, it is straightforward to derive the CS2 radar freeboard by removing the correction term as in the following equation.

$$F_r^{CS2} = F_i^{CS2} - (1 - \eta_s^{-1})h_s^{MW99} \quad (14)$$

Then CS2 ice thickness is re-produced from F_r^{CS2} and h_s^{MW99} by using Eq. (10) with the constant densities and the radar penetration factor described in Sect. 2.3. Those h_s^{MW99} and H_i (h_s^{MW99}, F_r^{CS2}) values are used for comparison.

3.5 Sea ice concentration

Calculation of α is done ~~over~~for those pixels where the ~~pixel whose~~ monthly SIC is greater than ~~98~~95% (as described in Sect. 2.3). To determine pixels that meet this SIC criterion, 'bootstrap sea ice concentrations from Nimbus-7 SMMR and DMSP SSM/I-SSMIS version 3' produced by Comiso (2017) are used. This SIC dataset is provided in the 25-km Polar Stereographic SSM/I grid format.

4 Results

4.1 The empirical relationship between α and $\Delta T_{snow}/\Delta T_{ice}$

We examine variables (i.e. T_{as}, T_{si}, T_{iw}, H, and h) obtained from buoy observations by applying the interface searching algorithm. In the scatter plot of weekly-averaged $\Delta T_{snow}/\Delta T_{ice}$ versus α (Fig. 4a), it appears that α linearly increases with $\Delta T_{snow}/\Delta T_{ice}$ when the ratio is smaller than 1.8, but the linear slope becomes smaller when $\Delta T_{snow}/\Delta T_{ice}$ is larger than 1.8. This ~~nature~~pattern of the slopes is found to be nearly invariant from year to year, as observed in different colors appearing in the entire range of $\Delta T_{snow}/\Delta T_{ice}$ ~~of~~in Fig. 4a. ~~Also~~We also found that this slope pattern is the consistent nature ~~of the slopes~~ even for different data sets; two different data sets (red points for SHEBA and other points for CRREL) covering various ranges of $\Delta T_{snow}/\Delta T_{ice}$, show similar distributions along the two different slopes. Thus, ~~it suffices to conclude that~~ the slope ~~change may~~pattern is not ~~be~~ due to different data sources or different data periods. ~~-~~Further analysis of the two slopes is found in Appendix A.

Taking such ~~changing~~ a two-slope pattern with $\Delta T_{snow}/\Delta T_{ice}$ into account, we introduce a piecewise linear function that may express the slope ~~change~~pattern, i.e.:

$$y = \begin{cases} a_1 x + b_1 & x \le x_0 \\ a_2 x + b_2 & x > x_0 \end{cases}, \quad x_0 = \frac{b_1 - b_2}{a_2 - a_1} \qquad \text{~~(8~~(15)}$$

In Eq. (~~8~~15), x and y correspond to $\Delta T_{snow}/\Delta T_{ice}$ and α, respectively, and x_0 is the point where the slope transition takes place. Applying Eq. (~~8~~15) to data points from buoy-based variables, the regression coefficients (a_1, b_1, a_2, b_2) and ~~the~~ transition point (x_0~~) in Eq. (8~~) are determined by minimizing the total variance - obtained regression line is plotted in Fig. 4a. α is predicted using the determined regression equation (hereafter referred to as α-prediction equation) and compared ~~against~~to the original α values to see how well the regression was performed. The comparison of α with predicted values in Fig. 4b shows that the regression equation is well fitted because of the ~~near~~ zero bias and 91.9% of explained variance.

Although the slope ~~change~~pattern discussed with Eq. (~~8~~15) and Fig. 4 is based on the weekly averages, the ~~nature of changing~~ slope pattern seems to be consistent among the data averaging periods except for ~~a very short~~an averaging period~~.~~ shorter than five days. Regressions ~~given~~ in the form of Eq. (~~8~~15) are performed with buoy data averaged with different averaging periods to understand the ~~nature of changing~~ slope pattern. Regression coefficients and transition point for the chosen averaging periods are examined, and results for four averaging periods are given in Table 2. Detailed information on the coefficients and

associated statistics varying with the averaging period is given in Fig. 5. The positions of slope change (x_0) are located at approximately 1.8, delineating a nearly invariant slope ~~change~~pattern, regardless of different data averaging periods. Fig. 5a shows that coefficients do not vary much with different averaging periods while coefficients of the first part of the regression line (a_1 and b_1, $x \leq x_0$) vary less than those of the second part (a_2 and b_2, $x > x_0$). The regression equations show that the explained variance (R^2) rises quickly when the averaging period is longer but levels off when data are averaged over a period that is longer than seven days. The bias appears to be near zero over the various averaging periods. Thus, regression performance is found to be comparable if data are averaged over a period that is longer than a week. ~~Further analysis of explanations of the possible causes of two slopes is found in Appendix A.~~

4.2 ~~Validation~~Evaluation against OIB estimates

According to the regression results, it is possible to estimate α from the $\Delta T_{snow}/\Delta T_{ice}$. Since the $\Delta T_{snow}/\Delta T_{ice}$ can be calculated from the satellite skin and interface temperature (as described in Sect. 3.2), the corresponding α can be estimated from satellite measurements. Thus, we are able to simultaneously retrieve sea ice thickness and snow depth from altimeter-based freeboard measurements, following Eqs. (~~6~~11) and (~~7~~12). We test and ~~validate~~evaluate this simultaneous retrieval approach using OIB data. Accordingly, ice thickness and snow depth are simultaneously estimated from OIB freeboard measurements and ~~validated~~evaluated against the OIB snow depth (~~h (OIB))~~h_s^{OIB}) and ice thickness (~~H (OIB)).~~H_i^{OIB}).

To calculate α, a data averaging period must be selected. Considering that the monthly composite of satellite freeboard measurements is needed to retrieve snow/ice thickness in the Arctic basin scale, it seems appropriate to use the monthly averaging period to calculate the monthly α distribution. Thus, we use the monthly averaged satellite temperatures and the coefficients for the 30-day averaging period (Table 2) to calculate α.

We simultaneously retrieved ~~H~~H_i and ~~h~~h_s for each year's March ~~of the~~during 2011—2015 period from the reformatted OIB freeboard measurements (Sect. 3.3) together with satellite-derived ~~α.~~α (α^{sat}). As expressed in Eqs. (~~6~~11) and (~~7~~12), two different ice thickness retrievals are possible, depending on the use of the freeboard type (i.e. total freeboard ~~h_f~~F_t vs. ~~ice~~radar freeboard ~~h_f~~F_r). Two accordingly associated retrievals of snow depth are available. Retrieved results of ice thickness (~~H~~H_i) and snow depth (~~h~~h_s) from the use of OIB total freeboard and ~~ice~~radar freeboard are given in the first and second row of Fig. 6, respectively. Corresponding OIB measurements are given at the bottom of Fig. 6. The comparison between any snow/ice retrievals and OIB measurements appear to be consistent with each other for both snow depth and ice thickness, in terms of magnitudes and distribution.

To compare the results quantitatively, scatterplots of comparing retrievals against OIB measurements are made, along with statistics for the snow depth and ice thickness retrievals, in the top four panels of Fig 7. The top-two left panels are derived from the use of OIB total freeboard (~~h_f~~F_t^{OIB}) while the top-two right panels are derived from the OIB ~~ice~~radar freeboard (~~h_f~~F_r^{OIB}). The comparison is done only for pixels where all four products (i.e. snow/ice thicknesses from two different freeboards) are available. This indicates that the snow depth from the total freeboard (top left) is fairly consistent with the OIB

snow depth, with a correlation coefficient of 0.73 and with a near-zero bias. The retrieved ice thickness from the total freeboard (middle left) appears to be consistent with OIB ice thickness, with a correlation coefficient of 0.93 and a bias around ~~2~~8.5 cm. The RMSEs for snow depth and ice thickness are 6.8 cm and 44.3 cm, respectively. Based on the comparison results, Eq. (~~8~~15) obtained from buoy measurements can be successfully implemented with space-borne total freeboard measurements for the simultaneous retrieval of snow depth and ice thickness.

Following Eq. (~~7~~12), snow depth and ice thickness retrievals are made from the use of ~~ice~~radar freeboard measurements, and results are presented in the top-two right panels in Fig. 7. ~~The~~On the one hand, the comparison of obtained ice thickness against the OIB ice thickness indicates that the retrieved ice thickness shows nearly the same quality as that retrieved from the total freeboard measurements. On the other hand, snow retrievals from the ~~ice~~radar freeboard show more scattered features, compared with snow retrieval results from the total freeboard. More scattered features found in the snow depth from the ~~ice~~radar freeboard are likely due to the ~~relatively more sensitive nature to~~larger sensitivity of the retrieved α and the prescribed densities, as noted in Eq. (~~7~~12). Note that Eq. (~~7~~12) has a smaller denominator than that for Eq. ~~(6).~~ (11). Results of associated sensitivity analysis can be found in Appendix B.

~~Examining~~We now examine how the ~~current practices~~use of MW99 for retrieving ~~the~~ sea ice thickness ~~through~~from ICESat and CS2 measurements ~~are compared~~compares with ~~the~~results from our simultaneous ~~retrievals is of interest. In doing~~method. To do so, OIB-measured total freeboard and ~~ice~~radar freeboard are converted into ice thickness using MW99 as input to solve Eqs. (4) and (~~5). These~~10). In this study, these two ice thickness retrievals with the use of MW99 are referred to as "ICESat-like" thickness and "CS2-like" thickness, respectively, and their comparisons are now observed in two panels at the bottom of Fig. 7. ~~Apparently~~According to our analysis, ICESat-like thickness tends to underestimate the ice thickness by about ~~50~~47.9 cm when MW99 is used, in comparison to OIB thickness~~. On the other hand,~~ and CS2-like ice thickness shows an overestimate of about ~~23~~25.5 cm. Nevertheless, their correlation coefficients and RMSEs are similar to the results obtained from the α method.

~~The different direction~~Better agreement of H_i from the simultaneous method with H_i^{OIB} may be due to the fact that the simultaneously estimated h_s is more consistent with h_s^{OIB} (h_s^{MW99} is likely larger than h_s^{OIB}, as shown in Fig. S1). Note that all inputs are the same except the snow depth. The negative bias ~~between~~of ICESat-like ~~and~~thickness and positive bias of CS2-like ~~thicknesses is thought to be attributable to the~~ thickness reflect expected responses in different signs to the same snow depth error ~~according to~~, as shown in different signs in the last terms of Eqs. (4) and (~~5). Therefore~~10) (also note Eq. (B2) in Appendix B). Because of this reasoning, if there are decreasing trends in ~~both~~not only ice thickness ~~and~~but also snow depth, the decreasing trend of ice thickness estimated from the constant snow depth will be diminished in radar, while being amplified in lidar. Because of this, the construction of the ice thickness (or volume) trend from the two different satellite altimeters would be problematic if MW99 ~~snow depth~~ is used for the freeboard to thickness conversion. For example, it would be hard to compare the sea ice thickness records estimated from ICESat and CS2 observations and to extend the current ice thickness record from CS2 with recently launched NASA's ICESat-2 which carries a lidar altimeter, for the same reason.

4.3 Simultaneous retrieval of ice thickness and snow depth from CS2 measurements

We have demonstrated that the method of simultaneously retrieving the sea ice thickness and snow depth was successfully implemented with OIB measurements. Now we extend the proposed approach to satellite freeboard measurements. Here, the method is tested with CS2 freeboard measurements, solving for ~~*H*~~H_i in Eq. (~~7~~12), and α is obtained from the collocated satellite skin and interface temperature data.

Monthly means of CS2-estimated freeboard (~~h_f~~F_r), retrieved α, ice thickness (~~*H*~~)H_i), and snow depth (~~h~~h_s) for December 2013 to March 2014 are given in Fig. 8. The geographical distribution of α indicates that α is largest in January and becomes smaller ~~in~~during the following months. Geographically, there seems to be no ~~coherent~~particular distribution of α between months, although interestingly the lowest α values are always found over the north of the Canadian Archipelago and the western part of the Arctic Ocean shows α values that is generally larger than that over the eastern part.

Retrieved ice thickness from the CS2 freeboard (~~h_f~~F_r) using obtained α is presented in the third row of Fig. 8. As expected, as noted in Eq. (~~7), *H*~~12), H_i shows a similar geographical distribution as shown in the freeboard (the first row). The thickest area is located north of the Canadian Archipelago, where the ice appears thicker than 4 m. On the other hand, most of the FYI thickness appears to range from 1.0 m to 2.0 m. The snow depth ~~h~~h_s is obtained by multiplying α by ~~*H*~~H_i (in 2nd and 3rd rows), following Eq. (3), and results are given at the bottom. The obtained snow distribution indicates that thicker snow areas are generally coincident with thicker MYI areas. Likewise, the thinner snow area coincides with the thinner FYI area. Such similarity should be consistent with the notion that MYI should accumulate more precipitation than FYI because of its longer existence.

The accuracies of CS2 retrievals using the current α approach can be indirectly tested ~~against~~with OIB measurements. We do so by examining whether the ~~relationship between *H* [α + h_f (OIB)]~~relationships of h_s (α^{sat}, F_r^{OIB}) vs. h_s^{MW99} and ~~*H* [*h* (MW99) + h_f (OIB)]~~,H_i (α^{sat}, F_r^{OIB}) vs. H_i (h_s^{MW99}, F_r^{OIB}), in which each snow/ice thickness retrieval has its own accuracy against OIB measurements, can be reproduced in CS2-based retrievals. If similar results are found, we can deduce respective accuracies against those found from the ~~validation~~evaluation efforts against OIB measurements. The ~~relationship~~relationships, which can be obtained from analysis in Fig. 7, is compared with the relationship found in the current results in Fig. 8, (i.e., ~~*H* [α + h_f (CS2)]~~h_s (α^{sat}, F_r^{CS2}) vs. h_s^{MW99} and ~~*H* [*h* (MW99) + h_f (CS2)]~~;H_i (α^{sat}, F_r^{CS2}) vs. H_i (h_s^{MW99}, F_r^{CS2})); the results are presented in Fig. 9. Observably, the ~~relationship~~relationships from CS2 freeboard data (Fig. 9b~~) is~~, d) are very similar to the relationship obtained from the comparison results from OIB measurements~~.~~ (Fig. 9a, c). This similarity of the slope strongly indicates that the CS2-based sea ice thickness from the current α method has similar accuracy to that found in the ~~validation~~evaluation against OIB measurements (Sect 4.2).

5. Conclusions and Discussion

A new approach towards simultaneously estimating snow depth and ice thickness from space-borne freeboard measurements was proposed and tested using OIB data and CS2 freeboard measurements. In developing the algorithm, the vertical temperature slopes were assumed to be linear within the snow and ice layers so that continuous heat flux could be maintained in both layers. This assumption allowed for the description of the snow–ice vertical thermal structure with snow skin temperature, snow–ice interface temperature, the water temperature at the ice–water interface, snow depth, and ice thickness. Based on the continuous heat transfer assumption, the snow–ice thickness ratio (α = ~~h / H~~h_s / H_i) was introduced and could then be embedded into the freeboard to ice thickness conversion equations. Thus, information on both ice thickness and snow depth can be derived once α is known in case of the availability of a freeboard, without relying on the snow depth information as an input to the conversion from freeboard to ice thickness. From the drifting buoy measurements of the temperature profile, snow depth, and ice thickness over the Arctic Ocean, we demonstrated that α can be reliably determined using the ratio of the vertical difference of the snow-layer temperature to the vertical difference of ice-layer temperature ($\Delta T_{snow}/\Delta T_{ice}$). An empirical regression equation was obtained for predicting α from three interface temperatures.

Before applying α-prediction equation to simultaneously retrieve the ice thickness and snow depth from satellite-borne freeboard measurements, the algorithm was ~~validated~~evaluated using OIB measurements, in conjunction with satellite-derived snow skin temperature and snow–ice interface temperature. ~~Validation~~Evaluation results demonstrated that our proposed algorithm adequately retrieved both parameters simultaneously. As a matter of fact, the ice thickness results were more accurate than they were from the current retrieval methods relying on the input of snow depth (this time MW99 snow climatology), in terms of mean bias and RMSE. It should be noted that in this case, snow depth is a retrieval product, instead of being input to the freeboard to ice thickness conversion adopted by CS2 or ICESat retrieval. ~~Application~~The application was finally made for the retrieval of the snow depth and ice thickness from CS2 ~~ice~~radar freeboard measurements from December 2013 to March 2014 using α as a constraint. Results showed that the quality of the obtained ice thickness was similar to that obtained from ~~validation~~evaluation results against OIB measurements. Retrieved snow depth distributions were also found to be consistent with expectations.

In the retrieval process, we may be concerned about the applicability of the algorithm developed with buoy observations representing the point ~~circumstances~~measurements, to the larger spatial and temporal scales ~~that are inevitable in the~~of satellite measurements. This concern may be relevant upon observing the range of α values. α in the satellite's monthly and 25 km x 25 km spatial scales was found to be generally smaller than 0.2. The smaller range of α compared to that shown in the buoy analysis results is likely due to the scale differences, indicating that extreme α values often shown in buoy measurements (due to very thick snow and/or very thin ice) may never be observed in satellite measurements. However, the range may not be a problem because the relationship (Eq. (3)) expresses the thermal equilibrium condition described by the temperature at three interfaces, the ratio of snow and ice thickness, and the ratio of thermal conductivity between snow and ice. Considering that the algorithm is based on the equilibrium conditions, results should be valid regardless of spatial and temporal scales if the

prerequisite equilibrium conditions are met. Apparently, buoy observations contain so many different cases that equilibrium conditions are met with different thermal and physical conditions of the snow–ice system. Sound ~~validation~~evaluation results and the consistency between OIB and CS2 ice thickness retrieval results, which are subject to different scales, all suggest that point-measured α-prediction equation can ~~be applicable~~apply to satellite measurements.

Overall, the developed α-based method yields ice thickness and snow depth, without relying on a priori 'uncertain' snow depth information~~,~~ (MW99), which results in uncertainty in the ice thickness retrieval. The results that ~~ice~~radar freeboard and the total freeboard yielded had nearly the same outputs when the α-approach was used. The proposed method ~~is applicable~~applies to both lidar and radar altimeter data, although lidar-based altimeter data tend to offer relatively more suitable snow depth information~~.~~ with smaller RMSE. We expect to continuously monitor the Arctic scale snow depth and ice thickness by applying the proposed α method to total freeboard observations by the recently launched ICESat-2, using temperature observations from the upcoming MetOp SG Meteorological Imager (MetImage), the Microwave Imager (MWI) and the proposed Copernicus Imaging Microwave Radiometer (CIMR).

Appendix A: Physical interpretation of the piecewise linearity between α and $\Delta T_{snow}/\Delta T_{ice}$

The relationship found between α and $\Delta T_{snow}/\Delta T_{ice}$ showed a piecewise linearity, which is almost invariant with the data averaging period. Because the slope change is neither attributable to different data sources nor different data periods, it is likely caused by the physical properties of the snow and ice, as shown in Fig. A1. If the slope change is caused by the snow/ice condition, there will be a significant difference in snow/ice properties between the two parts showing different slopes. Here, we examine the possibility of different physical properties causing the difference in slopes. Through this comparison using buoy data, we may identify important properties that might be responsible for the piecewise linearity.

First, the ~~mean~~averages of basic properties available from buoy measurements are compared. They include ice thickness, snow depth, snow–ice interface temperature, ice temperature ($T_{ice} = (T_{as} + T_{si}) / 2$), and so on. The comparison revealed that snow–ice system within the first part ($x \leq x_0$) is found to consist of relatively thicker ice (mean value: 1.84 m), thinner snow (0.29 m), and colder ice (-9.13 °C) while the second part ($x > x_0$) is found to consist of relatively thinner ice (1.10 m), thicker snow (0.46 m), and warmer ice (-5.00 °C). In general, a thicker snow or ice layer exhibits a greater temperature difference ~~within~~from top to bottom of the layer. There is no significant difference between the air–snow interface temperature (T_{as}) in the two slope parts.

The thermal conductivities, k_{snow} and k_{ice}, are also compared because what connects α and $\Delta T_{snow}/\Delta T_{ice}$ is the ratio of thermal conductivities. Before showing the results, we describe how to calculate k_{snow} and k_{ice}. First, the thermal conductivity ratio is calculated from buoy measured variables (i.e. T_{as}, T_{si}, T_{iw}, ~~h~~h_s, and ~~H~~H_i) using Eq. (3). Because the underlying physics in k_{snow} is significantly more complex, k_{ice} is estimated first, and then k_{snow} is obtained by multiplying the calculated k_{ice} and k_{snow}/k_{ice}. To calculate k_{ice}, the parameterization of Maykut and Untersteiner (1971), which describes k_{ice} as a function of salinity and temperature, is used.

$$k_{ice} = 2.03 + 0.117\frac{S_{ice}}{T_{ice}} \quad \text{(A1)}$$

Here, S_{ice} and T_{ice} is the salinity (in ppt) and temperature (in Celsius) of sea ice, respectively. For the calculation, S_{ice} is estimated according to the empirical relationship between sea ice thickness and mean salinity from Cox and Weeks (1974) as follows:

$$S_{ice} = \begin{cases} 14.24 - 19.39H, & H \leq 0.4\ m \\ 7.88 - 1.59H, & H > 0.4\ m \end{cases} \begin{cases} 14.24 - 19.39H_i, & H_i \leq 0.4\ m \\ 7.88 - 1.59H_i, & H_i > 0.4\ m \end{cases} \quad \text{(A2)}$$

Although Trodahl et al. (2001) reported that k_{ice} depends on depth and temperature; here we do not estimate accurate thermal conductivities but attempt to examine the physical consequences ~~within~~of the ~~piecewise linearity~~total ice layer.

The ~~comparison of~~ calculated thermal conductivities ~~is~~are presented in Fig. A2. The calculated k_{ice} ranges from 1.8 W K^{-1} m^{-1} to 2.0 W K^{-1} m^{-1} (left two panels in Fig. A2). These values are consistent with the in-situ measurements by Pringle et al. (2006). The mean values of k_{ice} of the first part (1.96 W K^{-1} m^{-1}) and the second part (1.88 W K^{-1} m^{-1}) show almost no difference. The calculated k_{snow} ranges from 0.2 W K^{-1} m^{-1} to 1.05 W K^{-1} m^{-1} (right two panels in Fig. A2). This range is consistent with reported values in Sturm et al. (1997). The first part shows the greater ~~and significantly~~ spread in the distribution of k_{snow} compared to the second part. The mean k_{snow} values are 0.44 and 0.27 for the first part and second part, respectively.

As a significant difference is observed in k_{snow}, ~~let us~~we would like to find a possible reason for this difference. To do so, we should first review the factors determining k_{snow}; they are density, temperature, and crystal structure (Sturm et al., 1997). Snow is a mixture of ice particles and air, and air has lower thermal conductivity than ice. Thus, snow with a relatively lower density including a greater portion of air should have relatively lower thermal conductivity. Besides, the thermal conductivity of ice particles depends on the temperature, and the path of heat transfer depends on the crystal structure which describes how the particles are connected. The heat transfer occurs not only by conduction but also by water vapor latent heat transportation and convection through the pore spaces (Sturm et al, 2002), which are hard to ~~be quantified~~quantify explicitly. These two factors are closely related to the temperature gradient (or difference) imposed within the snow layer.

Based on this knowledge, we can infer the condition of the snow layer of the two parts. The relatively higher and varying k_{snow} of the first part would be related to the compaction process resulting in high density, and metamorphic diversity which changes the crystal structure. According to Sturm et al. (2002), the value of k_{snow} of hard wind slap attains up to 0.5 W m^{-1} K^{-1}, while that of k_{snow} of depth hoar is below 0.1 W m^{-1} K^{-1}. On the other hand, the lower and nearly constant k_{snow} of the second part implies that the snow layer of the second part would consist of fresh and dry snow having relatively lower density and a relatively lower likelihood of experiencing particular metamorphism.

In summary, it is concluded that the physical properties of snow and ice can account for the piecewise linearity, based on the differences in the physical properties between the first and second parts. Especially, the thermal conductivity of the snow, k_{snow}, seems to play an important role. Nevertheless, further analysis is required to fully understand this phenomenon.

Appendix B: Sensitivity test for the proposed method

Here we present results of a sensitivity test for showing how the snow depth and ice thickness retrieval results are dependent on the uncertainties in α. To do so, the uncertainty in the snow depth (Δh_s) due to the α error (i.e. $\Delta\alpha$) and associated ice thickness error (ΔH_i) are estimated. From this sensitivity test, we expect to understand why the simultaneous method for the radar freeboard shows more scattered features than those from the lidar total freeboard.

First, Δh_s is defined by the difference of retrieved h_s between with error ($\alpha+\Delta\alpha$) and without error (α).

$$\Delta h_s = \begin{cases} h_s(\alpha+\Delta\alpha, F_t) - h_s(\alpha, F_t) & (\text{using } F_t) \\ h_s(\alpha+\Delta\alpha, F_r) - h_s(\alpha, F_r) & (\text{using } F_r) \end{cases} \quad \text{(B1)}$$

Then, Δh_s can be converted to the error in the ice thickness (ΔH_i) using the following equation derived from Eq. (10).

$$\Delta H_i = \frac{(f\eta_s - 1)\rho_w + \rho_s}{\rho_w - \rho_i}\Delta h_s = \begin{cases} -6.46\Delta h_s & (\text{using } F_t) \\ 3.44\Delta h_s & (\text{using } F_r) \end{cases} \quad \text{(B2)}$$

Because h_s is a combination of freeboard and α, as in Eqs. (11) and (12), we only examine the uncertainty with some typical sea ice types. Here physical states for thicker ice (type A), moderate ice (type B), and thinner ice (type C) are chosen, which are summarized in Table B1. Typical values for those three types are shown in the scatterplots of OIB-based (α^{OIB} vs. F_t^{OIB}) and of satellite-based (α^{sat} vs. F_r^{CS2}) – Fig. B1. It is shown that the majority of data points are located around type B, followed by type A. There seems a very small portion of total samples showing values around type C.

With $\Delta\alpha = \pm 0.03$, which is an RMSE range in the α-prediction equation, Δh_s and ΔH_i are estimated for three ice types. Table B2 summarizing results show that $|\Delta h_s|$ is within 5 cm and it tends to decrease as the ice becomes thinner when the current method is applied to the total freeboard. On the other hand, the use of radar freeboard shows that $|\Delta h_s|$ tends to be more sensitive for the same $\Delta\alpha$. Especially, the sensitivity of type C is the greatest. This is because the denominator of Eq. (12) becomes smaller when α approaches to α_{crit}, resulting in an unstable solution. For the ice thickness, $|\Delta H_i|$ is smaller when the total freeboard is used since ΔH_i is proportional to Δh_s. However, the gap between the results from two freeboards has narrowed because H_i from the total freeboard is more sensitive than the radar freeboard to Δh_s, according to Eq. (B2). The sensitivity characteristics shown here are consistent with the analysis results given in Sect 4.2. Because there is a much small number of data points belonging to type C, at least in the data used for this study, the overall sensitivity would likely be in between B and A types.

It is also of importance to ask to what degree of retrievals is successfully yielded. In this study, cases showing $T_{as} > T_{si}$ or retrieved $\alpha \geq \alpha_{crit}$ are considered to be failures. Statistics on success/fail ratio of α retrieval for December–March of 2011–2015 period are provided in Table B3. Overall, the success ratio was over 82% in December–February, while it was reduced to ~74% in March. Most of the failures appear associated with cases showing the temperature inversion (i.e. $T_{as} > T_{si}$), whose areas are shaded with grey in the α-distributions of Fig. 8. Those failure areas are generally found around the marginal ice zones and in

the east of Greenland. On the other hand, there was a near-zero failure (0.02% of total pixels) for retrieved $\alpha \geq \alpha_{crit}$. This near-zero failure implies that almost all calculated α meet the satisfactory condition after the removal of cases showing the temperature inversion. It may be concluded that the calculated α appears to be physically reasonable (i.e. $\alpha < \alpha_{crit}$) as long as presumed thermodynamic conditions are met.

Data availability

The SHEBA buoy data were obtained from NCAR/EOL (https://doi.org/10.5065/D6KS6PZ7, last access: 14 September 2019) and CRREL IMB buoy data were obtained from the CRREL-Dartmouth Mass Balance Buoy Program (http://imb-crrel-dartmouth.org, last access: 14 September 2019). AASTI-v2 and SIIT data are available upon request to authors. Other data sets were obtained from NSIDC; They are OIB data (https://doi.org/10.5067/G519SHCKWQV6, last access: 10 September 2019), OIB quick look data (https://doi.org/10.5067/7Q8HCCWS4I0R, last access: 10 September 2019), CS2 data (https://doi.org/10.5067/96JO0KIFDAS8, last access: 10 September 2019), and SIC data (https://doi.org/10.5067/7Q8HCCWS4I0R, last access: 12 September 2019).

Author contribution

HS and BJS conceptualized and developed the methodology and HS conducted data analysis and visualization. GD and RTT gave important feedback for the algorithm development and result interpretation. GD provided AASTI data. All of the authors participated in writing the manuscript; HS prepared the original draft under the supervision of BJS and GD, and BJS critically revised the manuscript.

Competing interests

The authors declare that they have no conflict of interest.

Acknowledgments

This study has been supported by the Space Core Technology Development Program (NRF-2018M1A3A3A02065661) of the National Research Foundation of Korea. Authors also acknowledge that this study is also supported by the International Network Programme of the Ministry of Higher Education and Science, Denmark (Grant ref. no. 8073-00079B). We appreciate NSIDC for producing and providing the OIB, CS2, and SIC dataset. We also give thanks to CRREL and NCAR/EOL under the sponsorship of the National Science Foundation for providing IMB and SHEBA buoy data.

References

Alexandrov, V., Sandven, S., Wahlin, J., and Johannessen, O. M.: The relation between sea ice thickness and freeboard in the Arctic, The Cryosphere, 4, 373-380, doi: 10.5194/tc-4-373-2010, 2010.

Armitage, T. W. K., and Ridout, A. L.: Arctic sea ice freeboard from AltiKa and comparison with CryoSat-2 and Operation IceBridge, Geophys. Res. Lett., 42, 6724–6731, doi: 10.1002/2015GL064823, 2015.

Berg, W., Kroodsma, R., Kummerow, C. D., and McKague, D. S.: Fundamental Climate Data Records of Microwave Brightness Temperatures, Remote Sens., 10(8), 1306, doi: 10.3390/rs10081306, 2018.

Braakmann-Folgmann, A., and Donlon, C.: Estimating snow depth on Arctic sea ice using satellite microwave radiometry and a neural network, The Cryosphere, 13, 2421–2438, doi: 10.5194/tc-13-2421-2019, 2019.

Brucker, L., and Markus, T.: Arctic-scale assessment of satellite passive microwave-derived snow depth on sea ice using Operation IceBridge airborne data, J. Geophys. Res.-Oceans, 118(6), 2892–2905, doi: 10.1002/jgrc.20228, 2013.

Comiso, J. C.: Bootstrap Sea Ice Concentrations from Nimbus-7 SMMR and DMSP SSM/I-SSMIS, Version 3, Boulder, Colorado USA. NASA National Snow and Ice Data Center, doi: 10.5067/7Q8HCCWS4I0R, 2017.

Comiso, J. C., Cavalieri, D. J., and Markus, T.: Sea ice concentration, ice temperature, and snow depth using AMSR-E data, IEEE Trans. Geosci. Remote Sens., 41(2), 243–252, doi: 10.1109/TGRS.2002.808317, 2003.

Cox, G. F. N., and Weeks, W. F.: Salinity variations in sea ice, J. Glaciol., 13(67), 109–120, doi: 10.3189/S0022143000023418, 1974.

Dybkjær, G., and Eastwood, S.: Validation Report for the OSI SAF High Latitude L2 Sea and Sea Ice Surface Temperature, OSI-205, Version 1.1, OSI SAF, 30 pp., 2016.

Dybkjær, G., Eastwood, S., Borg, A. L., Højer, J., and Tonboe, R.: Algorithm theoretical basis document for the OSI SAF Sea and Sea Ice Surface Temperature L2 processing chain, OSI-205-a and OSI-205-b, Version 1.4, OSI SAF, 40 pp., 2018.

Dybkjær, G., Tonboe, R., Højer, J., and Eastwood, S.: Arctic and Antarctic snow and ice Surface Temperatures from AVHRR thermal Infrared satellite sensors, 1982-2015, 2020. (Manuscript in preparation)

Guerreiro, K., Fleury, S., Zakharova, E., Rémy, F., and Kouraev, A.: Potential for estimation of snow depth on Arctic sea ice from CryoSat-2 and SARAL/AltiKa missions, Remote Sens. Environ., 186, 339–349, doi: 10.1016/j.rse.2016.07.013, 2016.

Guerreiro, K., Fleury, S., Zakharova, E., Kouraev, A., Rémy, F., and Maisongrande, P.: Comparison of CryoSat-2 and ENVISAT radar freeboard over Arctic sea ice: toward an improved Envisat freeboard retrieval, The Cryosphere, 11, 2059–2073, doi: 10.5194/tc-11-2059-2017, 2017.

Hendricks, S., Ricker, R., and Helm, V.: User Guide – AWI CryoSat-2 sea Ice thickness data product (v1.2), doi: 10013/epic.48201, 2016.

Karlsson, K.-G., Anttila, K., Trentmann, J., Stengel, M., Meirink, J. F., Devasthale, A., Hanschmann, T., Kothe, S., Jääskeläinen, E., Sedlar, J., Benas, N., van Zadelhoff, G.-J., Schlundt, C., Stein, D., Finkensieper, S., Håkansson, N., Hollmann, R., Fuchs, P., and Werscheck, M.: CLARA-A2: CM SAF cLoud, Albedo and surface RAdiation dataset from AVHRR data -

Edition 2, Satellite Application Facility on Climate Monitoring (CM SAF), doi: 10.5676/EUM_SAF_CM/CLARA_AVHRR/V002, 2017.

Kern, S., Khvorostovsky, K., Skourup, H., Rinne, E., Parsakhoo, Z. S., Djepa, V., Wadhams, P., and Sandven S.: The impact of snow depth, snow density and ice density on sea ice thickness retrieval from satellite radar altimetry: results from the ESA-CCI Sea Ice ECV Project Round Robin Exercise, The Cryosphere, 9, 37–52, doi: 10.5194/tc-9-37-2015, 2015.

Kilic, L., Tonboe, R. T., Prigent, C., and Heygster, G.: Estimating the snow depth, the snow-ice interface temperature, and the effective temperature of Arctic sea ice using Advanced Microwave Scanning Radiometer 2 and ice mass balance buoy data, The Cryosphere, 13, 1283–1296, doi: 10.5194/tc-13-1283-2019, 2019.

Kurtz, N. T., and Farrell, S. L.: Large-scale surveys of snow depth on Arctic sea ice from Operation IceBridge, Geophys. Res. Lett., 38, L20505, doi:10.1029/2011GL049216, 2011.

Kurtz, N. T., Farrell, S. L., Studinger, M., Galin, N., Harbeck, J. P., Lindsay, R., Onana, V. D., Panzer, B., and Sonntag, J. G.: Sea ice thickness, freeboard, and snow depth products from Operation IceBridge airborne data, The Cryosphere, 7, 1035–1056., doi: 10.5194/tc-7-1035-2013, 2013.

Kurtz, N. T., Galin, N., and Studinger, M.: An improved CryoSat-2 sea ice freeboard retrieval algorithm through the use of waveform fitting, The Cryosphere, 8, 1217–1237, doi: 10.5194/tc-8-1217-2014, 2014.

Kurtz, N. and Harbeck, J.: CryoSat-2 Level-4 Sea Ice Elevation, Freeboard, and Thickness, Version 1, Boulder, Colorado USA. NASA National Snow and Ice Data Center Distributed Active Archive Center, doi: 10.5067/96JO0KIFDAS8, 2017.

Kurtz, N., M. Studinger, J. Harbeck, V. Onana, and D. Yi.: IceBridge L4 Sea Ice Freeboard, Snow Depth, and Thickness, Version 1, Boulder, Colorado USA. NASA National Snow and Ice Data Center, doi: 10.5067/G519SHCKWQV6, 2015.

Kwok, R., and Cunningham, G. F.: Variability of Arctic sea ice thickness and volume from CryoSat-2, Phil. Trans. R. Soc. A, 373(2045), 20140157, doi: 10.1098/rsta.2014.0157, 2015.

Kwok, R., and Markus, T.: Potential basin-scale estimates of Arctic snow depth with sea ice freeboards from CryoSat-2 and ICESat-2: An exploratory analysis, Adv. Space Res., 62(6), 1243–1250, doi: 10.1016/j.asr.2017.09.007, 2018.

Kwok, R., Cunningham, G. F., Wensnahan, M., Rigor, I., Zwally, H. J., and Yi, D.: Thinning and volume loss of the Arctic Ocean sea ice cover: 2003–2008, J. Geophys. Res.-Oceans, 114(C7), C07005, doi: 10.1029/2009JC005312, 2009.

Lawrence, I. R., Tsamados, M. C., Stroeve, J. C., Armitage, T. W. K., and Ridout, A. L.: Estimating snow depth over Arctic sea ice from calibrated dual-frequency radar freeboards, The Cryosphere, 12, 3551–3564, doi:10.5194/tc-12-3551-2018, 2018.

Laxon, S., Peacock, N., and Smith, D.: High interannual variablility of sea ice thickness in the Arctic region, Nature, 425, 947–950, doi: 10.1038/nature02050, 2003.

Laxon, S. W., Giles, K. A., Ridout, A. L., Wingham, D. J., Willatt, R., Cullen, R., Kwok, R., Schweiger, A., Zhang, J., Haas, C., Hendricks, S., Krishfield, R., Kurtz, N., Farrell, S., and Davidson, M.: CryoSat-2 estimates of Arctic sea ice thickness and volume, Geophys. Res. Lett., 40, 732– 737, doi: 10.1002/grl.50193, 2013.

Lee, S.-M., Sohn, B.-J., and Kummerow, C. D.: Long-term Arctic snow/ice interface temperature from special sensor for Microwave imager measurements, Remote Sens., 10(11), 1795, doi: 10.3390/rs10111795, 2018.

Maaß, N., Kaleschke, L., Tian-Kunze, X., and Drusch, M.: Snow thickness retrieval over thick Arctic sea ice using SMOS satellite data, The Cryosphere, 7(6), 1971–1989, doi: 10.5194/tc-7-1971-2013, 2013.

Mallett, R. D. C., Lawrence, I. R., Stroeve, J. C., Landy, J. C., and Tsamados, M.: Brief communication: Conventional assumptions involving the speed of radar waves in snow introduce systematic underestimates to sea ice thickness and seasonal growth rate estimates, The Cryosphere, 14, 251-260, doi: 10.5194/tc-14-251-2020, 2020.

Markus, T. and Cavalieri, D. J.: Snow depth distribution over sea ice in the Southern Ocean from satellite passive microwave data, Antarct. Res. Ser., 74, 19–39, 1998.

Markus, T., Neumann, T., Martino, A., Abdalati, W., Brunt, K., Csatho, B., Farrell, S., Fricker, H., Gardner, A., Harding, D., Jasinski, M., Kwok, R., Magruder, L., Lubin, D., Luthcke, S., Morison, J., Nelson, R., Neuenschwander, A., Stephen, P., Popescu, S., Shum, CK, Schutz, B. E., Smith, B., Yang. Y., Zwally, J.: The Ice, Cloud, and land Elevation Satellite-2 (ICESat-2): Science requirements, concept, and implementation, Remote Sens. Environ, 190, 260–273, doi: 10.1016/j.rse.2016.12.029, 2017.

Maykut, G. A., and Untersteiner, N.: Some results from a time-dependent thermodynamic model of sea ice, J. Geophys. Res., 76(6), 1550–1575, doi: 10.1029/JC076i006p01550, 1971.

Nandan, V., Geldsetzer, T., Yackel, J., Mahmud, M., Scharien, R., Howell, S., King, J., Ricker, R., and Else, B.: Effect of Snow Salinity on CryoSat-2 Arctic First-Year Sea Ice Freeboard Measurements, Geophys. Res. Lett., 44(20), 10,419–10,426, doi:10.1002/2017GL074506, 2017.

Perovich, D., Richter-Menge, J., and Polashenski, C.: Observing and understanding climate change: Monitoring the mass balance, motion, and thickness of Arctic sea ice, CRREL-Dartmouth mass balance buoy program, http://imb-crrel-dartmouth.org, 2019.

Perovich, D., Richter-Menge, J., Tucker, W., Elder, B., and Bosworth, B.: Snow and Ice Temperature Profiles. Version 1.0. UCAR/NCAR - Earth Observing Laboratory, doi:10.5065/D6KS6PZ7, 2007.

~~Petty, A. A., Webster, M., Boisvert, J., and Markus, T.: The NASA Eulerian Snow On Sea Ice Model (NESOSIM) v1.0: initial model development and analysis, Geosci. Model Dev., 11(11), 4577–4602, doi: 10.5194/gmd-11-4577-2018, 2018.~~

Pringle, D. J., Trodahl, H. J., and Haskell, T. G.: Direct measurement of sea ice thermal conductivity: no surface reduction, J. Geophys. Res.-Oceans, 111(C5), C05020, doi: 10.1029/2005JC002990, 2006.

Ricker, R., Hendricks, S., Helm, V., Skourup, H., and Davidson, M.: Sensitivity of CryoSat-2 Arctic sea-ice freeboard and thickness on radar-waveform interpretation, The Cryosphere, 8, 1607–1622, doi: 10.5194/tc-8-1607-2014, 2014.

Rostosky, P., Spreen, G., Farrell, S. L., Frost, T., Heygster, G., and Melsheimer, C.: Snow depth retrieval on Arctic sea ice from passive microwave radiometers – improvements and extensions to multiyear ice using lower frequencies, J. Geophys. Res.-Oceans, 123(10), 7120–7138, doi: 10.1029/2018JC014028, 2018.

Sturm, M., Holmgren, J., König, M., and Morris, K.: The thermal conductivity of seasonal snow, J. Glaciol., 43(143), 26–41, doi: 10.3189/S0022143000002781, 1997.

Sturm, M., Perovich, D. K., and Holmgren, J.: Thermal conductivity and heat transfer through the snow on the ice of the Beaufort Sea, J. Geophys. Res., 107(C21), 8043, doi: 10.1029/2000JC000409, 2002.

Tilling, R. L., Ridout, A., and Shepherd, A.: Estimating Arctic sea ice thickness and volume using CryoSat-2 radar altimeter data, Adv. Space Res., 62, 1203–1225, doi: 10.1016/j.asr.2017.10.051, 2018.

Tiuri, M., A. Sihvola, E. Nyfors, and M. Hallikainen, The complex dielectric constant of snow at microwave frequencies, IEEE J. Ocean. Eng., 9, 377–382, 1984.

Tonboe, R. T., Pedersen, L. T., Haas, C.: Simulation of the CryoSat-2 satellite radar altimeter sea ice thickness retrieval uncertainty, Can. J. Remote Sens., 36(1), 55–67, doi: 10.5589/m10-027, 2010.

Trodahl, H. J., Wilkinson, S. O. F., McGuinness, M. J., and Haskell, T. G.: Thermal conductivity of sea ice; dependence on temperature and depth, Geophys. Res. Lett., 28(7), 1279–1282, doi: 10.1029/2000GL012088, 2001.

Ulaby, F. T., Moore, R. K., and Fung, A. K.: Microwave remote sensing: Active and passive, Volume 3 - From theory to applications, 1986.

Warren, S. G., Rigor, I. G., Untersteiner, N., Radionov, V. F., Bryazgin, N. N., Aleksandrov, Y. I., and Colony, R.: Snow depth on Arctic sea ice, J. Climate, 12(6), 1814–1829, doi: 10.1175/1520-0442(1999)012<1814:SDOASI>2.0.CO;2, 1999.

Webster, M. A., Rigor, I. G., Nghiem, S. V., Kurtz, N. T., Farrell, S. L., Perovich, D. K., and Sturm, M.: Interdecadal changes in snow depth on Arctic sea ice, J. Geophys. Res.-Oceans, 119(8), 5395–5406, doi: 10.1002/2014JC009985, 2014.

Wingham, D. J., Francis, C. R., Baker, S., Bouzinac, C., Brockley, D., Cullen, R., Chateau-Thierry, P., Laxon, S. W., Mallow, U., Mavrocordatos, C., Phalippou, L., Ratier, G., Rey, L., Rostan, F., Viau, P., and Wallis, D. W.: CryoSat: a mission to determine the fluctuations in Earth's land and marine ice fields, Adv. Space Res., 37(4), 841–871, doi: 10.1016/j.asr.2005.07.027, 2006.

Willatt, R., Laxon, S., Giles, K., Cullen, R., Haas, C., and Helm, V.: Ku-band radar penetration into snow cover on Arctic sea ice using airborne data, Ann. Glaciol., 52, 197–205, doi:10.3189/172756411795931589, 2011.

Zhou, L., Xu, S., Liu, J., and Wang, B.: On the retrieval of sea ice thickness and snow depth using concurrent laser altimetry and L-band remote sensing data~~.~~, The Cryosphere, 12(3), 993–1012, doi: 10.5194/tc-12-993-2018, 2018.

Zwally, H. J., Schutz, B., Abdalati, W., Abshire, J., Bentley, C., Brenner, A., Bufton, J., Dezio, J., Hancock, D., Harding, D., Herring, T., Minster, B., Quinn, K., Palm, S., Spinhirne, J., and Thomas, R.: ICESat's laser measurements of polar ice, atmosphere, ocean, and land, J. Geodyn., 34, 405–445, doi: 10.1016/S0264-3707(02)00042-X, 2002.

Zygmuntowska, M., Rampal, P., Ivanova, N., and Smedsrud, L. H.: Uncertainties in Arctic sea ice thickness and volume: new estimates and implications for trends, The Cryosphere, 8(2), 705–720, doi: 10.5194/tc-8-705-2014, 2014.

Table 1. Information on the measurement sites of buoys whose observations were used in this study.

Name		Deployment Location	Ice Type	Initial Snow Depth [m]	Initial Ice Thickness [m]
CRREL	2010F	Beaufort Sea	Multi-Year	0.25	1.97
	2011M	Central Arctic	Multi-Year	0.07	1.67
	2012G	Central Arctic	First-Year	0.16	1.41
	2013F	Beaufort Sea	Multi-Year	0.00	1.40
	2013G	Beaufort Sea	Multi-Year	0.00	1.40
	2014G	Beaufort Sea	Multi-Year	0.10	1.08
	2014I	Beaufort Sea	Multi-Year	0.23	1.32
SHEBA	Q2	Beaufort Sea	Multi-Year	0.06*	1.75*
	PIT	Beaufort Sea	Multi-Year	0.12*	2.01*
	BALT	Beaufort Sea	First Year	0.07*	1.40*
	R4	Beaufort Sea	Second-Year Ridge	0.09*	4.23*
	SEA	Beaufort Sea	Ponded Area	0.10*	1.54*

*The initial snow depth and ice thickness of the SHEBA sites are average values of all thickness gauge measurements in the corresponding site because there was one thermistor string but several thickness gauges in each measurement site

Table 2. Coefficients of the regression equation for averaging periods of 1, 7, 15, and 30 days. a_1, b_1, a_2, b_2, and x_0 are given in Eq. (~~8~~15).

Averaging Periods	a_1	b_1	a_2	b_2	x_0
1 day	0.166	0.047	0.050	0.263	1.864
7 days	0.179	0.028	0.053	0.254	1.796
15 days	0.180	0.034	0.029	0.339	2.022
30 days	0.185	0.022	0.076	0.214	1.769

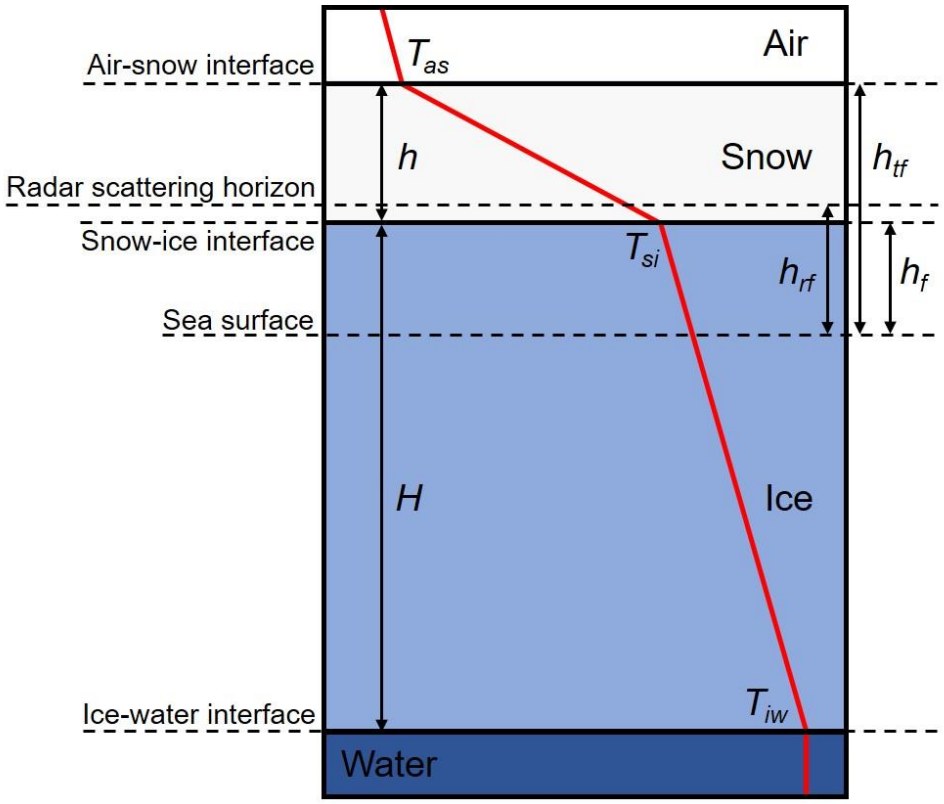

690

695 **Table B1.** The physical state of typical cases of points A, B, and C.

Type	H_i [m]	h_s [m]	α	F_t [m]	F_r [m]
A	3.961	0.332	0.084	0.65	0.30
B	1.646	0.123	0.075	0.26	0.13
C	0.616	0.152	0.246	0.17	0.01

700

Table B2. Errors of snow depth (Δh_s) and ice thickness (ΔH_i) for snow depth to ice thickness ratio error ($\Delta\alpha$) of ±0.03.

	Total Freeboard Method		Radar Freeboard Method	
$\Delta\alpha$	-0.03	0.03	-0.03	0.03
		Δh_s (cm)		
A	-4.070	3.161	-14.59	19.54
B	-1.913	1.471	-5.840	7.730
C	-0.045	0.039	-7.230	37.62
		ΔH_i (m)		
A	0.263	-0.204	-0.502	0.672
B	0.124	-0.095	-0.201	0.266
C	0.003	-0.003	-0.249	1.294

Table B3. Statistics of success/fail ratio α retrieval for 2011-2015 winter.

Year Month	Total Pixels (SIC > 95%)	Success		Fail ($T_{as} > T_{si}$)		Fail ($\alpha > \alpha_{crit}$)	
2010 12	13879	12080	(87.04%)	1799	(12.96%)	0	(0.00%)
2011 01	16246	14004	(86.20%)	2242	(13.80%)	0	(0.00%)
2011 02	17986	14779	(82.17%)	3206	(17.82%)	1	(0.01%)
2011 03	17610	12871	(73.09%)	4738	(26.91%)	1	(0.01%)
2011 12	13915	11405	(81.96%)	2510	(18.04%)	0	(0.00%)
2012 01	16812	13765	(81.88%)	3047	(18.12%)	0	(0.00%)
2012 02	17528	14131	(80.62%)	3397	(19.38%)	0	(0.00%)
2012 03	18741	13586	(72.49%)	5155	(27.51%)	0	(0.00%)
2012 12	14059	11144	(79.27%)	2915	(20.73%)	0	(0.00%)
2013 01	16413	13510	(82.31%)	2903	(17.69%)	0	(0.00%)
2013 02	18640	15526	(83.29%)	3114	(16.71%)	0	(0.00%)
2013 03	19078	14134	(74.09%)	4944	(25.91%)	0	(0.00%)
2013 12	14515	12071	(83.16%)	2444	(16.84%)	0	(0.00%)
2014 01	16880	14201	(84.13%)	2678	(15.86%)	1	(0.01%)
2014 02	16987	14731	(86.72%)	2247	(13.23%)	9	(0.05%)
2014 03	17699	13300	(75.15%)	4391	(24.81%)	8	(0.05%)
2014 12	14071	11119	(79.02%)	2952	(20.98%)	0	(0.00%)
2015 01	17008	15095	(88.75%)	1913	(11.25%)	0	(0.00%)
2015 02	18076	15907	(88.00%)	2169	(12.00%)	0	(0.00%)
2015 03	17618	14042	(79.70%)	3576	(20.30%)	0	(0.00%)
December	70439	57819	(82.08%)	12620	(17.92%)	0	(0.00%)
January	83359	70575	(84.66%)	12783	(15.33%)	1	(0.00%)
February	89217	75074	(84.15%)	14133	(15.84%)	10	(0.01%)
March	90746	67933	(74.86%)	22804	(25.13%)	9	(0.01%)

α_{crit}=0.291 for ρ_s=320 kg m^{-3}, ρ_i=915 kg m^{-3}, ρ_w=1024 kg m^{-3}, and f=0.84.

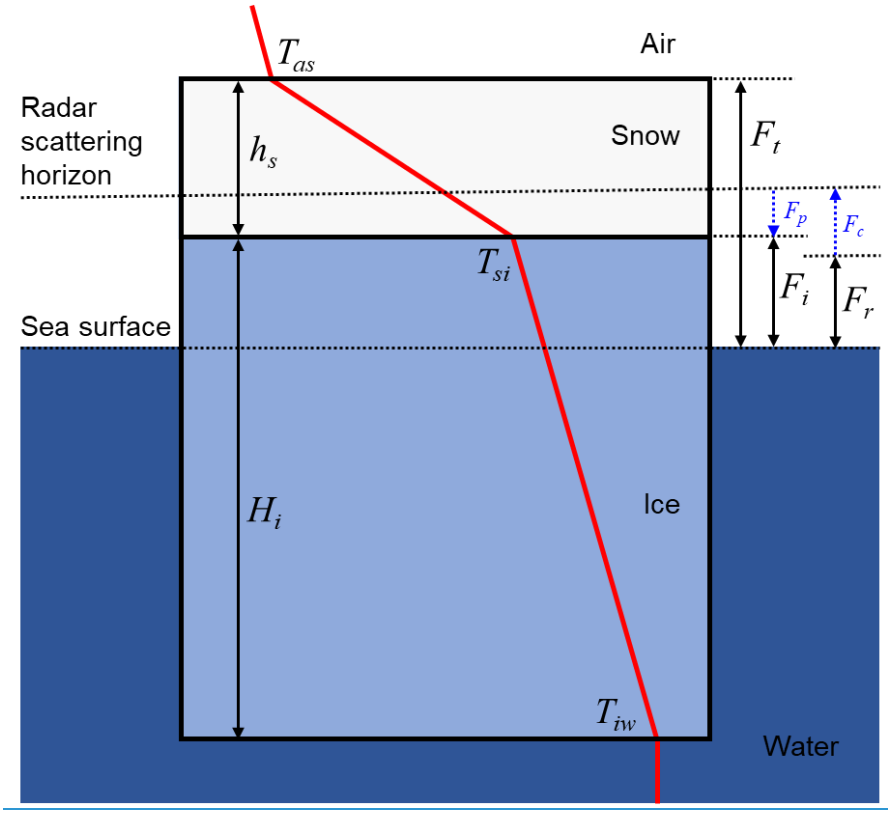

Figure 1. Schematic diagram of a typical snow–ice system during the winter. Snow depth (~~h~~h_s), ice thickness (~~H~~H_i), total freeboard (~~h_f~~F_t), radar freeboard (~~h_r~~F_r), and ice freeboard (~~h_f~~F_i) are indicated. Correction terms regarding the wave propagation speed change in snow layer (F_c) and the displacement of the scattering horizon from the ice surface (F_p) are indicated by blue arrows. The red line denotes a typical temperature profile with air–snow interface temperature (T_{as}), snow–ice interface temperature (T_{si}~~)~~), and ice–water interface temperature (T_{iw}).

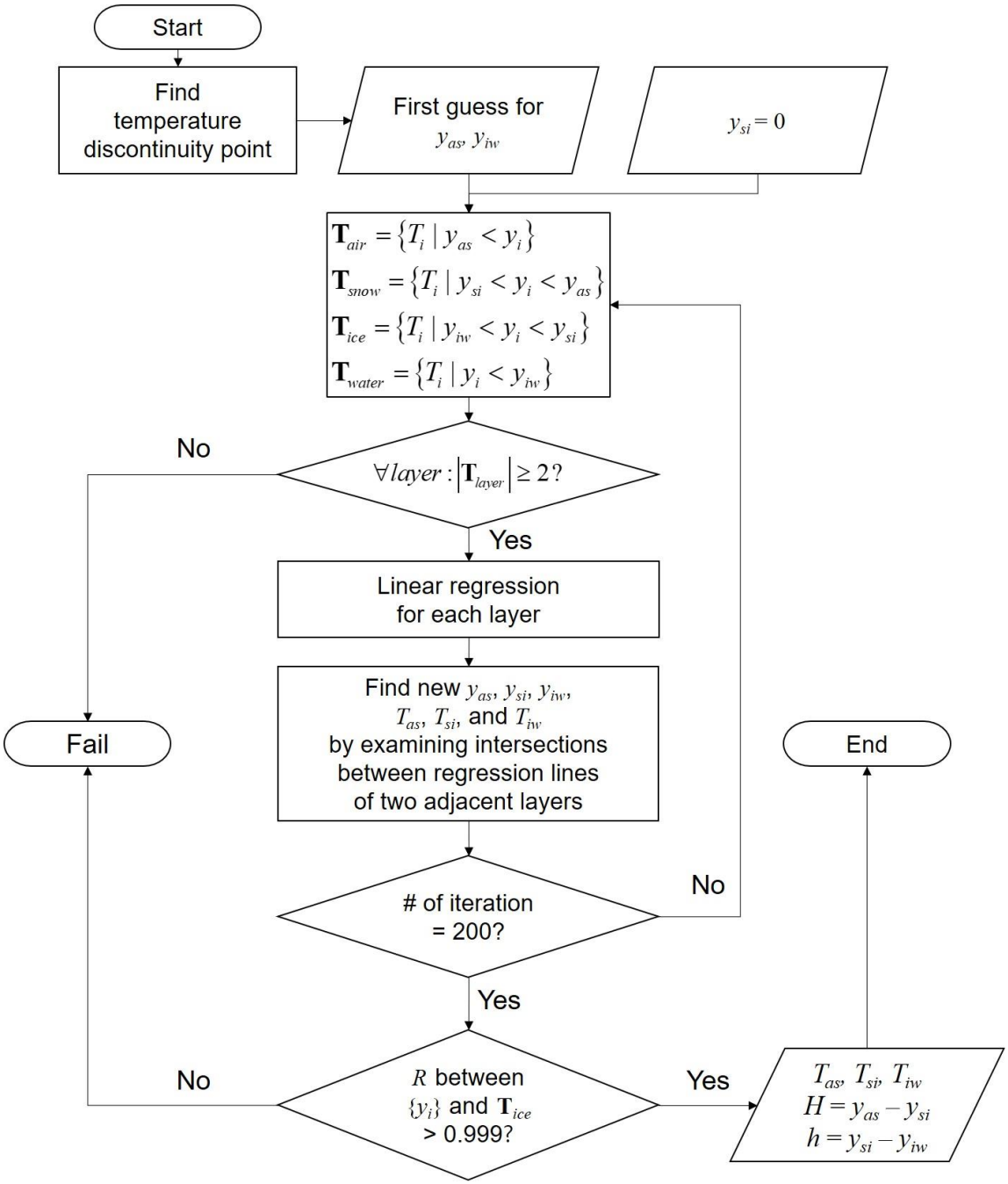
Start
Find temperature discontinuity point
First guess for y_{as}, y_{iw}
$y_{si} = 0$
$\mathbf{T}_{air} = \{T_i \mid y_{as} < y_i\}$
$\mathbf{T}_{snow} = \{T_i \mid y_{si} < y_i < y_{as}\}$
$\mathbf{T}_{ice} = \{T_i \mid y_{iw} < y_i < y_{si}\}$
$\mathbf{T}_{water} = \{T_i \mid y_i < y_{iw}\}$
$\forall layer : |\mathbf{T}_{layer}| \geq 2$?
No
Yes
Linear regression for each layer
Find new y_{as}, y_{si}, y_{iw}, T_{as}, T_{si}, and T_{iw} by examining intersections between regression lines of two adjacent layers
# of iteration = 200?
No
Yes
R between $\{y_i\}$ and $\mathbf{T}_{ice}$ > 0.999?
No
Yes
Fail
End
T_{as}, T_{si}, T_{iw}
$H = y_{as} - y_{si}$
$h = y_{si} - y_{iw}$

715

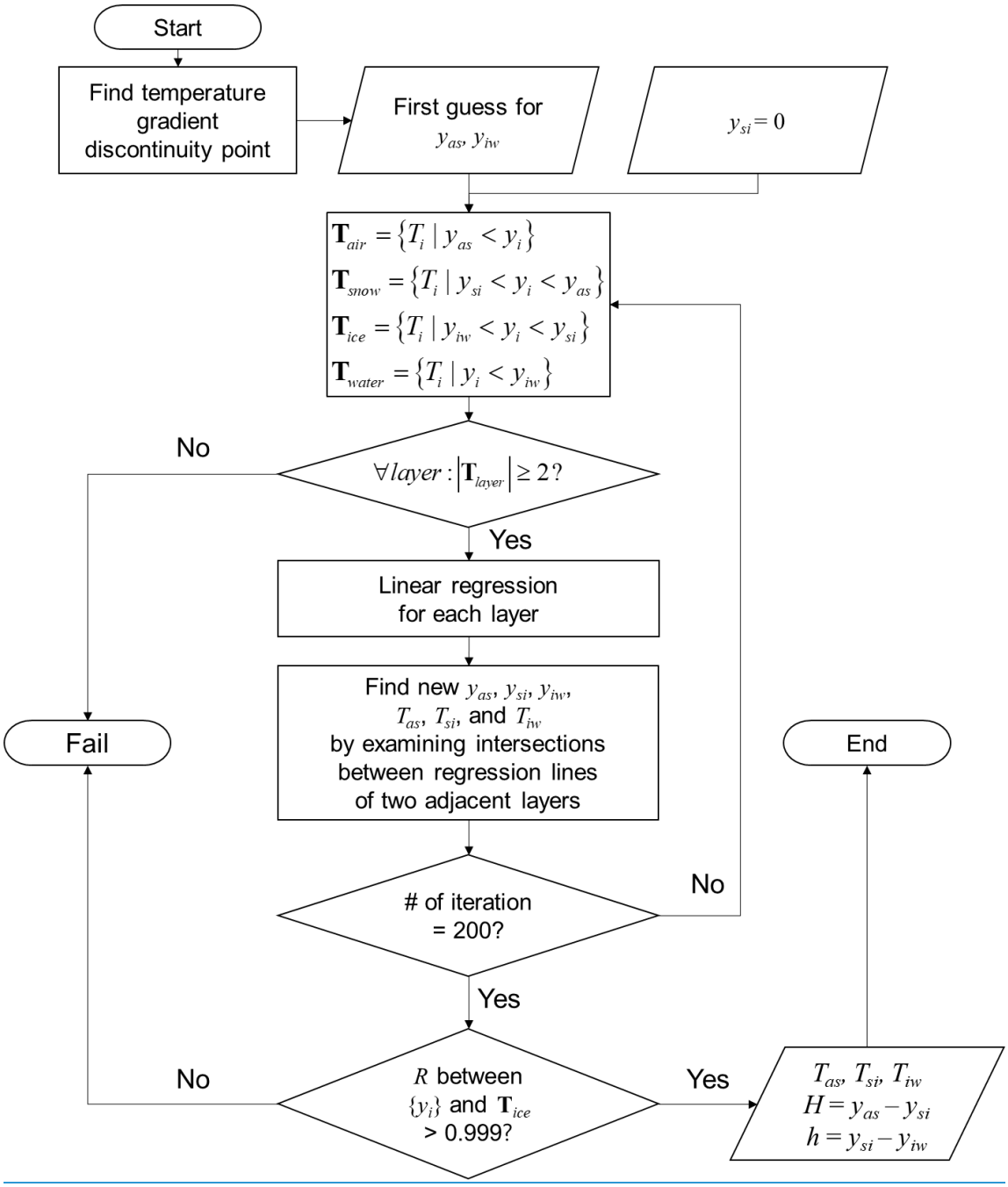

Figure 2. The flow chart of the interface searching algorithm. y_i and T_i denote the position and temperature of a data point in the temperature profile. y_{as}, y_{si}, and y_{iw} denote the position of the interfaces, and $\mathbf{T}_{layer}$ denotes a set of temperature data points.

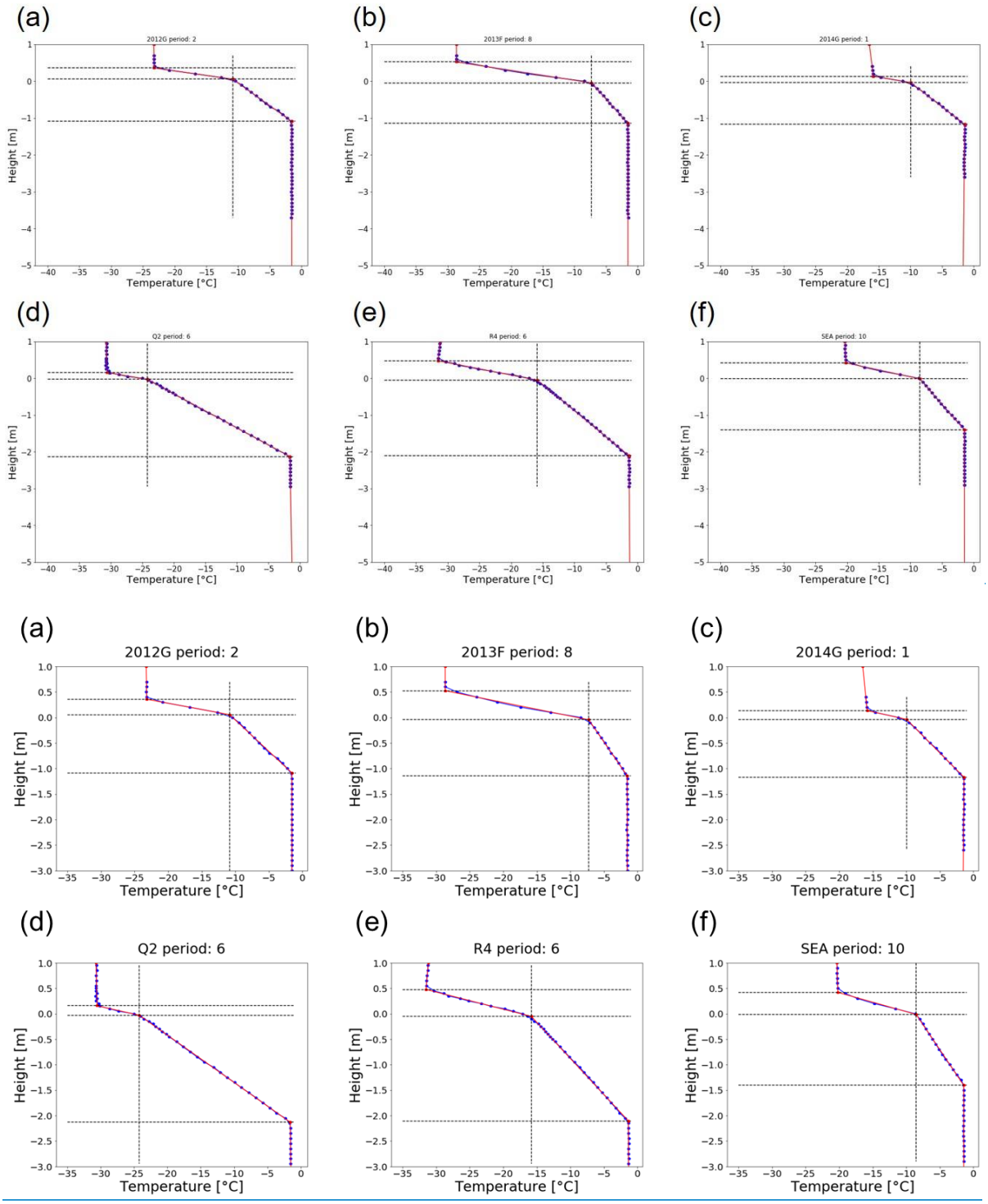

Figure 3. Examples of interface searching results with an averaging period of 15 days: (a) 2012G period 2, (b) 2013F period 8, (c) 2014G period 1, (d) Q2 period 6, (e) R4 period 6, and (f) SEA period 10. The period number is equivalent to the number of time–averaging bin.

Blue dots are buoy-measured temperature profiles and red lines are regression lines. Black dashed lines indicate the intersections between
725 adjacent regression lines.

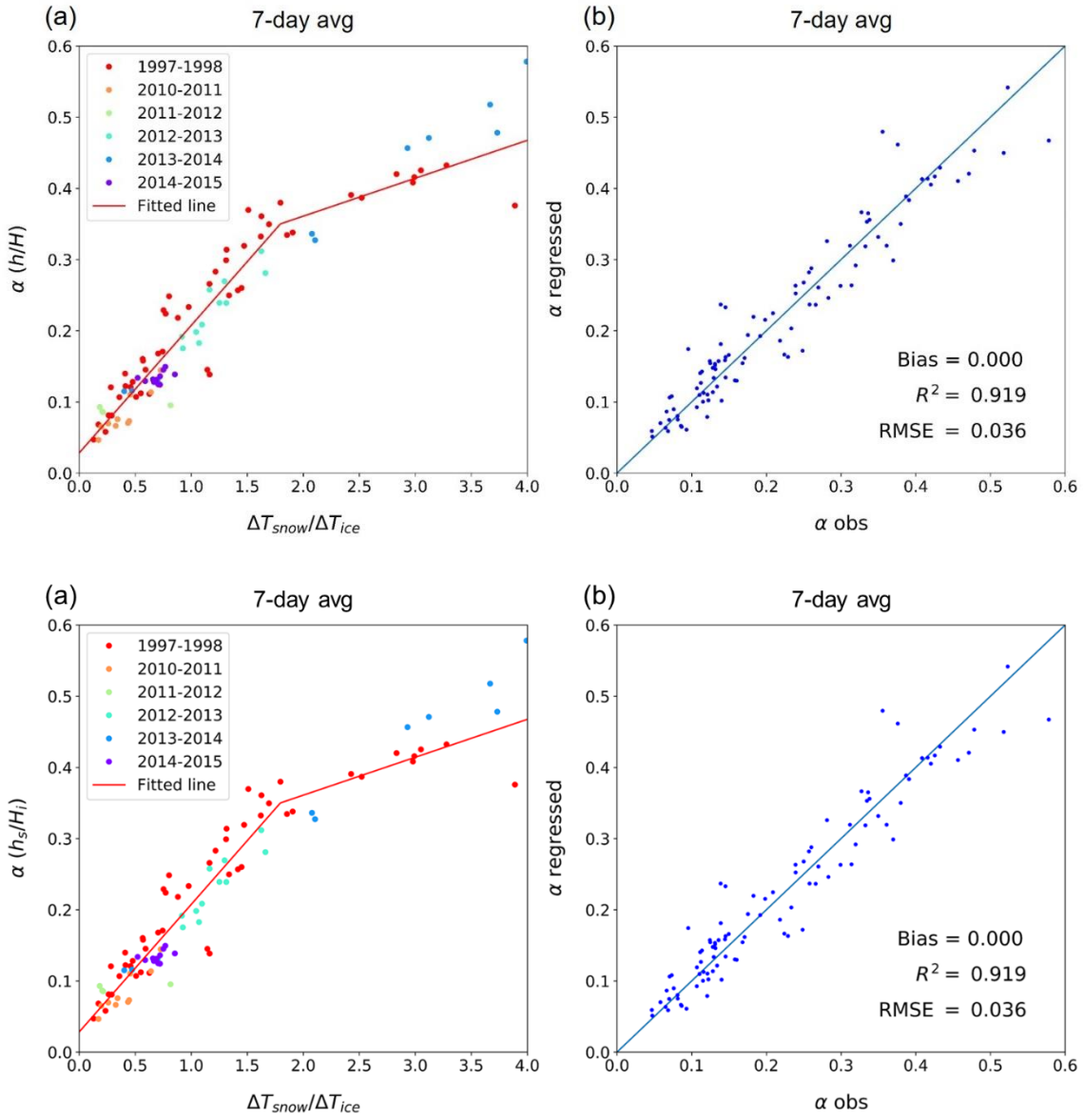

Figure 4. (a) Scatterplots of the temperature difference ratio of the snow and ice layer ($\Delta T_{snow}/\Delta T_{ice}$) and the snow–ice thickness ratio (α). Color denotes the collected year of buoy data. The red lines are the regression lines (defined in Eq. (~~8~~15)). (b) The scatter plot of observed and regressed α.

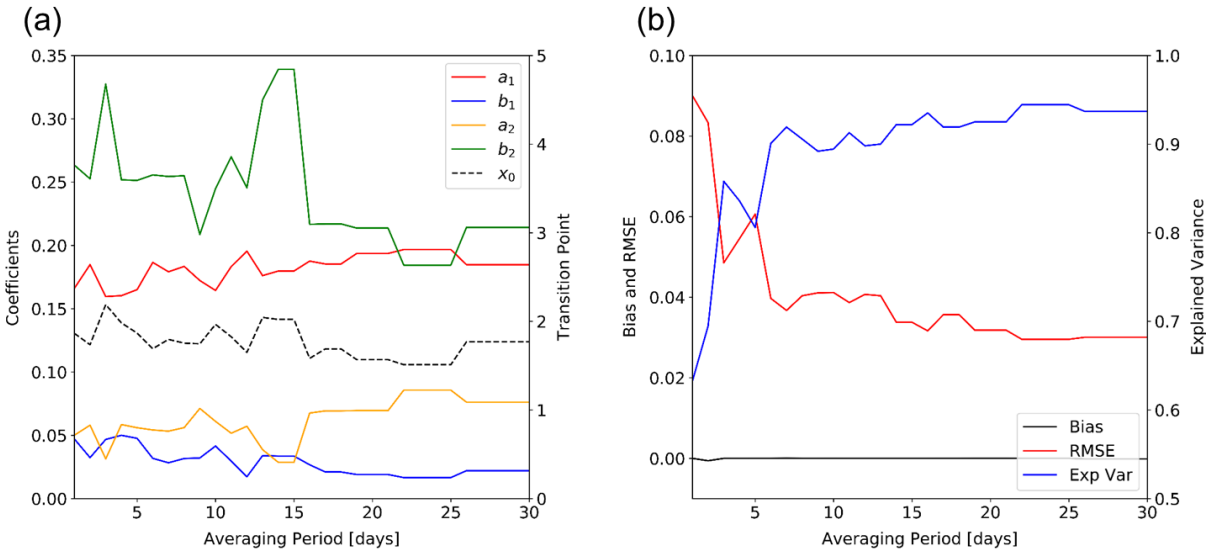

Figure 5. (a) The regression coefficients (a_1, b_1, a_2, b_2) in Eq. (~~8~~15) and (b) the error statistics of the regression with averaging periods from 1 to 30 days.

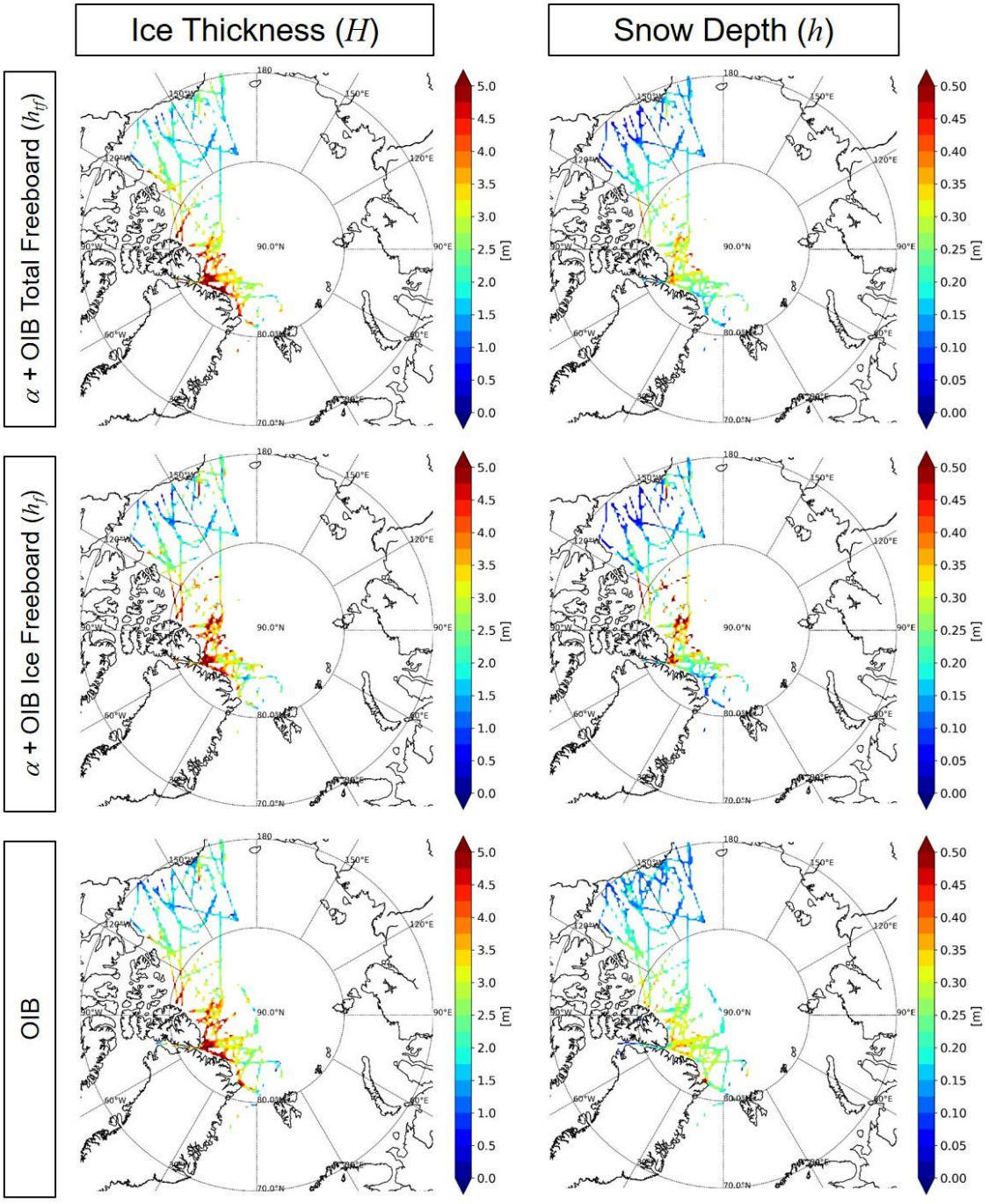
Ice Thickness (H)
Snow Depth (h)
α + OIB Total Freeboard (h_{tf})
α + OIB Ice Freeboard (h_f)
OIB
[m]

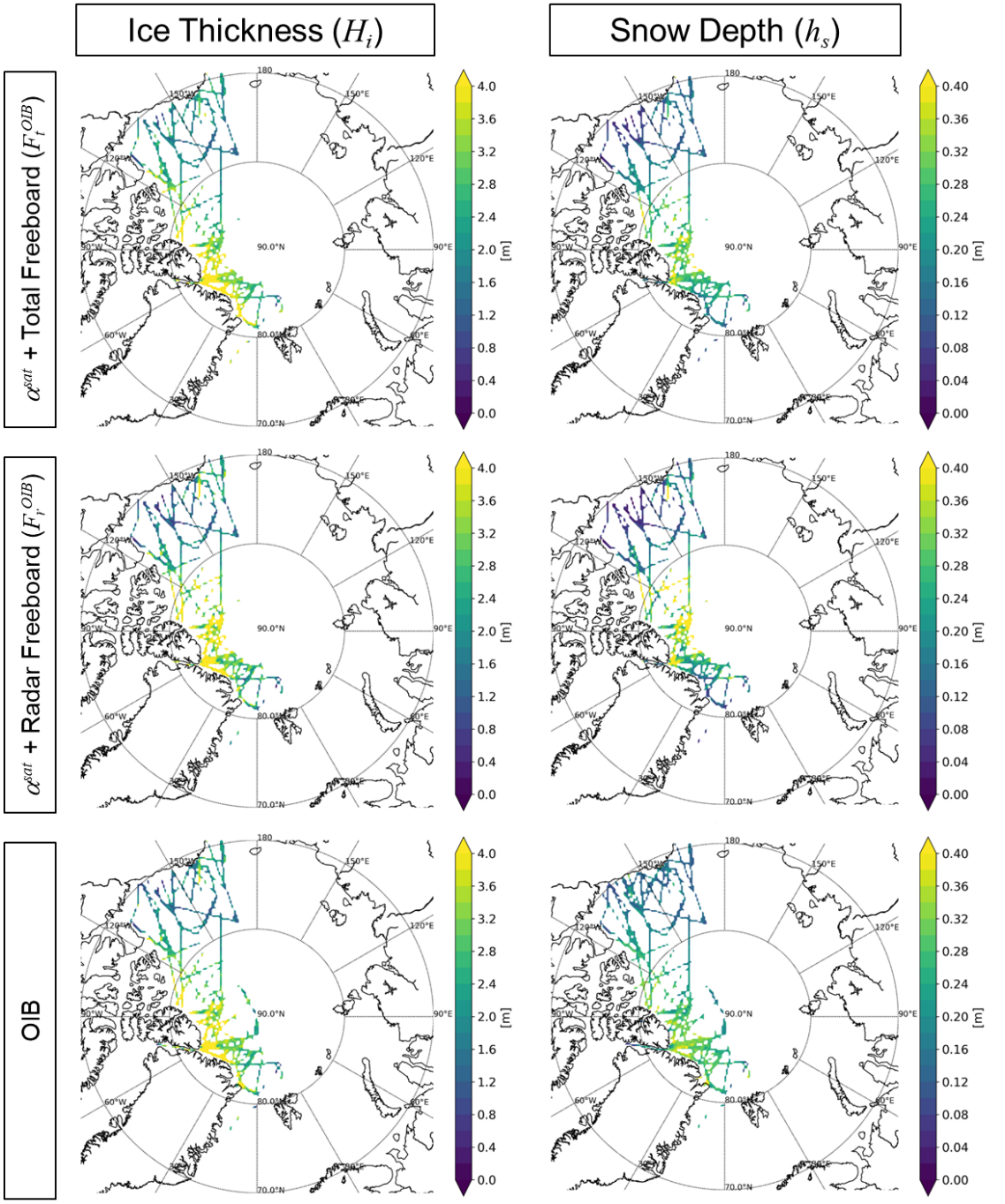

Figure 6. Simultaneously retrieved ice thickness and snow depth from OIB total/~~ice~~radar freeboard in March of the 2011–2015 period. Corresponding OIB products are at the bottom.

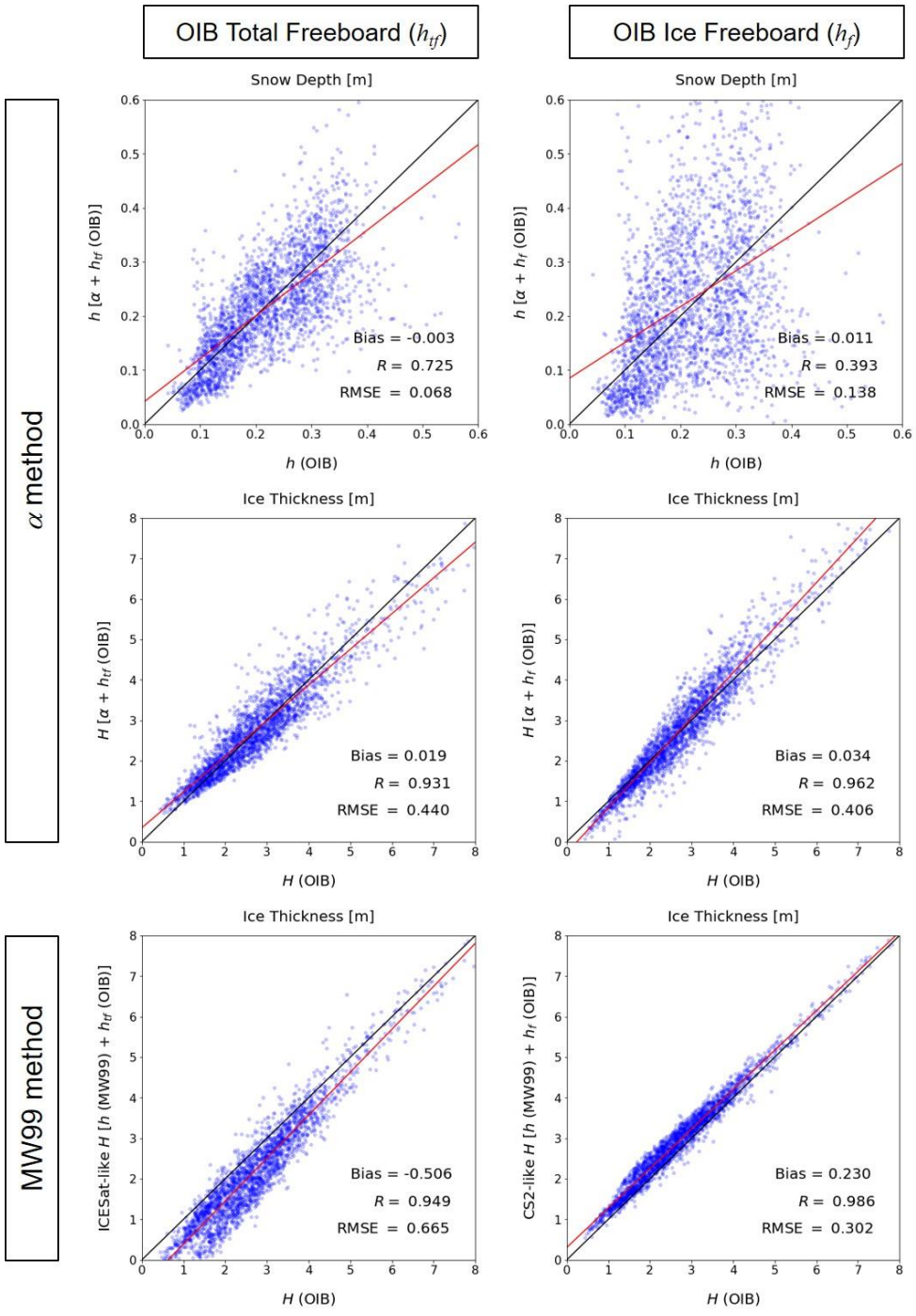
OIB Total Freeboard (h_{tf})
OIB Ice Freeboard (h_f)
α method
MW99 method
Snow Depth [m]
Ice Thickness [m]
h [α + h_{tf} (OIB)]
h [α + h_f (OIB)]
H [α + h_{tf} (OIB)]
H [α + h_f (OIB)]
ICESat-like H [h (MW99) + h_{tf} (OIB)]
CS2-like H [h (MW99) + h_f (OIB)]
h (OIB)
H (OIB)
Bias = -0.003
R = 0.725
RMSE = 0.068
Bias = 0.011
R = 0.393
RMSE = 0.138
Bias = 0.019
R = 0.931
RMSE = 0.440
Bias = 0.034
R = 0.962
RMSE = 0.406
Bias = -0.506
R = 0.949
RMSE = 0.665
Bias = 0.230
R = 0.986
RMSE = 0.302

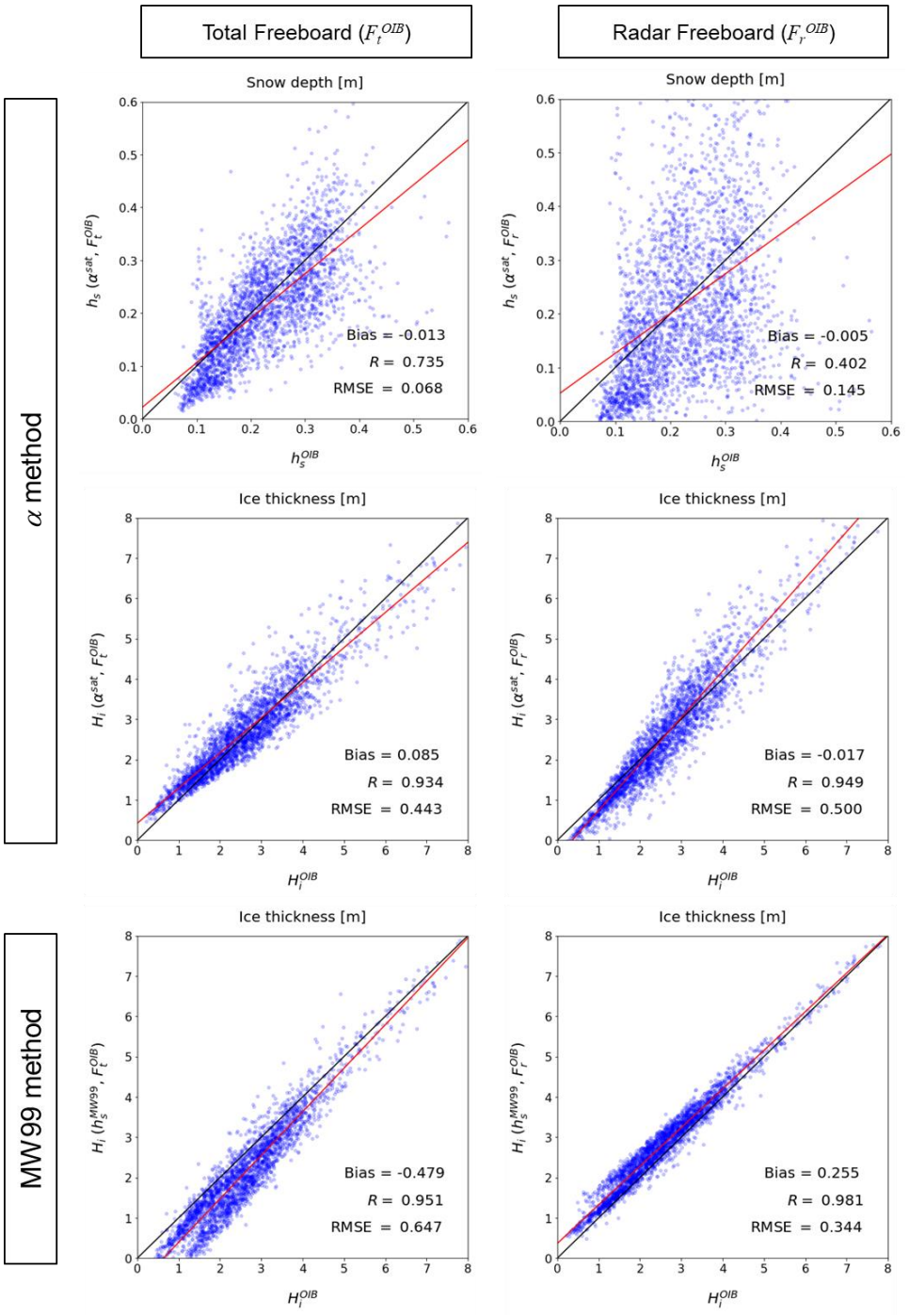

Figure 7. Scatter plots between OIB products and the simultaneously retrieved snow depth and ice thickness from OIB total/~~ice~~radar freeboards during the March 2011–2015 period. Corresponding ice thicknesses estimated from MW99 ~~snow depth~~ are in the third row. The red lines are linear regression lines.

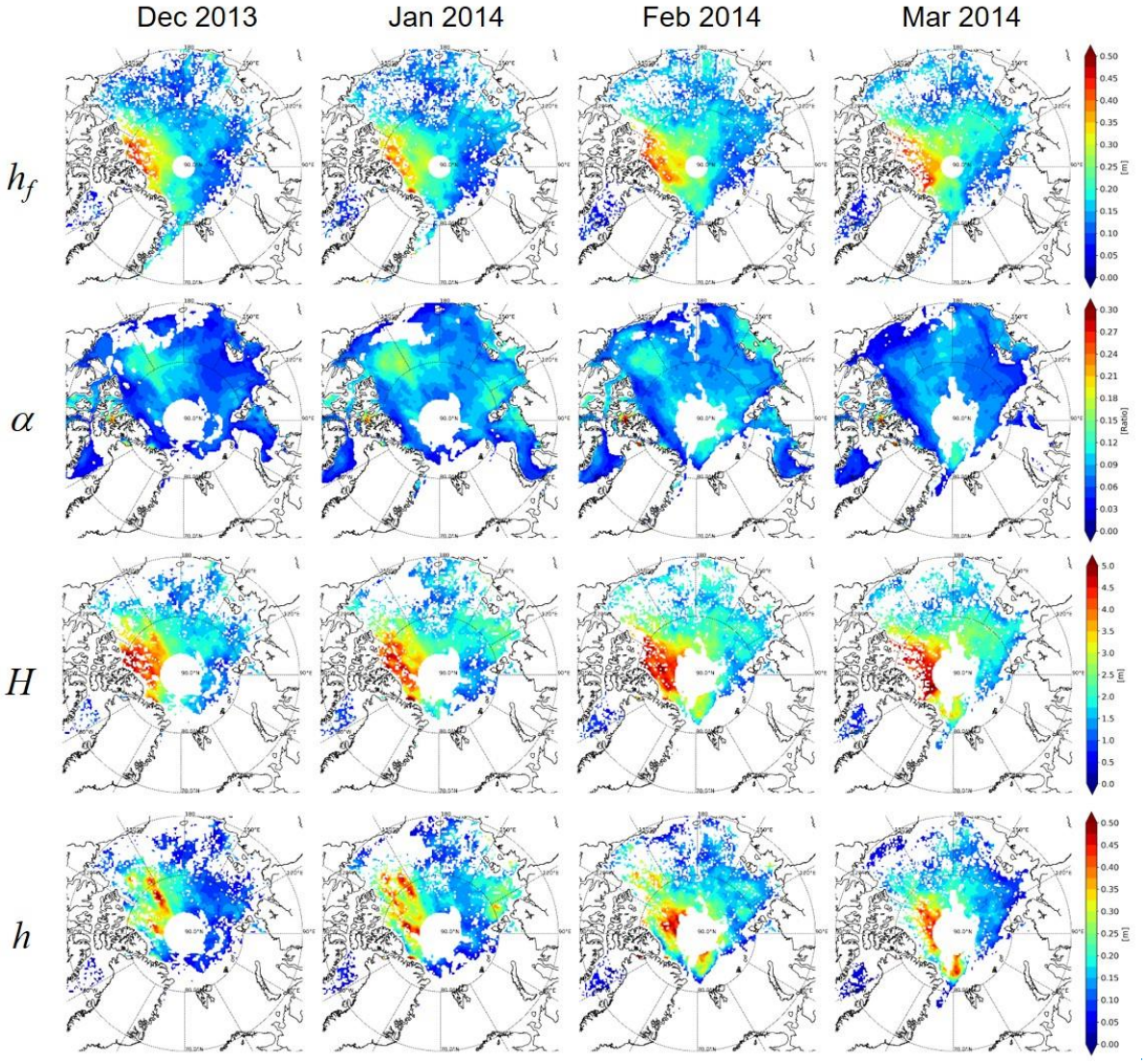
Dec 2013
Jan 2014
Feb 2014
Mar 2014
h_f
α
H
h
[m]
[Ratio]
[m]
[m]

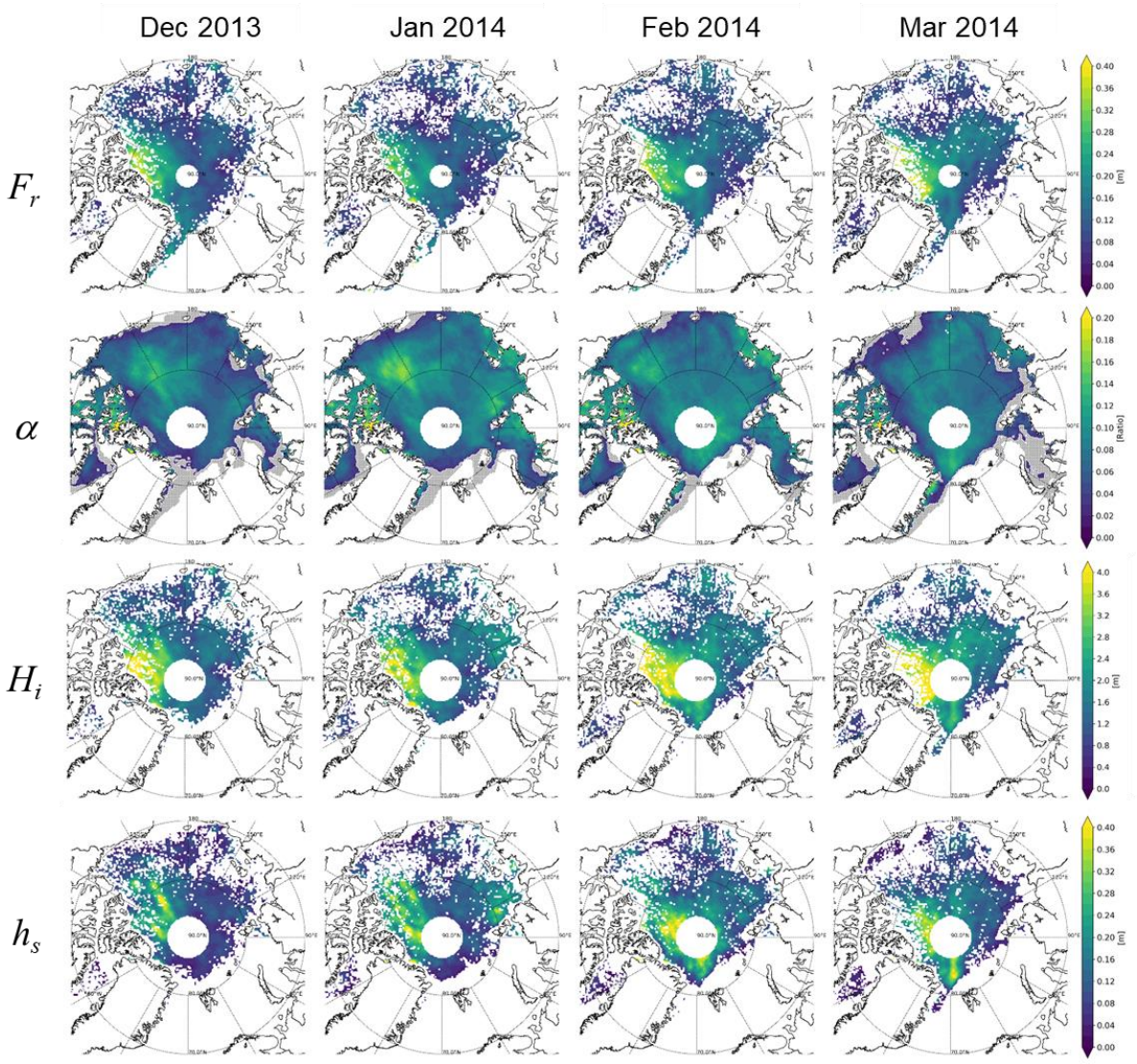

Figure 8. Geographical distributions of observed CS2 ~~ice~~radar freeboard (~~h_i~~F_r) and estimated snow–ice thickness ratio (α), ice thickness (~~H~~H_i), and snow depth (~~h~~h_s) from December 2013 to March 2014. Grey areas in the second row denote where α retrieval is failed because T_{as} is warmer than T_{as}.

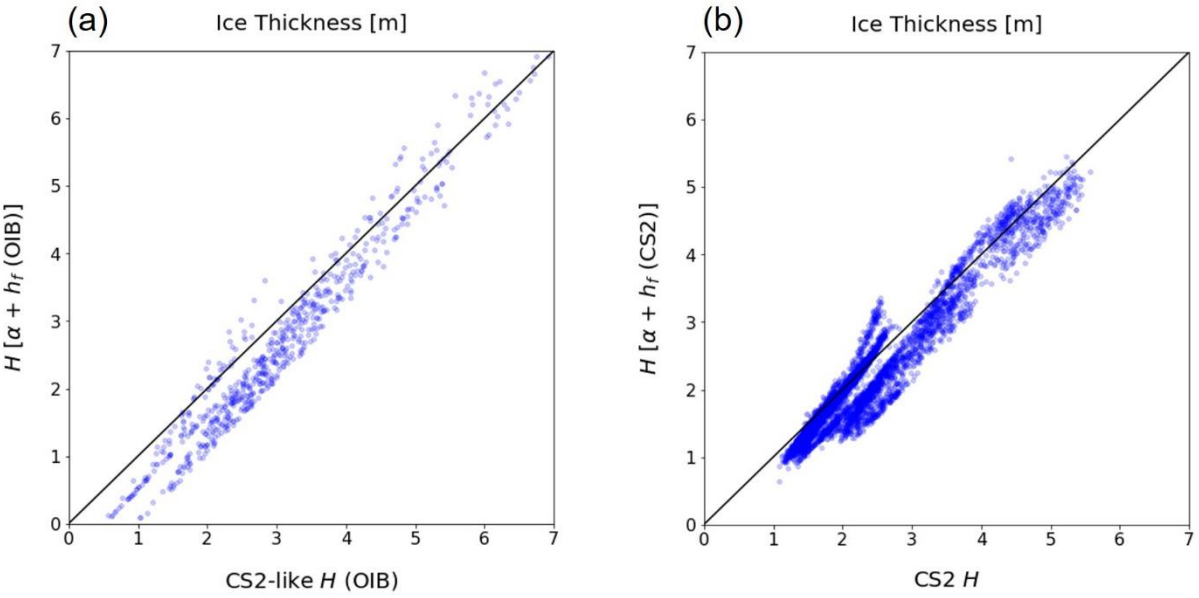
(a)
Ice Thickness [m]
H [α + h_f (OIB)]
CS2-like H (OIB)
(b)
Ice Thickness [m]
H [α + h_f (CS2)]
CS2 H

755

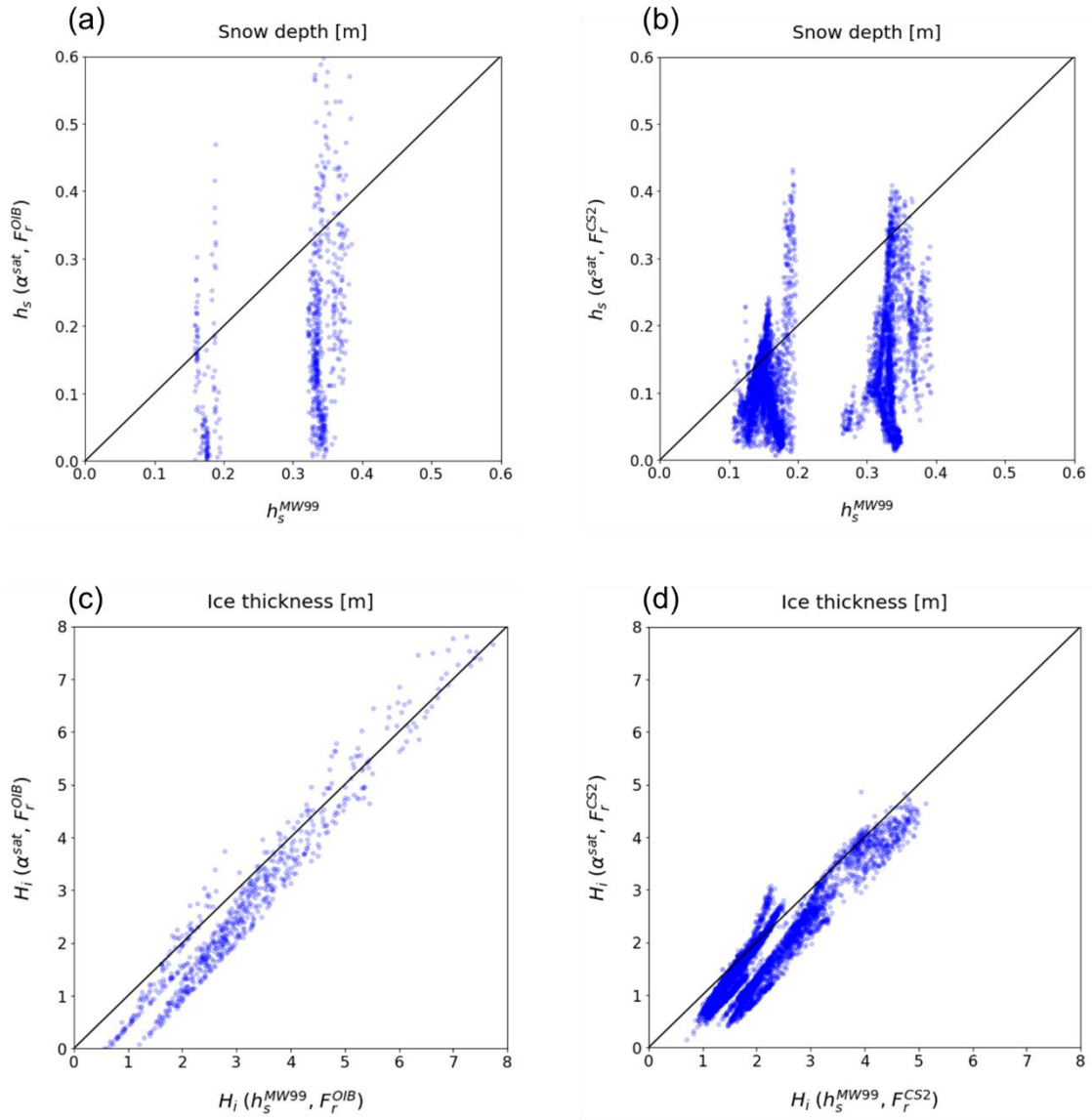

Figure 9. Comparison of simultaneous retrieved snow depth and ice thickness ~~between~~to those from the MW99 method ~~and the α method using.~~ (a) Snow depth from OIB ~~ice~~radar freeboard ~~and,~~ (b) snow depth from CS2 radar freeboard ~~on March 2014. CS2-like H (OIB) denotes the,~~ (c) ice thickness ~~estimated~~ from ~~the MW99 snow depth and~~ OIB ~~ice~~radar freeboard~~.~~, and (d) ice thickness from CS2 radar freeboard.

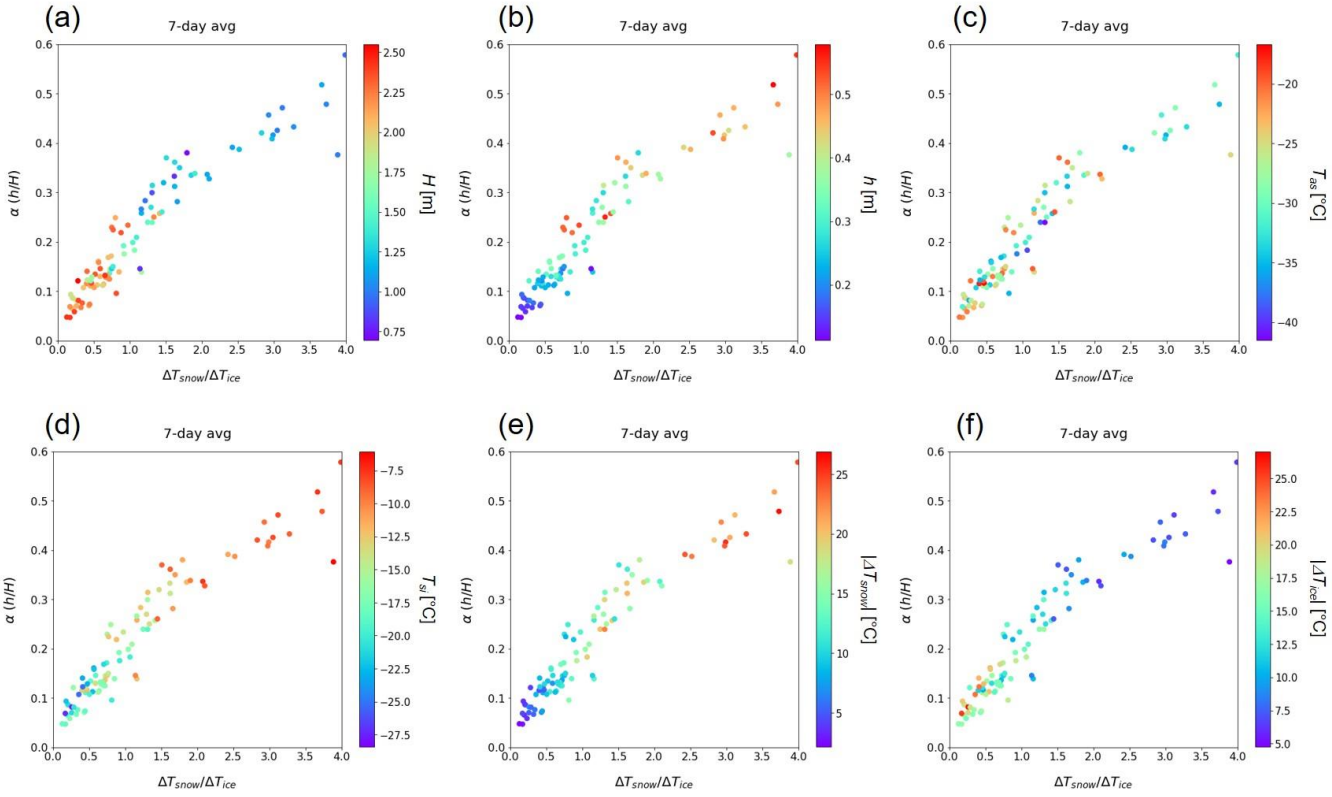
(a)
7-day avg
α (h/H)
ΔT_snow/ΔT_ice
H [m]
(b)
7-day avg
α (h/H)
ΔT_snow/ΔT_ice
h [m]
(c)
7-day avg
α (h/H)
ΔT_snow/ΔT_ice
T_as [°C]
(d)
7-day avg
α (h/H)
ΔT_snow/ΔT_ice
T_si [°C]
(e)
7-day avg
α (h/H)
ΔT_snow/ΔT_ice
|ΔT_snow| [°C]
(f)
7-day avg
α (h/H)
ΔT_snow/ΔT_ice
|ΔT_ice| [°C]

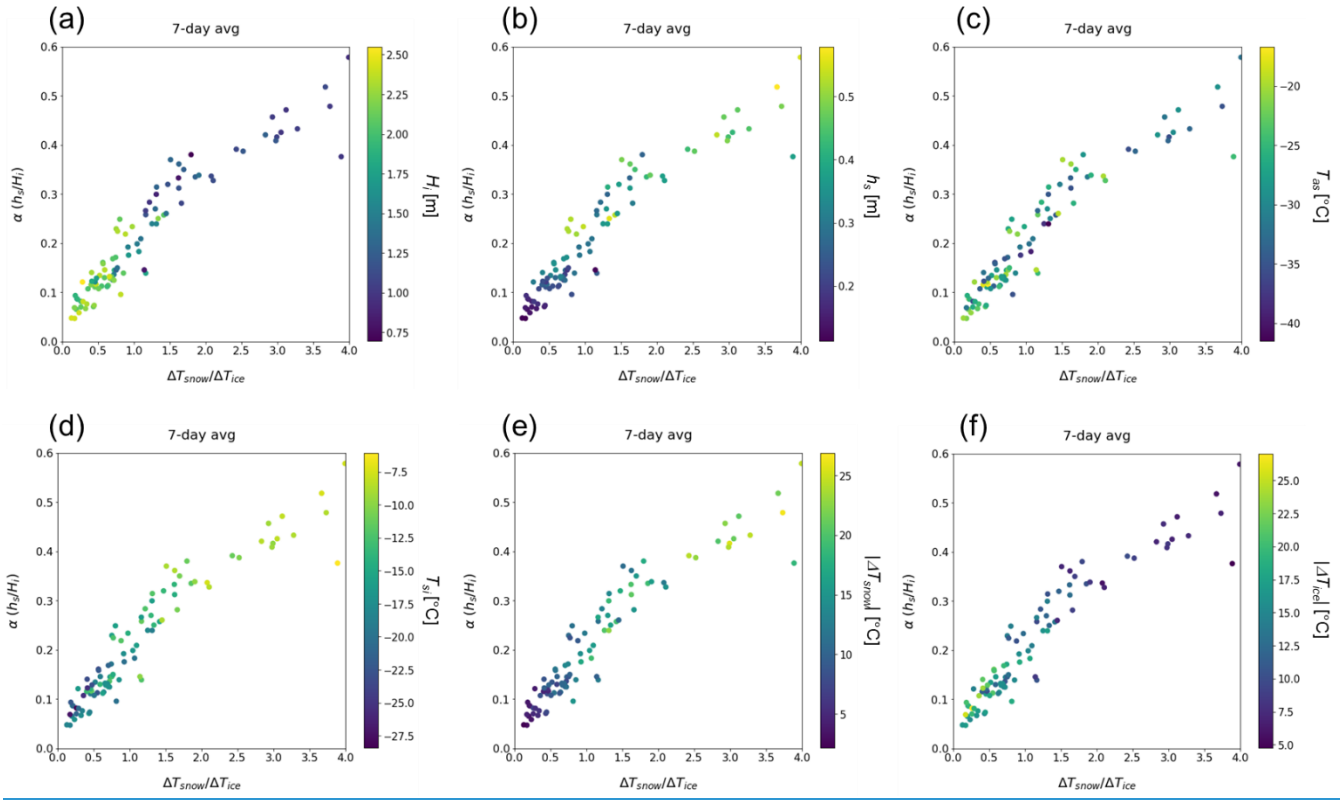

Figure A1. Distribution of physical variables on scatterplots of the temperature difference ratio of snow and ice layer ($\Delta T_{snow}/\Delta T_{ice}$) and the snow–ice thickness ratio (α). Color denotes the value of physical variables: (a) ice thickness (H), (b) snow depth (h), (c) air–snow interface temperature (T_{as}), (d) snow–ice interface temperature (T_{si}), (e) temperature difference within snow layer ($|\Delta T_{snow}|$), and (f) temperature difference within ice layer ($|\Delta T_{ice}|$).

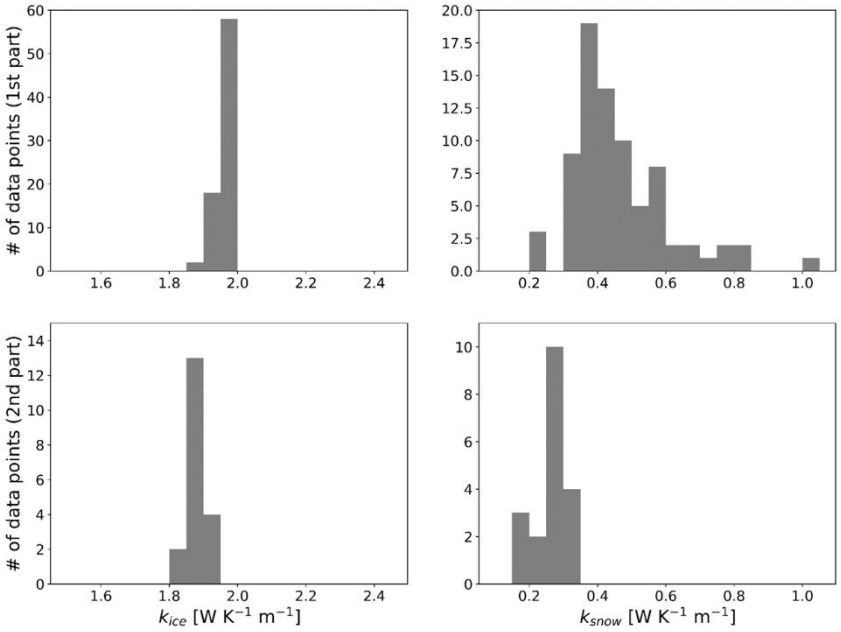

Figure A2. Histogram of estimated (left column) k_{ice} and (right column) k_{snow}. The top and bottom row denote the first and the second part, respectively. The size of the bins is 0.05 W K^{-1} m^{-1}.

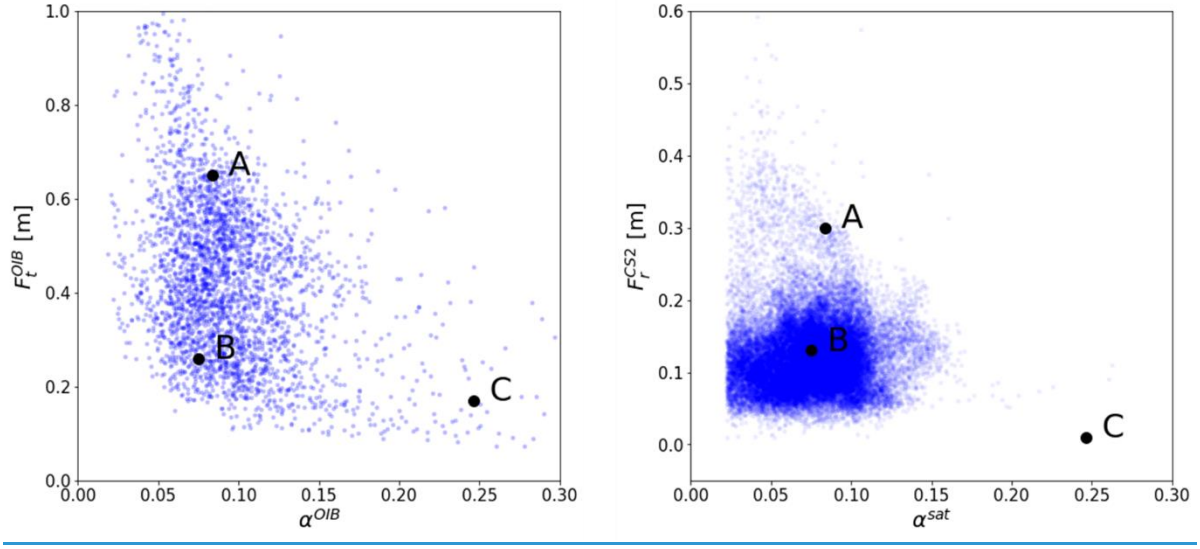

Figure B1. Locations of physical states for typical types (A, B, C) on the freeboard-thickness ratio space. Blue dots are from (left) OIB data and (right) retrieved thickness ratio and CS2 radar freeboard.

Response to Reviewer 2

General comment

The authors have done a thorough job responding to and addressing my comments. In particular, the application of the methodology to radar freeboard from CryoSat-2 has been demonstrated (I apologise for assuming it would not be possible!). The only thing outstanding is an uncertainty estimate for the CS2-derived snow depth and ice thickness. The sensitivity analysis that has been included in the appendix explores the impact $\Delta\alpha$ has on snow depth and sea ice thickness, but this alone is not sufficient to describe the uncertainty on these products since, for example, error on radar freeboard should also be accounted for. If these products are to be made available, in particular to the modelling community, they must come with an error budget.

The methodology presented in this manuscript is a novel and valuable addition to the sea ice community. I therefore recommend the paper for publication following minor revisions.

Authors appreciate Dr. Isobel R. Lawrence for providing constructive comments. This time, we included uncertainty budget analysis by conducting error propagation analysis. Please find the following point-by-point responses to the referee's comments below. A marked-up version of the revised manuscript regarding the changes is attached at the end of this authors' response.

Minor revisions

The accuracies of CS2 retrievals / Error budget

I find the final paragraph of section 4.3 (L359-369) extremely difficult to follow. Indeed, after studying Figure 9 for some ten minutes I am still at a loss as to what these plots actually tell us. If the aim is to perform a validation against OIB measurements, why not just show a scatter plot of h_s^{OIB} vs $h_s(\alpha^{sat}, F_r^{CS2})$ and H_i^{OIB} vs $H_i(\alpha^{sat}, F_r^{CS2})$? That would be a far simpler and more relevant plot which the reader will understand immediately.

Sorry for the confusion. We should have provided the reason why we did it in an indirect way. We clarify the paragraph and provide the reason.

"To assess the accuracy of CS2 retrievals, reference snow depth and ice thickness collocated with CS2 freeboard in space and time are necessary. However, different from simultaneous retrievals from OIB freeboards in Sect. 4.2, evaluation with the required matching data may not be possible from the monthly composite of CS2 data used in this study. Here, instead of using monthly collocated match-up data, an indirect way is used to examine the accuracy of CS2 retrievals. We do so by examining whether the relationship between the simultaneous method and the MW99 method, based on retrievals from the OIB freeboard, can be reproduced by CS2-based retrievals. If similar results are obtained, respective accuracies can be deduced against those noted from the evaluation against OIB measurements."

I think an uncertainty estimate for the satellite-derived products needs including in section 4.3. A simple propagation of errors could be performed on Equation 12 to estimate the error on Hi, and similarly error on h_s could then be propagated from Equation 3. For this, the uncertainty on radar freeboard and α are required. In the manuscript $\Delta\alpha$ is estimated to be 0.036, equal to the RMSE between observed and regressed α, where regressed α are derived from buoy-measured interface temperatures. Does the same $\Delta\alpha$ apply for α derived from satellite temperatures? Evidently errors in T_{si}^{sat} and T_{as}^{sat} will result in errors in α. This should at least be discussed in section 4.3, even if it is not possible to incorporate errors on T_{si}^{sat} and T_{as}^{sat} into the final uncertainty budget (if for example the satellite temperature products do not come with an uncertainty). Errors on radar freeboard should be available with the CS2 product you are using. If not, see discussion in Tilling et al (2018) for their estimate of CS2 radar freeboard uncertainty.

Your understanding is correct. The value of 0.036 is for buoy temperatures, not for satellite derived temperatures. Incorporating your comment, the difference in root mean square between α^{OIB} and α^{sat} is calculated and is used for $\Delta\alpha$. Appendix B is updated accordingly.

Then, we calculated the uncertainty budget for satellite derived α and CS2 freeboard measurements on ice thickness and snow depth by using Gaussian error propagation equation. The results are in Appendix C and referred at the end of Sect. 4.3.

In the case of ice thickness, freeboard-related uncertainty is greater than α-related uncertainty. Total uncertainty of ice thickness estimate ranges from 0.8 m to 2.0 m and total uncertainty of snow depth estimate ranges from 4 cm to 40 cm. It is noted that α-related uncertainty is greater than freeboard-related uncertainty for snow depth estimation. Both uncertainties in ice thickness and snow depth are greater for MYI region than for FYI region. It is thought that the improvement of accuracy in satellite derived temperatures can reduce the snow depth uncertainty while the improvement of freeboard accuracy can reduce the ice thickness uncertainty.

Other minor comments

L15: "retrieved ice thickness was found to be better than the methods relying on the use of snow depth climatology as input, in terms of mean bias and RMSE." - This is not true, RMSE on ice thickness from radar freeboard is smaller using the MW99 method (0.344 vs 0.5 α-method, figure 7)

The sentence is corrected by removing RMSE. Now the new sentence reads as follow.

"retrieved ice thickness was found to be better than the methods relying on the use of snow depth climatology as input, in terms of mean bias."

L68: "Other satellite remote sensing approaches include the snow depth retrieval using dual-frequency altimetry (Guerreiro et al., 2016; Lawrence et al., 2018, 70 Kwok and Markus, 2018),

multilinear regression (Kilic et al., 2019), and a neural network approach (Braakmann-Folgmann and Donlon, 2019).” – I think here you need to add something about the limitations of these methods. Otherwise it is unclear why a new snow product is necessary.

The following sentence is now added regarding limitations of those studies.

“In spite of promising results, the dual frequency altimetry method is available only for regions where two altimeters overlap with each other, reducing the great deal of spatial coverage. On the other hands, the regression/neural network methods based on AMSR-2 TBs are prone to the overfitting problem, limiting their applications to other microwave sensors.”

L170: “A sensitivity test indicated that the influence of a 0.3°C difference in the freezing temperature on α was negligible”. Could you give a percentage value or some quantification of it being negligible?

Additional information is now provided at the end of the sentence.

“… (e.g. approximately 1.2% difference for typical interface temperatures of T_{as} = -30 °C and T_{si} = -20 °C)”

L233: The Quicklook dataset URL you provide takes you to ‘Bootstrap Sea ice concentrations”. Please check the DOI. Also I suggest moving the url to the end of the sentence.

Thanks for the comment. DOI is corrected and the url has been moved to the data availability section. It is now located at the end of the sentence.

L235: “The OIB data are also reformatted into the 25 km grid format for comparison. If the location of one OIB individual data point falls within a certain 25 km grid area, then the point data is binned in a corresponding grid. After completing the grid assignment, grid value is determined by calculating a simple arithmetic mean of all data within that grid area.” – Do you just mean “the OIB data are averaged on the same 25km grid”?

The sentence is now clarified, as follows:

“The OIB data are also reformatted into the 25 km grid format by averaging pixel-level OIB observations on the 25 km grid.”

L251: I find lines 245 to 250 slightly confusing. I suggest you move the equation for η_s to after equation 14. i.e:

“[Eq 14],

where η_s = […] and ρ_s is taken from the Warren climatology, after Kurtz (2017)”

Following the comment, the equation for η_s is located after Eq. (14):

[Eq. (14)]

"Here, η_s was parameterized as a function of the snow density, i.e. $\eta_s = (1 + 1.7\rho_s + 0.7\rho_s^2)^{0.5}$ (Tiuri et al., 1984), and ρ_s is taken from the W99 climatology, after Kurtz and Harbeck (2017)."

Figure 3 caption: "The period number is equivalent to the number of time-averaging bin." – I do not understand what the period number is.

If time averaging period is 15 days, there are 10 time-averaging bins because 151 days (November 1 to March 30) are divided into 15-day increments. We sequentially numbered each time averaging bin which has a 15-day length. That number is the period number in Fig. 3 caption. The following figure for the averaging period of 15 days would help understanding.

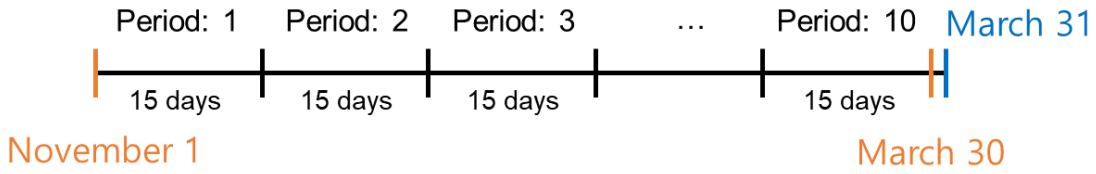

For clarification, the description is changed as follow.

"The period number indicates the sequential 15-day period from November 1 (e.g. 'period: 2' denotes a time-averaging period of November 16th to November 30th)."

Typos / Grammar

L19: "…buoyancy equation and radar penetration…" -> "…buoyancy equation or the radar penetration…"

L26: "…the height from the sea surface in cracks and leads to the snow surface." -> "…the height from the sea surface in leads, to the snow surface."

L51: "variation of snow–ice system" -> "variation of the snow–ice system"

L58: "TB's" -> "TBs"

L156: Remove "respectively"

L181: "…by multiplying the obtained sea ice thickness and α." -> "…by multiplying the obtained sea ice thickness and α (Eq. (3))."

L194 "…as parts…" -> "…as part…"

L201: "depending" -> "dependent"

Sentences are corrected following your suggestion.

L248: "In this dataset, η_s was parameterized as a function of the snow density" -> "η_s was parameterized as a function of the snow density" – The 'in this dataset' suggests to me that you mean your dataset!

Sorry for the confusion. 'in this dataset' is now removed from the sentence.

L253: "…values are used for comparison." -> "…values are used for comparison with results from our simultaneous method."

L307: "scatterplots of comparing retrievals" -> "scatterplots comparing retrievals"

L351: "shows α values that is generally larger than that over" -> "shows α values that are generally larger than those over"

L353: "H_i shows a similar geographical distribution as shown in the freeboard (the first row)" -> "H_i shows a similar geographical distribution to radar freeboard (the first row)"

L356: "and results are given at the bottom" -> "and results are shown in the bottom row"

L356: "The obtained snow distribution indicates that thicker snow areas are generally coincident with thicker MYI areas. Likewise, the thinner snow area coincides with the thinner FYI area" -> "The obtained snow distribution indicates that thicker (thinner) snow areas are generally coincident with thicker MYI (thinner FYI) areas."

Sentences are corrected following your suggestion.

L385: "As a matter of fact, the ice thickness results were more accurate than they were from the current retrieval methods relying on the input of snow depth (this time MW99 snow climatology), in terms of mean bias and RMSE." – This sentence is not accurate. RMSE on ice thickness from radar freeboard is smaller using the MW99 method (0.344 vs 0.5 α-method, figure 7)

Sentence is corrected (removed RMSE).

L406: "The results that radar freeboard and the total freeboard yielded had nearly the same outputs when the α-approach was used" – This sentence does not make sense to me.

This sentence is removed.

L455: "hard wind slap" -> "hard wind slab"

Sentence is corrected.

L471: "Because hs is a combination of freeboard and α" - Do you mean "Because Hi is a combination of freeboard and α"?

Both ice thickness and snow depth are combination of freeboard and α. Sentence is corrected as follow.

"Because H_i and h_s are the combination of freeboard and α"

L476: "With $\Delta\alpha$= ±0.03, which is an RMSE range in the α-prediction equation" – From figure 4b, the RMSE = 0.04, not 0.03.

±0.03 was RMSE range in the α-prediction equation for the 30-day averaging period. However, regarding your comment, root mean square difference value between α^{OIB} *and* α^{sat} is used for $\Delta\alpha$. This part has changed as follow:

"With $\Delta\alpha$ = ±0.05, which is the root mean square difference (RMSD) value between α^{OIB} *and* α^{sat}"

L483: "a much small number" -> "a much smaller number"

Figure 8 caption: "Grey areas in the second row denote where α retrieval is failed because Tas is warmer than Tas." -> "Grey areas in the second row denote where α retrieval failed because T_{as} is warmer than T_{si}."

The sentences are corrected accordingly.

Simultaneous estimation of wintertime sea ice thickness and snow depth from space-borne freeboard measurements

Hoyeon Shi[1], Byung-Ju Sohn[1,2], Gorm Dybkjær[2]r[3], Rasmus Tage ~~Tonboe[2]~~Tonboe[3], Sang-Moo Lee[1,3,4,5]

[1]School of Earth and Environmental Sciences, Seoul National University, Seoul, Republic of Korea
[2]~~Danish~~Key Laboratory for Aerosol-Cloud-Precipitation of China Meteorological Administration, School of Atmospheric Physics, Nanjing University of Information Science & Technology, Nanjing, China
[3]Danish Meteorological Institute, Copenhagen, Denmark
[3]~~Center~~Center for Environmental Technology, ECEE, University of Colorado-Boulder, Boulder, Colorado, USA
[4]~~National~~National Snow and Ice Data Center, CIRES, University of Colorado-Boulder, Boulder, Colorado, USA

Correspondence to: Byung-Ju Sohn (sohn@snu.ac.kr)

Abstract. A method of simultaneously estimating snow depth and sea ice thickness using satellite-based freeboard measurements over the Arctic Ocean during winter was proposed. The ratio of snow depth to ice thickness (referred to as α) was defined and used in constraining the conversion from the freeboard to ice thickness in satellite altimetry without prior knowledge of snow depth. Then, α was empirically determined using the ratio of temperature difference of the snow layer to the difference of the ice layer, to allow the determination of α from satellite-derived snow surface temperature and snow–ice interface temperature. The proposed method was evaluated against NASA's Operation IceBridge measurements, and results indicated that the algorithm adequately retrieves snow depth and ice thickness simultaneously: retrieved ice thickness was found to be better than the methods relying on the use of snow depth climatology as input, in terms of mean bias ~~and RMSE~~. The application of the proposed method to CryoSat-2 radar freeboard measurements yields similar results. In conclusion, the developed α-based method has the capacity to derive ice thickness and snow depth, without relying on the snow depth information as input to the buoyancy equation ~~and~~or the radar penetration correction for converting freeboard to ice thickness.

1 Introduction

Satellite altimeters have been used to estimate sea ice thickness for nearly two decades (Laxon et al., 2003; Kwok et al., 2009; Laxon et al., 2013). The altimeters do not measure sea ice thickness directly but measure the sea ice freeboard which is then converted to sea ice thickness with assumptions, for example, regarding the snow depth, snow/ice densities, and radar penetration (Ricker et al., 2014). We hereafter refer to this procedure as 'freeboard to thickness conversion'.

Generally, there are two types of satellite altimeters measuring different sea ice freeboards: 1) Lidar altimeters such as NASA's ICESat (Zwally et al., 2002) and ICESat-2 (Markus et al., 2017) missions measure the total freeboard (F_t): the height from the sea surface in ~~cracks and~~ leads, to the snow surface. 2) Radar altimeters such as ESA's CryoSat-2 (CS2) (Wingham et al., 2006) measure the radar freeboard (F_r): difference in the radar ranging between the sea surface and the radar scattering horizon.

By applying two corrections terms regarding the wave propagation speed change in the snow layer (F_c) and displacement of the scattering horizon from the ice surface (F_p), the radar freeboard is converted to the ice freeboard (F_i): the height from the sea surface to the snow–ice interface (F_i). Several studies indicate that the radar scattering horizon is at or above the snow–ice interface depending on ice type and snow/ice conditions (Nandan et al., 2017; Armitage and Ridout, 2015; Willatt et al., 2011; Tonboe et al. 2010). However, the radar scattering horizon is often treated as the snow–ice interface (Kurtz et al., 2014; Kwok and Cunningham, 2015; Hendricks et al., 2016; Guerreiro et al., 2017, Tilling et al., 2018). The three different freeboards are indicated in Fig. 1.

For both lidar and radar altimeters, snow depth (h_s) is required as an input to constrain the freeboard to thickness conversion; thus, the conversion results are highly dependent on snow depth (Ricker et al., 2014; Zygmuntowska et al., 2014; Kern et al. 2015). The buoyancy equation used in the freeboard to thickness conversion describes the balance between buoyancy and the weight of snow and ice. For a given freeboard, snow/ice densities, and assumptions on radar penetration of the snow layer, sea ice thickness (H_i) is a function of h_s. According to Zygmuntowska et al. (2014), up to 70% of uncertainty in the freeboard to thickness conversion stems from the poorly constrained snow depth. However, mapping the Arctic scale snow depth distribution is challenging. The most commonly used snow depth information necessary for the freeboard to thickness conversion is the modified version of the snow depth climatology by Warren et al. (1999) (hereafter W99). W99 is based on in-situ measurements at Soviet drifting stations (1954–1991) mostly on multi-year ice (MYI). Kurtz and Farrell (2011) compared W99 with Operation IceBridge (OIB) snow depth measurements in 2009 and claimed that W99 was still valid in the MYI region and significantly differed from OIB snow depth on first-year ice (FYI). Based on that study, Modified W99 (hereafter MW99) was developed, which halves W99 snow depth in regions covered by FYI. MW99 is often used in CS2 ice thickness products available at CPOM-UCL (Laxon et al., 2013), AWI (Ricker et al., 2014), and NSIDC (Kurtz ~~et al.,~~and Harbeck, 2017).

However, the use of MW99 for the freeboard to thickness conversion understandably yields a substantial error, considering that W99 is climatology and not actual snow depth. This is because the actual snow depth distribution is subject to the year-to-year variation of the snow–ice system, thus the climatology based on the 37-year measurements of snow depth would deviate significantly from the actual distribution (Webster et al., 2014). Accordingly, such deviation causes errors in the estimation of ice thickness. Thus, additional snow observations covering both MYI and FYI on the Arctic basin-scale would be ideal as a replacement of MW99.

There have been various approaches aimed at obtaining the snow depth distribution over the Arctic scale using satellite observations. Markus and Cavalieri (1998) developed an algorithm based on the Brightness Temperatures (TBs) of Special Sensor Microwave/Imager (SSM/I) based on the negative correlation of the snow depth with the spectral gradient ratio between 18 and 37 GHz of vertically polarized ~~TB's~~TBs on the Antarctic FYI. Comiso et al. (2003) have updated the coefficients of this algorithm for the Advanced Microwave Scanning Radiometer for EOS (AMSR-E). However, snow depth retrieval using this algorithm is relatively less accurate when the MYI fraction within the grid cell is significant (Brucker and Markus, 2013).

Recently, Rostosky et al. (2018) suggested a new method: using the lower frequency pair of 7 and 19 GHz to overcome this limitation. Nonetheless, estimating the basin-scale snow depth distribution seems to be a difficult task.

There are other approaches involving the use of the lower frequency measurements at L-band. Using Soil Moisture Ocean Salinity (SMOS) measurements, Maaß et al. (2013) found that 1.4 GHz TB depends on the snow depth through the insulation effect of snow layer, and they determined snow depth by matching Radiative Transfer Model (RTM) simulated TBs with SMOS-measured TBs. Zhou et al. (2018) simultaneously estimated the sea ice thickness and snow depth by adding additional laser altimeter freeboard information, improving the Maaß et al. (2013) approach. However, both of these RTM-based approaches require a priori information on ice properties (e.g. temperature and salinity profiles).

Other satellite remote sensing approaches include the snow depth retrieval using dual-frequency altimetry (Guerreiro et al., 2016; Lawrence et al., 2018, Kwok and Markus, 2018), multilinear regression (Kilic et al., 2019), and a neural network approach (Braakmann-Folgmann and Donlon, 2019). In spite of promising results, the dual frequency altimetry method is available only for regions where two altimeters overlap with each other, reducing the great deal of spatial coverage. On the other hands, the regression/neural network methods based on AMSR-2 TBs are prone to the overfitting problem, limiting their applications to other microwave sensors.

Here, let us switch our point of view to solving the buoyancy equation instead of retrieving snow depth directly. Remember that there are two unknowns (snow depth and ice thickness) in the buoyancy equation for given snow/ice densities, freeboard, and assumptions on radar penetration of the snow layer. The attempt so far has been to add one constraint (snow depth information) to the buoyancy equation for solving ice thickness. However, if a particular relationship between two unknowns is available, it can be used to constrain the equation yielding both ice thickness and snow depth simultaneously.

To identify such a relationship, this study examines the vertical thermal structure within the snow/ice layers observed by drifting buoys. The vertical thermal structure of a snow–ice system in winter is rather simple; the temperature profile of the snow–ice system can be assumed to be piecewise linear, as illustrated in Fig. 1. Therefore, the temperatures at three interfaces can represent the thermal state of the snow–ice system fairly well; they are (1) air–snow interface temperature (T_{as}), (2) snow–ice interface temperature (T_{si}), and (3) ice–water interface temperature (T_{iw}). T_{iw} is assumed to be nearly constant at the freezing temperature of seawater (Maaß et al., 2013), implying that two other interface temperatures (T_{as} and T_{si}) are sufficient to describe the thermal structure of the system.

Based on this thermal structure, there is a constraint relating the snow depth and ice thickness. In identifying this constraint, conductive heat flux is assumed to be continuous through the snow–ice interface (Maykut and Untersteiner, 1971), implying that conductive heat fluxes within the snow and ice layers are same under the steady-state assumed in the given thermal structure. As the conductive heat flux is proportional to the bulk temperature difference of the layer divided by its thickness, it is possible to deduce the relationship between snow depth and ice thickness from the given thermal structure.

Once the relationship is obtained, then it is possible to apply it to the Arctic Ocean basin-scale because the thermal structure can be resolved from satellites, as shown in the recently available basin-scale and long-term satellite-derived interface temperatures (Dybkjær et al., 2020; Lee et al., 2018). In determining the snow depth along with the ice thickness, instead of

using the snow depth as an input to solve for the ice thickness, we intend to (1) examine the relationship between the vertical thermal structure of a snow–ice system (T_{as} and T_{si}) and the thicknesses of the snow and ice layer (h_s and H_i) using buoy measurements, (2) retrieve the sea ice thickness and the snow depth simultaneously by applying their relationship to the freeboard to thickness conversion as a constraint, thus replacing the snow depth information. The result may reduce uncertainty in the freeboard to ice thickness conversion by replacing the currently used snow depth climatology.

2 Method

Here, we provide the theoretical background of how the snow–ice thickness ratio ($\alpha = h_s / H_i$) can be related to T_{as} and T_{si}. Then, after empirically determining the relationship of α to T_{as} and T_{si} from buoy measured temperature profiles, α obtained from satellite-observed T_{as} and T_{si} is then used to constrain the conversion from freeboard to ice thickness over the Arctic Ocean during winter.

2.1 Theoretical background

We intend to find a relationship between snow depth and ice thickness in terms of the vertical thermal structure of the snow–ice system. Because the temperature gradients within the snow and ice layers are linked to both temperature and thickness, we focus on the temperature gradient. Owing to the physical reasoning that the conductive heat flux is continuous across the snow–ice interface (Maykut and Untersteiner, 1971), the following relationship is valid at the snow–ice interface:

$$k_{snow} \frac{\partial T_{snow}}{\partial z}\Big|_{z=0} = k_{ice} \frac{\partial T_{ice}}{\partial z}\Big|_{z=0} \quad (1)$$

In Eq. (1), the subscripts *snow* and *ice* denote their respective layers while T, k, and z denote temperature, thermal conductivity, and depth, respectively. The snow–ice interface is defined as $z = 0$. Assuming a piecewise linear temperature profile within the snow–ice layer, Eq. (1) can be rewritten as follows:

$$k_{snow} \frac{T_{as} - T_{si}}{h_s} = k_{ice} \frac{T_{si} - T_{iw}}{H_i} \quad (2)$$

where subscripts *as*, *si*, and *iw* denote the air–snow, snow–ice, and ice–water interface, respectively, and H_i and h_s denote the sea ice thickness and snow depth as in Fig. 1. Introducing a variable α, which is the snow–ice thickness ratio, Eq. (2) becomes:

$$\alpha = \frac{h_s}{H_i} = \frac{k_{snow}}{k_{ice}} \frac{\Delta T_{snow}}{\Delta T_{ice}} \quad (3)$$

Here, ΔT denotes the temperature difference between the top and bottom of each of the snow and ice layers (i.e. $\Delta T_{snow} = T_{as} - T_{si}$, $\Delta T_{ice} = T_{si} - T_{iw}$). As explained in detail in Sect. 2.3, α can be used to constrain the freeboard to thickness conversion. Thus, once α is known, both snow depth and ice thickness can be simultaneously estimated from altimeter-measured freeboard, instead of using snow depth data for ice thickness retrieval.

2.2 Empirical determination of 'α-prediction equation' from buoy measurements

To obtain α, the conductivity ratio (k_{snow}/k_{ice}) should be known even if the temperature difference ratio ($\Delta T_{snow}/\Delta T_{ice}$) is given. In this study, instead of using the conventional conductivity ratio found in literature, it is empirically determined using buoy-measured α and $\Delta T_{snow}/\Delta T_{ice}$. Thus, the interface should be defined and determined from buoy-measured temperature profiles, which show a piecewise linear temperature profile as shown in Fig. 1.

The buoy-measured temperature profiles in the vertical resolution of 10 cm are used in this study (Sect. 3.1). Although the instrument initially sets the zero-depth reference position to be approximately at the snow–ice interface, the reference position can deviate from the initial location if the ice deforms, or if the snow refreezes after the temporary melt into snow-ice. In addition, the interfaces (air–snow, snow–ice, and ice–water) may be located in between measurement levels in a 10 cm spacing. Therefore, an interface searching algorithm is developed to determine three interfaces (y_{as}, y_{si}, y_{iw}) and their respective temperatures (T_{as}, T_{si}, T_{iw}) by extrapolating each piecewise linear temperature profile iteratively.

The interface searching algorithm iterates three processes to find the location and temperature of each interface: it (1) divides temperature profile into four layers using the most recently available locations of the three interfaces, (2) finds a linear regression line of the temperature profile at each layer, and (3) updates the location and temperature of each interface by finding an intersection between two adjacent regression lines. The algorithm fails if the temperature profile is far from linear, or the thickness of a certain layer is too thin to have less than two data points. More detailed procedures for determining the interface are provided in Fig. 2, as a flow chart. The outputs are T_{as}, T_{si}, T_{iw}, H_i (= y_{as} - y_{si}), and h_s (= y_{si} - y_{iw}). Examples of the interface searching results for 15-day averaged temperature profiles are shown in Fig. 3. The algorithm works adequately for both CRREL-IMB (Fig. 3a–c) and SHEBA buoy data (Fig. 3d–f).

Since T_{as}, T_{si}, T_{iw}, H_i, and h_s can be obtained from the previous interface determination with buoy data, the calculation of $\Delta T_{snow}/\Delta T_{ice}$ and α is straightforward. Then, an empirical relationship can be obtained by relating α to $\Delta T_{snow}/\Delta T_{ice}$ by running a regression model, and details are given in Sect. 4. However, for the time being, we assume that the regression equation (referred to as an 'α-prediction equation' that will be discussed in Sect. 4) is used to predict α from $\Delta T_{snow}/\Delta T_{ice}$.

2.3 Simultaneous estimation of ice thickness and snow depth from satellite-based freeboard using α

In this section, we describe how α can be used to constrain the freeboard to thickness conversion. Based on the assumed hydrostatic balance, ice thickness can be obtained from satellite-borne total freeboard or ice freeboard as follows:

$$H_i = \frac{\rho_w}{\rho_w - \rho_i} F_t - \frac{\rho_w - \rho_s}{\rho_w - \rho_i} h_s \tag{4}$$

$$H_i = \frac{\rho_w}{\rho_w - \rho_i} F_i + \frac{\rho_s}{\rho_w - \rho_i} h_s \tag{5}$$

Here, ρ_w, ρ_i, and ρ_s denote the bulk densities of water, ice, and snow layer, respectively. Ice freeboard is obtained from radar freeboard by applying two correction terms regarding the change of the wave propagation speed in snow layer (F_c) and the displacement of the scattering horizon from the ice surface (F_p) (Kwok and Cunningham, 2015).

$$F_i = F_r + (F_c - F_p) \tag{6}$$

The correction terms are expressed in the following equations (Armitage and Ridout, 2015; Kwok and Markus, 2018).

$$F_c = (\eta_s - 1) f h_s \tag{7}$$

$$F_p = (1 - f) h_s \tag{8}$$

Here, η_s denotes the refractive index of the snow layer and f denotes the radar penetration factor (Armitage and Ridout, 2015), which is the depth of the radar scattering horizon relative to the snow depth (e.g. $f = 1$ if the radar scattering horizon is at snow–ice interface and $f = 0$ if the radar scattering horizon is at air-snow interface~~), respectively.)~~. Combination of Eqs. (6~~) – ()~~ – (8) yields the following relationship.

$$F_i = F_r + (f\eta_s - 1) h_s \tag{9}$$

Ice freeboard in Eq. (5) can be substituted by radar freeboard and snow depth using Eq. (9), i.e.:

$$H_i = \frac{\rho_w}{\rho_w - \rho_i} F_r + \frac{(f\eta_s - 1)\rho_w + \rho_s}{\rho_w - \rho_i} h_s \tag{10}$$

According to Eq. (10), the ice thickness can be estimated from the radar freeboard and the snow depth. Note that Eq. (10) becomes equivalent to the equation for the total freeboard (Eq. (4)) if $f = 0$ (i.e. if there is no radar penetration into snow layer). With the use of α, defined in Eq. (3), Eqs. (4) and (10) become

$$H_i = \frac{\rho_w}{\rho_w - \rho_i + \alpha(\rho_w - \rho_s)} F_t \tag{11}$$

$$H_i = \frac{\rho_w}{\rho_w - \rho_i - \alpha\{(f\eta_s - 1)\rho_w + \rho_s\}} F_r \tag{12}$$

From Eqs. (3), (11) and (12), it is evident that the snow depth and ice thickness can be simultaneously estimated from the freeboards once α, ρ, f and η_s are known.

In order to obtain α from satellite measurements of T_{as} and T_{si}, we need to calculate the temperature difference ratio ($\Delta T_{snow}/\Delta T_{ice}$). For the calculation, T_{iw} is set to be -1.5 °C. The freezing temperature of seawater is often assumed to be -1.8 °C; however, the value of -1.5 °C is chosen, based on the buoy observations. A sensitivity test indicated that the influence of a 0.3 °C difference in the freezing temperature on α was negligible~~.~~ (e.g. approximately 1.2% difference for typical interface temperatures of T_{as} = -30 °C and T_{si} = -20 °C). α values are calculated only at the pixel whose monthly sea ice concentration (SIC) is greater than 95% and rejected if T_{as} is warmer than T_{si}. The densities are prescribed with those used for OIB data processing: ρ_s, ρ_i, and ρ_w are 0.320 g cm^{-3}, 0.915 g cm^{-3}, and 1.024 g cm^{-3}, respectively (Kurtz et al., 2013). Although ρ_s varies

seasonally (Warren et al., 1999) and ρ_i is greater for MYI than FYI (Alexandrov et al., 2010), we use the same densities as those of OIB data because we intend to compare outputs against OIB data. In solving Eq. (12), cases showing negative ice thickness ($\alpha \geq \alpha_{crit} = 0.291$ for the given densities and radar penetration factor) are rejected. Radar penetration factor f is set to be 0.84 for CS2 (Armitage and Ridout, 2015) and η_s is parameterized as a function of the snow density, i.e., $\eta_s = (1+0.51\rho_s)^{1.5}$ (Ulaby et al., 1986).

Before the Arctic basin-scale retrieval, ice thickness is estimated from OIB total freeboard measurement using Eq. (11), and from OIB-derived radar freeboards (Sect. 3.3) using Eq. (12), using satellite-derived α as a constraint. At the same time, the corresponding snow depth is derived by multiplying the obtained sea ice thickness and ~~α.~~α (Eq. (3)). Sea ice thicknesses are also calculated from Eqs. (4) and (10), using MW99 as snow depth, to examine how simultaneous retrievals compare with ice thickness estimation using MW99. To differentiate various outputs, obtained snow depth and ice thickness are expressed with nomenclature such as '(constraint, freeboard source)'. For example, the snow depth estimated from satellite-derived α and OIB total freeboard is referred to as 'h_s (α^{sat}, ~~F_t^{OIB}~~)', and sea ice thickness from the MW99 and OIB radar freeboard is referred to as 'H_i (h_s^{MW99}, F_r^{OIB})'. Finally, ice thickness and snow depth are estimated from CS2 radar freeboard (Sect. 3.4) over the Arctic Ocean.

3 Data

Here, we provide detailed information on the data sets used for the development of the retrieval algorithm, evaluation, and application to the Arctic ocean basin scale.

3.1 CRREL and SHEBA buoy data

To determine the empirical relationship between α and $\Delta T_{snow}/\Delta T_{ice}$ using Eq. (3), we need information regarding ~~h, H~~h_s, H_i, T_{as}, T_{si}, and T_{iw} (as depicted in Fig. 1). These are sourced from temperature profiles observed by buoys deployed over the Arctic, as ~~parts~~part of the Surface Heat Energy Budget of the Arctic (SHEBA) campaign (Perovich et al., 2007) and the Cold Regions Research and Engineering Laboratory Ice Mass Balance (CRREL-IMB) buoy program (Perovich et al., 2019). Those buoy observations are stored for further analysis if there are no missing records over the entire period ranging from November to March of the following year. Detailed information regarding ice type and initial snow/ice thickness at deployment locations are given in Table 1.

Time averages of temperature profiles are used as input to the interface searching algorithm (described in Sect. 2.2) to meet the required near-equilibrium states (e.g. linear temperature profile). However, because of the possibility that the results are ~~depending~~dependent on the averaging period, we examine the results using various averaging periods from one to 30 days.

3.2 Satellite-derived skin and interface temperatures

For applying the buoy-based α-prediction equation in retrieving the snow/ice thicknesses over the Arctic Ocean, satellite-derived T_{as} and T_{si} data are necessary. In this study, T_{as} is obtained from Arctic and Antarctic ice Surface Temperatures from thermal Infrared satellites sensors – version 2 (AASTI-v2) data (Dybkjær et al., 2020), and the monthly mean for the 1982–2015 period is obtained from daily products. AASTI T_{as} is derived from CM SAF cLoud, Albedo and surface Radiation dataset from AVHRR data - Edition 2 (CLARA-A2) dataset (Karlsson et al., 2017), based on the algorithm described in Dybkjær et al. (2018). Information on the validation of this product is found in Dybkjær and Eastwood (2016). It is available in a 0.25° grid format, however, because other satellite data sets such as SIC are available in a 25 km Polar Stereographic SSM/I Grid, AASTI-v2 data are re-gridded in the same 25 km grid format. This reformatted AASTI-v2 dataset is called 'satellite skin temperature'.

T_{si} is obtained from Snow/Ice Interface Temperature (SIIT) produced by Lee et al. (2018) over 30 years (1988–2017) of wintertime (December to February) using SSM/I and Special Sensor Microwave Imager/Sounder (SSMIS) homogenized TBs (Berg et al., 2018). The daily data are in the 25 km grid format. Lee et al. (2018) reported that the satellite-derived T_{si} is consistent with snow–ice interface temperatures observed by CRREL-IMB buoys, with the correlation coefficient, bias, and RMSE of 0.95, 0.15 K and 1.48 K, respectively. In this study, we also produced T_{si} for March using the same algorithm of Lee et al. (2018) for evaluating results against OIB data which are mostly collected during spring. Monthly composites are constructed by averaging daily data for grid cells where the data frequency is over 20 days. This product is called 'satellite interface temperature'.

3.3 OIB data

In this study, OIB snow depth (h_s^{OIB}) and total freeboard (F_t^{OIB}) are used as a reference in the evaluation of snow depth and ice thickness retrieved from the developed algorithm. NASA's OIB is an aircraft mission and it measures snow depth and total freeboard over the Arctic using the snow radar, Digital Mapping System (DMS), and Airborne Topographic Mapper (ATM) (Kurtz et al., 2013). OIB ice thickness is derived from measured snow depth and total freeboard, for the given snow and ice densities using Eq. (4). In this study, the OIB radar freeboard (F_r^{OIB}) is derived from F_t^{OIB} and h_s^{OIB} using the combined relationship of $F_i = F_t - h_s$ and Eq. (9) as follows:

$$F_r^{OIB} = F_t^{OIB} - h_s^{OIB} - (f\eta_s - 1)h_s^{OIB} \tag{13}$$

Because the main objective of using OIB data is to evaluate the relative performance of the simultaneous retrieval method when the method is applied to CS2 data, the radar penetration factor (f) for OIB data processing is also set to be 0.84. In the data processing chain, h_s^{OIB} is removed if it is smaller than the given uncertainty level of the dataset (~5.7 cm) or it is larger than the total freeboard F_t^{OIB}.

Five years of OIB data during 2011-2015 period are utilized in this study. The level 4 dataset (Kurtz et al., 2015) during 2011-2013 period and Quick look dataset ~~(https://doi.org/10.5067/7Q8HCCWS4I0R, last access: 20 May 2020)~~ during 2014-2015 period are obtained from the NSIDC website~~.~~ (see the data availability section). Because we use the November–March period for the buoy analysis, only March OIB data are considered for the evaluation. The OIB data are also reformatted into the 25 km grid format ~~for comparison. If the location of one OIB individual data point falls within a certain 25 km grid area, then the point data is binned in a corresponding grid. After completing the grid assignment, grid value is determined by calculating a simple arithmetic mean of all data within that grid area.~~by averaging pixel-level OIB observations on the 25 km grid.

3.4 CS2 data

For examining the Arctic Ocean basin distribution of ice thickness and snow depth, CS2 freeboard measurement summary data are used (Kurtz ~~et al.,~~and Harbeck, 2017). They are monthly mean composites of CS2 ice freeboard data in the 25 km Polar Stereographic SSM/I Grid format, covering the entire Arctic, and available from September 2010. Detailed descriptions of the retracker algorithm used in this dataset are found in the study by Kurtz et al. (2014). The dataset also includes MW99 (h_s^{MW99}) and W99 snow density climatology used for producing the ice freeboard.

The CS2 ice freeboard data (F_i^{CS2}) distributed by NSIDC (Kurtz ~~et al.~~and Harbeck, 2017) assumed that the radar scattering horizon is at the snow–ice interface and applied a wave propagation speed correction. However, the correction was made using h_s^{MW99} and W99 snow density climatology with an erroneous form of $h_c = (1 - \eta_s^{-1})\, h_s$, instead of the proper form of $h_c = (\eta_s - 1)\, h_s$ (Mallett et al., 2020). ~~In this dataset, η_s was parameterized as a function of the snow density, i.e., $\eta_s = (1 + 1.7\rho_s + 0.7\rho_s^2)^{0.5}$ (Tiuri et al., 1984).~~ Thus, at this point, it is straightforward to derive the CS2 radar freeboard by removing the correction term as in the following equation.

$$F_r^{CS2} = F_i^{CS2} - (1 - \eta_s^{-1}) h_s^{MW99} \tag{14}$$

Here, η_s was parameterized as a function of the snow density, i.e. $\eta_s = (1 + 1.7\rho_s + 0.7\rho_s^2)^{0.5}$ (Tiuri et al., 1984), and ρ_s is taken from the W99 climatology, after Kurtz and Harbeck (2017). Then CS2 ice thickness is re-produced from F_r^{CS2} and h_s^{MW99} by using Eq. (10) with the constant densities and the radar penetration factor described in Sect. 2.3. Those h_s^{MW99} and H_i (h_s^{MW99}, F_r^{CS2}) values are used for comparison~~.~~ with results from our simultaneous method.

3.5 Sea ice concentration

Calculation of α is done for those pixels where the monthly SIC is greater than 95% (as described in Sect. 2.3). To determine pixels that meet this SIC criterion, 'bootstrap sea ice concentrations from Nimbus-7 SMMR and DMSP SSM/I-SSMIS version 3' produced by Comiso (2017) are used. This SIC dataset is provided in the 25-km Polar Stereographic SSM/I grid format.

4 Results

4.1 The empirical relationship between α and $\Delta T_{snow}/\Delta T_{ice}$

We examine variables (i.e. T_{as}, T_{si}, T_{iw}, ~~H~~H_i, and ~~h~~h_s) obtained from buoy observations by applying the interface searching algorithm. In the scatter plot of weekly-averaged $\Delta T_{snow}/\Delta T_{ice}$ versus α (Fig. 4a), it appears that α linearly increases with $\Delta T_{snow}/\Delta T_{ice}$ when the ratio is smaller than 1.8, but the linear slope becomes smaller when $\Delta T_{snow}/\Delta T_{ice}$ is larger than 1.8. This pattern of the slopes is found to be nearly invariant from year to year, as observed in different colors appearing in the entire range of $\Delta T_{snow}/\Delta T_{ice}$ in Fig. 4a. We also found that this slope pattern is the consistent nature even for different data sets; two different data sets (red points for SHEBA and other points for CRREL) covering various ranges of $\Delta T_{snow}/\Delta T_{ice}$, show similar distributions along the two different slopes. Thus, the slope pattern is not due to different data sources or different data periods. Further analysis of the two slopes is found in Appendix A.

Taking such a two-slope pattern with $\Delta T_{snow}/\Delta T_{ice}$ into account, we introduce a piecewise linear function that may express the slope pattern, i.e.:

$$y = \begin{cases} a_1 x + b_1 & x \le x_0 \\ a_2 x + b_2 & x > x_0 \end{cases}, \quad x_0 = \frac{b_1 - b_2}{a_2 - a_1} \tag{15}$$

In Eq. (15), x and y correspond to $\Delta T_{snow}/\Delta T_{ice}$ and α, respectively, and x_0 is the point where the slope transition takes place. Applying Eq. (15) to data points from buoy-based variables, the regression coefficients (a_1, b_1, a_2, b_2) and transition point (x_0) are determined by minimizing the total variance - obtained regression line is plotted in Fig. 4a. α is predicted using the determined regression equation (hereafter referred to as α-prediction equation) and compared to the original α values to see how well the regression was performed. The comparison of α with predicted values in Fig. 4b shows that the regression equation is well fitted because of the zero bias and 91.9% of explained variance.

Although the slope pattern discussed with Eq. (15) and Fig. 4 is based on the weekly averages, the slope pattern seems to be consistent among the data averaging periods except for an averaging period shorter than five days. Regressions in the form of Eq. (15) are performed with buoy data averaged with different averaging periods to understand the slope pattern. Regression coefficients and transition point for the chosen averaging periods are examined, and results for four averaging periods are given in Table 2. Detailed information on the coefficients and associated statistics varying with the averaging period is given in Fig. 5. The positions of slope change (x_0) are located at approximately 1.8, delineating a nearly invariant slope pattern, regardless of different data averaging periods. Fig. 5a shows that coefficients do not vary much with different averaging periods while coefficients of the first part of the regression line (a_1 and b_1, $x \le x_0$) vary less than those of the second part (a_2 and b_2, $x > x_0$). The regression equations show that the explained variance (R^2) rises quickly when the averaging period is longer but levels off when data are averaged over a period that is longer than seven days. The bias appears to be near zero over the various averaging periods. Thus, regression performance is found to be comparable if data are averaged over a period that is longer than a week.

4.2 Evaluation against OIB estimates

According to the regression results, it is possible to estimate α from the $\Delta T_{snow}/\Delta T_{ice}$. Since the $\Delta T_{snow}/\Delta T_{ice}$ can be calculated from the satellite skin and interface temperature (as described in Sect. 3.2), the corresponding α can be estimated from satellite measurements. Thus, we are able to simultaneously retrieve sea ice thickness and snow depth from altimeter-based freeboard measurements, following Eqs. (11) and (12). We test and evaluate this simultaneous retrieval approach using OIB data. Accordingly, ice thickness and snow depth are simultaneously estimated from OIB freeboard measurements and evaluated against the OIB snow depth (h_s^{OIB}) and ice thickness (H_i^{OIB}).

To calculate α, a data averaging period must be selected. Considering that the monthly composite of satellite freeboard measurements is needed to retrieve snow/ice thickness in the Arctic basin scale, it seems appropriate to use the monthly averaging period to calculate the monthly α distribution. Thus, we use the monthly averaged satellite temperatures and the coefficients for the 30-day averaging period (Table 2) to calculate α.

We simultaneously retrieved H_i and h_s for each year's March during 2011–2015 period from the reformatted OIB freeboard measurements (Sect. 3.3) together with satellite-derived α (α^{sat}). As expressed in Eqs. (11) and (12), two different ice thickness retrievals are possible, depending on the use of the freeboard type (i.e. total freeboard F_t vs. radar freeboard F_r). Two accordingly associated retrievals of snow depth are available. Retrieved results of ice thickness (H_i) and snow depth (h_s) from the use of OIB total freeboard and radar freeboard are given in the first and second row of Fig. 6, respectively. Corresponding OIB measurements are given at the bottom of Fig. 6. The comparison between any snow/ice retrievals and OIB measurements appear to be consistent with each other for both snow depth and ice thickness, in terms of magnitudes and distribution.

To compare the results quantitatively, scatterplots ~~of~~ comparing retrievals against OIB measurements are made, along with statistics for the snow depth and ice thickness retrievals, in the top four panels of Fig 7. The top-two left panels are derived from the use of OIB total freeboard (F_t^{OIB}) while the top-two right panels are derived from the OIB radar freeboard (F_r^{OIB}). The comparison is done only for pixels where all four products (i.e. snow/ice thicknesses from two different freeboards) are available. This indicates that the snow depth from the total freeboard (top left) is fairly consistent with the OIB snow depth, with a correlation coefficient of 0.73 and with a near-zero bias. The retrieved ice thickness from the total freeboard (middle left) appears to be consistent with OIB ice thickness, with a correlation coefficient of 0.93 and a bias around 8.5 cm. The RMSEs for snow depth and ice thickness are 6.8 cm and 44.3 cm, respectively. Based on the comparison results, Eq. (15) obtained from buoy measurements can be successfully implemented with space-borne total freeboard measurements for the simultaneous retrieval of snow depth and ice thickness.

Following Eq. (12), snow depth and ice thickness retrievals are made from the use of radar freeboard measurements, and results are presented in the top-two right panels in Fig. 7. On the one hand, the comparison of obtained ice thickness against the OIB ice thickness indicates that the retrieved ice thickness shows ~~nearly the same~~similar quality as that retrieved from the total freeboard measurements. On the other hand, snow retrievals from the radar freeboard show more scattered features, compared with snow retrieval results from the total freeboard. More scattered features found in the snow depth from the radar freeboard

are likely due to the larger sensitivity of the retrieved α and the prescribed densities, as noted in Eq. (12). Note that Eq. (12) has a smaller denominator than that for Eq. (11). Results of associated sensitivity analysis can be found in Appendix B.

We now examine how the use of MW99 for retrieving sea ice thickness from ICESat and CS2 measurements compares with results from our simultaneous method. To do so, OIB-measured total freeboard and radar freeboard are converted into ice thickness using MW99 as input to solve Eqs. (4) and (10). In this study, these two ice thickness retrievals with the use of MW99 are referred to as "ICESat-like" thickness and "CS2-like" thickness, respectively, and their comparisons are now observed in two panels at the bottom of Fig. 7. According to our analysis, ICESat-like thickness tends to underestimate the ice thickness by about 47.9 cm when MW99 is used, in comparison to OIB thickness and CS2-like ice thickness shows an overestimate of about 25.5 cm. Nevertheless, their correlation coefficients and RMSEs are similar to the results obtained from the α method.

Better agreement of H_i from the simultaneous method with H_i^{OIB} may be due to the fact that the simultaneously estimated h_s is more consistent with h_s^{OIB} (h_s^{MW99} is likely larger than h_s^{OIB}, as shown in Fig. S1). Note that all inputs are the same except the snow depth. The negative bias of ICESat-like thickness and positive bias of CS2-like thickness reflect expected responses in different signs to the same snow depth error, as shown in different signs in the last terms of Eqs. (4) and (10) (also note Eq. (B2) in Appendix B). Because of this reasoning, if there are decreasing trends in not only ice thickness but also snow depth, the decreasing trend of ice thickness estimated from the constant snow depth will be diminished in radar, while being amplified in lidar. Because of this, the construction of the ice thickness (or volume) trend from the two different satellite altimeters would be problematic if MW99 is used for the freeboard to thickness conversion. For example, it would be hard to compare the sea ice thickness records estimated from ICESat and CS2 observations and to extend the current ice thickness record from CS2 with recently launched NASA's ICESat-2 which carries a lidar altimeter, for the same reason.

4.3 Simultaneous retrieval of ice thickness and snow depth from CS2 measurements

We have demonstrated that the method of simultaneously retrieving the sea ice thickness and snow depth was successfully implemented with OIB measurements. Now we extend the proposed approach to satellite freeboard measurements. Here, the method is tested with CS2 freeboard measurements, solving for H_i in Eq. (12), and α is obtained from the collocated satellite skin and interface temperature data.

Monthly means of CS2-estimated freeboard (F_r), retrieved α, ice thickness (H_i), and snow depth (h_s) for December 2013 to March 2014 are given in Fig. 8. The geographical distribution of α indicates that α is largest in January and becomes smaller during the following months. Geographically, there seems to be no particular distribution of α between months, although interestingly the lowest α values are always found over the north of the Canadian Archipelago and the western part of the Arctic Ocean shows α values that ~~is~~are generally larger than ~~that~~those over the eastern part.

Retrieved ice thickness from the CS2 freeboard (F_r) using obtained α is presented in the third row of Fig. 8. As expected, as noted in Eq. (12), H_i shows a similar geographical distribution ~~as shown in the~~to radar freeboard (the first row). The thickest

area is located north of the Canadian Archipelago, where the ice appears thicker than 4 m. On the other hand, most of the FYI thickness appears to range from 1.0 m to 2.0 m. The snow depth h_s is obtained by multiplying α by H_i (in 2nd and 3rd rows), following Eq. (3), and results are ~~given at~~shown in the bottom row. The obtained snow distribution indicates that thicker (thinner) snow areas are generally coincident with thicker MYI ~~areas. Likewise, the thinner snow area coincides with the (~~thinner FYI~~ area)~~ areas. Such similarity should be consistent with the notion that MYI should accumulate more precipitation than FYI because of its longer existence.

~~The accuracies~~ To assess the accuracy of CS2 retrievals ~~using the current α approach can be indirectly tested with OIB measurements. We do so by examining whether the relationships of~~, reference ~~h_s (α^{sat}, F_r^{OIB}) vs. h_s^{MW99} and H_i (α^{sat}, F_r^{OIB}) vs. H_i (h_s^{MW99}, F_r^{OIB}), in which each~~ snow~~/~~ depth and ice thickness ~~retrieval has its own accuracy against OIB measurements, can be reproduced in~~ collocated with CS2 ~~based~~ freeboard in space and time are necessary. However, different from simultaneous retrievals~~. If similar results are found, we can deduce respective accuracies against those found from the~~ from OIB freeboards in Sect. 4.2, evaluation ~~efforts~~with the required matching data may not be possible from the monthly composite of CS2 data used in this study. Here, instead of using monthly collocated match-up data, an indirect way is used to examine the accuracy of CS2 retrievals. We do so by examining whether the relationship between the simultaneous method and the MW99 method, based on retrievals from the OIB freeboard, can be reproduced by CS2-based retrievals. If similar results are obtained, respective accuracies can be deduced against those noted from the evaluation against OIB measurements.

The relationships, which can be obtained from analysis in Sect. 4.2 (i.e. h_s (α^{sat}, F_r^{OIB}) vs. h_s^{MW99} and H_i (α^{sat}, F_r^{OIB}) vs. ~~Fig. 7, is H_i (h_s^{MW99}, F_r^{OIB})~~), are compared with the ~~relationship~~ relationships found in the current results in Fig. 8~~,~~ (i.e~~.,~~ h_s (α^{sat}, F_r^{CS2}) vs. h_s^{MW99} and H_i (α^{sat}, F_r^{CS2}) vs. H_i (h_s^{MW99}, F_r^{CS2})); the results are presented in Fig. 9. Observably, the relationships from CS2 freeboard data (Fig. 9b, d) are very similar to the relationship obtained from the comparison results from OIB measurements (Fig. 9a, c). This similarity of the slope strongly indicates that the CS2-based sea ice thickness from the current α method has similar accuracy to that found in the evaluation against OIB measurements (Sect 4.2). Further uncertainty estimates for CS2-derived products can be found in Appendix C.

5. Conclusions and Discussion

A new approach towards simultaneously estimating snow depth and ice thickness from space-borne freeboard measurements was proposed and tested using OIB data and CS2 freeboard measurements. In developing the algorithm, the vertical temperature slopes were assumed to be linear within the snow and ice layers so that continuous heat flux could be maintained in both layers. This assumption allowed for the description of the snow–ice vertical thermal structure with snow skin temperature, snow–ice interface temperature, the water temperature at the ice–water interface, snow depth, and ice thickness. Based on the continuous heat transfer assumption, the snow–ice thickness ratio ($\alpha = h_s / H_i$) was introduced and could then be embedded into the freeboard to ice thickness conversion equations. Thus, information on both ice thickness and snow depth

can be derived once α is known in case of the availability of a freeboard, without relying on the snow depth information as an input to the conversion from freeboard to ice thickness. From the drifting buoy measurements of the temperature profile, snow depth, and ice thickness over the Arctic Ocean, we demonstrated that α can be reliably determined using the ratio of the vertical difference of the snow-layer temperature to the vertical difference of ice-layer temperature ($\Delta T_{snow}/\Delta T_{ice}$). An empirical regression equation was obtained for predicting α from three interface temperatures.

Before applying α-prediction equation to simultaneously retrieve the ice thickness and snow depth from satellite-borne freeboard measurements, the algorithm was evaluated using OIB measurements, in conjunction with satellite-derived snow skin temperature and snow–ice interface temperature. Evaluation results demonstrated that our proposed algorithm adequately retrieved both parameters simultaneously. As a matter of fact, the ice thickness results were more accurate than they were from the current retrieval methods relying on the input of snow depth (this time MW99 snow climatology), in terms of mean bias ~~and RMSE~~. It should be noted that in this case, snow depth is a retrieval product, instead of being input to the freeboard to ice thickness conversion adopted by CS2 or ICESat retrieval. The application was finally made for the retrieval of the snow depth and ice thickness from CS2 radar freeboard measurements from December 2013 to March 2014 using α as a constraint. Results showed that the quality of the obtained ice thickness was similar to that obtained from evaluation results against OIB measurements. Retrieved snow depth distributions were also found to be consistent with expectations.

In the retrieval process, we may be concerned about the applicability of the algorithm developed with buoy observations representing the point measurements, to the larger spatial and temporal scales of satellite measurements. This concern may be relevant upon observing the range of α values. α in the satellite's monthly and 25 km x 25 km spatial scales was found to be generally smaller than 0.2. The smaller range of α compared to that shown in the buoy analysis results is likely due to the scale differences, indicating that extreme α values often shown in buoy measurements (due to very thick snow and/or very thin ice) may never be observed in satellite measurements. However, the range may not be a problem because the relationship (Eq. (3)) expresses the thermal equilibrium condition described by the temperature at three interfaces, the ratio of snow and ice thickness, and the ratio of thermal conductivity between snow and ice. Considering that the algorithm is based on the equilibrium conditions, results should be valid regardless of spatial and temporal scales if the prerequisite equilibrium conditions are met. Apparently, buoy observations contain so many different cases that equilibrium conditions are met with different thermal and physical conditions of the snow–ice system. Sound evaluation results and the consistency between OIB and CS2 ice thickness retrieval results, which are subject to different scales, all suggest that point-measured α-prediction equation can apply to satellite measurements.

Overall, the developed α-based method yields ice thickness and snow depth, without relying on a priori 'uncertain' snow depth information (MW99), which results in uncertainty in the ice thickness retrieval. ~~The results that radar freeboard and the total freeboard yielded had nearly the same outputs when the α approach was used.~~ The proposed method applies to both lidar and radar altimeter data, although lidar-based altimeter data tend to offer relatively more suitable snow depth information with smaller RMSE. We expect to continuously monitor the Arctic scale snow depth and ice thickness by applying the proposed α

method to total freeboard observations by the recently launched ICESat-2, using temperature observations from the upcoming MetOp SG Meteorological Imager (MetImage), the Microwave Imager (MWI) and the proposed Copernicus Imaging Microwave Radiometer (CIMR).

Appendix A: Physical interpretation of the piecewise linearity between α and $\Delta T_{snow}/\Delta T_{ice}$

The relationship found between α and $\Delta T_{snow}/\Delta T_{ice}$ showed a piecewise linearity, which is almost invariant with the data averaging period. Because the slope change is neither attributable to different data sources nor different data periods, it is likely caused by the physical properties of the snow and ice, as shown in Fig. A1. If the slope change is caused by the snow/ice condition, there will be a significant difference in snow/ice properties between the two parts showing different slopes. Here, we examine the possibility of different physical properties causing the difference in slopes. Through this comparison using buoy data, we may identify important properties that might be responsible for the piecewise linearity.

First, the averages of basic properties available from buoy measurements are compared. They include ice thickness, snow depth, snow–ice interface temperature, ice temperature ($T_{ice} = (T_{as} + T_{si}) / 2$), and so on. The comparison revealed that snow–ice system within the first part ($x \leq x_0$) is found to consist of relatively thicker ice (mean value: 1.84 m), thinner snow (0.29 m), and colder ice (-9.13 °C) while the second part ($x > x_0$) is found to consist of relatively thinner ice (1.10 m), thicker snow (0.46 m), and warmer ice (-5.00 °C). In general, a thicker snow or ice layer exhibits a greater temperature difference from top to bottom of the layer. There is no significant difference between the air–snow interface temperature (T_{as}) in the two slope parts.

The thermal conductivities, k_{snow} and k_{ice}, are also compared because what connects α and $\Delta T_{snow}/\Delta T_{ice}$ is the ratio of thermal conductivities. Before showing the results, we describe how to calculate k_{snow} and k_{ice}. First, the thermal conductivity ratio is calculated from buoy measured variables (i.e. T_{as}, T_{si}, T_{iw}, h_s, and H_i) using Eq. (3). Because the underlying physics in k_{snow} is significantly more complex, k_{ice} is estimated first, and then k_{snow} is obtained by multiplying the calculated k_{ice} and k_{snow}/k_{ice}. To calculate k_{ice}, the parameterization of Maykut and Untersteiner (1971), which describes k_{ice} as a function of salinity and temperature, is used.

$$k_{ice} = 2.03 + 0.117\frac{S_{ice}}{T_{ice}} \quad \text{(A1)}$$

Here, S_{ice} and T_{ice} is the salinity (in ppt) and temperature (in Celsius) of sea ice, respectively. For the calculation, S_{ice} is estimated according to the empirical relationship between sea ice thickness and mean salinity from Cox and Weeks (1974) as follows:

$$S_{ice} = \begin{cases} 14.24 - 19.39H_i, & H_i \leq 0.4\ m \\ 7.88 - 1.59H_i, & H_i > 0.4\ m \end{cases} \quad \text{(A2)}$$

Although Trodahl et al. (2001) reported that k_{ice} depends on depth and temperature; here we do not estimate accurate thermal conductivities but attempt to examine the physical consequences of the total ice layer.

The calculated thermal conductivities are presented in Fig. A2. The calculated k_{ice} ranges from 1.8 W K^{-1} m^{-1} to 2.0 W K^{-1} m^{-1} (left two panels in Fig. A2). These values are consistent with the in-situ measurements by Pringle et al. (2006). The mean values of k_{ice} of the first part (1.96 W K^{-1} m^{-1}) and the second part (1.88 W K^{-1} m^{-1}) show almost no difference. The calculated k_{snow} ranges from 0.2 W K^{-1} m^{-1} to 1.05 W K^{-1} m^{-1} (right two panels in Fig. A2). This range is consistent with reported values in Sturm et al. (1997). The first part shows the greater spread in the distribution of k_{snow} compared to the second part. The mean k_{snow} values are 0.44 and 0.27 for the first part and second part, respectively.

As a significant difference is observed in k_{snow}, we would like to find a possible reason for this difference. To do so, we should first review the factors determining k_{snow}; they are density, temperature, and crystal structure (Sturm et al., 1997). Snow is a mixture of ice particles and air, and air has lower thermal conductivity than ice. Thus, snow with a relatively lower density including a greater portion of air should have relatively lower thermal conductivity. Besides, the thermal conductivity of ice particles depends on the temperature, and the path of heat transfer depends on the crystal structure which describes how the particles are connected. The heat transfer occurs not only by conduction but also by water vapor latent heat transportation and convection through the pore spaces (Sturm et al, 2002), which are hard to quantify explicitly. These two factors are closely related to the temperature gradient (or difference) imposed within the snow layer.

Based on this knowledge, we can infer the condition of the snow layer of the two parts. The relatively higher and varying k_{snow} of the first part would be related to the compaction process resulting in high density, and metamorphic diversity which changes the crystal structure. According to Sturm et al. (2002), the value of k_{snow} of hard wind ~~slap~~slab attains up to 0.5 W m^{-1} K^{-1}, while that of k_{snow} of depth hoar is below 0.1 W m^{-1} K^{-1}. On the other hand, the lower and nearly constant k_{snow} of the second part implies that the snow layer of the second part would consist of fresh and dry snow having relatively lower density and a relatively lower likelihood of experiencing particular metamorphism.

In summary, it is concluded that the physical properties of snow and ice can account for the piecewise linearity, based on the differences in the physical properties between the first and second parts. Especially, the thermal conductivity of the snow, k_{snow}, seems to play an important role. Nevertheless, further analysis is required to fully understand this phenomenon.

Appendix B: Sensitivity test for the proposed method

Here we present results of a sensitivity test for showing how the snow depth and ice thickness retrieval results are dependent on the uncertainties in α. To do so, the uncertainty in the snow depth (Δh_s) due to the α error (i.e. $\Delta\alpha$) and associated ice thickness error (ΔH_i) are estimated. From this sensitivity test, we expect to understand why the simultaneous method for the radar freeboard shows more scattered features than those from the lidar total freeboard.

First, Δh_s is defined by the difference of retrieved h_s between with error ($\alpha + \Delta\alpha$) and without error (α).

$$\Delta h_s = \begin{cases} h_s(\alpha + \Delta\alpha, F_t) - h_s(\alpha, F_t) & (\text{using } F_t) \\ h_s(\alpha + \Delta\alpha, F_r) - h_s(\alpha, F_r) & (\text{using } F_r) \end{cases} \quad \text{(B1)}$$

Then, Δh_s can be converted to the error in the ice thickness (ΔH_i) using the following equation derived from Eq. (10).

$$\Delta H_i = \frac{(f\eta_s - 1)\rho_w + \rho_s}{\rho_w - \rho_i}\Delta h_s = \begin{cases} -6.46\Delta h_s & (\text{using } F_t) \\ 3.44\Delta h_s & (\text{using } F_r) \end{cases} \quad \text{(B2)}$$

Because H_i and h_s ~~is a~~are the combination of freeboard and α, as in Eqs. (3), (11) and (12), we only examine the uncertainty with some typical sea ice types. Here physical states for thicker ice (type A), moderate ice (type B), and thinner ice (type C) are chosen, which are summarized in Table B1. Typical values for those three types are shown in the scatterplots of OIB-based (α^{OIB} vs. F_t^{OIB}) and of satellite-based (α^{sat} vs. F_r^{CS2}) – Fig. B1. It is shown that the majority of data points are located around type B, followed by type A. There seems a very small portion of total samples showing values around type C.

With $\Delta\alpha = \pm 0.0305$, which is ~~an RMSE range in~~ the ~~α prediction equation~~root mean square difference (RMSD) value between α^{OIB} and α^{sat}, Δh_s and ΔH_i are estimated for three ice types. Table B2 summarizing results show that $|\Delta h_s|$ is within ~~5~~8 cm and it tends to decrease as the ice becomes thinner when the current method is applied to the total freeboard. On the other hand, the use of radar freeboard shows that $|\Delta h_s|$ tends to be more sensitive for the same $\Delta\alpha$. Especially, the sensitivity of type C is the greatest. This is because the denominator of Eq. (12) becomes smaller when α approaches to α_{crit}, resulting in an unstable solution. For the ice thickness, $|\Delta H_i|$ is smaller when the total freeboard is used since ΔH_i is proportional to Δh_s. However, the gap between the results from two freeboards has narrowed because H_i from the total freeboard is more sensitive than the radar freeboard to Δh_s, according to Eq. (B2). The sensitivity characteristics shown here are consistent with the analysis results given in Sect 4.2. Because there is a much ~~small~~smaller number of data points belonging to type C, at least in the data used for this study, the overall sensitivity would likely be in between B and A types.

It is also of importance to ask to what degree of retrievals is successfully yielded. In this study, cases showing $T_{as} > T_{si}$ or retrieved $\alpha \geq \alpha_{crit}$ are considered to be failures. Statistics on success/fail ratio of α retrieval for December–March of 2011–2015 period are provided in Table B3. Overall, the success ratio was over 82% in December–February, while it was reduced to ~74% in March. Most of the failures appear associated with cases showing the temperature inversion (i.e. $T_{as} > T_{si}$), whose areas are shaded with grey in the α-distributions of Fig. 8. Those failure areas are generally found around the marginal ice zones and in the east of Greenland. On the other hand, there was a near-zero failure (0.02% of total pixels) for retrieved $\alpha \geq \alpha_{crit}$. This near-zero failure implies that almost all calculated α meet the satisfactory condition after the removal of cases showing the temperature inversion. It may be concluded that the calculated α appears to be physically reasonable (i.e. $\alpha < \alpha_{crit}$) as long as presumed thermodynamic conditions are met.

Appendix C: Uncertainty estimation for CS2 retrievals

Although the sensitivity test regarding uncertainty of satellite derived α has been conducted in Appendix B, the uncertainty of CS2 freeboard measurements and prescribed parameters should be considered as well for the satellite snow depth and ice thickness estimates. To do so, a simple propagation analysis of errors is performed, regarding the uncertainty of satellite

products (α^{sat} and F_r^{CS2}) and prescribed parameters (ρ_i, ρ_s, and f). Uncertainty due to the variability of ρ_w is neglected (Kurtz and Harbeck, 2017; Hendricks et al., 2016; Ricker et al., 2014). Here we assume that α^{sat} and F_r^{CS2} are not correlated, with no systematic bias. Such assumption may not be true in the real world. However, it allows us to estimate the retrieval uncertainty from satellite-derived products, with a certain limit. Uncertainty of ice thickness can be estimated by following Gaussian error propagation equation.

$$\epsilon_{y,total}^2 = \sum_x \epsilon_y(x)^2 \quad \text{(C1)}$$

Here, $\varepsilon_{y,total}$ denotes the total uncertainty of retrieved variable y (h_s or H_i) and $\varepsilon_y(x)$ denotes the uncertainty of y related to input variable x (α, F_r, ρ_i, ρ_s, or f). The uncertainties on the right-hand side are obtained by following equation.

$$\epsilon_y(x) = \frac{\partial y}{\partial x}\sigma_x = \lim_{\delta \to 0} \frac{y(x+\delta)-y(x)}{\delta}\sigma_x \quad \text{(C2)}$$

Here, σ_x denotes the uncertainty of x and δ is set to be 10^{-6} for numerical calculation of the partial derivative using Eqs. (3) and (12). σ_α is estimated to be an RMSD value between α^{OIB} and α^{sat}. σ_{Fr} is given by Kurtz and Harbeck (2017) and σ_f is adopted from Armitage and Ridout (2015). Uncertainties of snow/ice densities are from relevant literatures (Alexandrov et al., 2020; Hendricks et al., 2016; Kern and Spreen, 2015; Ricker et al., 2014; Warren et al., 1999). Those values are summarized in Table C1.

Using Eqs. (C1) and (C2), uncertainties of snow depth and ice thickness retrievals can be estimated. Ice thickness uncertainty estimates are presented in Fig. C1. Total uncertainty of ice thickness estimate ranges from 0.8 m to 2.0 m. Generally, F_r-related uncertainty in the third row is greater than α-related uncertainty in the second row. Snow depth uncertainty estimates are presented in Fig. C2. Total uncertainty of snow depth ranges from 0.04 m to 0.4 m. In the case of the snow depth, α-related uncertainty is greater than F_r-related uncertainty. Both uncertainties of ice thickness and snow depth are greater for MYI region than FYI region. It is thought that the improvement of accuracy in satellite derived temperatures can reduce the snow depth uncertainty while the improvement of freeboard accuracy can reduce the ice thickness uncertainty. Uncertainties induced from densities and radar penetration factors are found to be relatively smaller than uncertainties related to α and F_r (shown in Fig. S2 and Fig. S3).

Data availability

The SHEBA buoy data were obtained from NCAR/EOL (https://doi.org/10.5065/D6KS6PZ7, last access: 14 September 2019) and CRREL IMB buoy data were obtained from the CRREL-Dartmouth Mass Balance Buoy Program (http://imb-crrel-dartmouth.org, last access: 14 September 2019). AASTI-v2 and SIIT data are available upon request to authors. Other data sets were obtained from NSIDC; They are OIB data (https://doi.org/10.5067/G519SHCKWQV6, last access: 10 September 2019), OIB quick look data (https://doi.org/10.5067/~~7Q8HCCWS4I0R~~GRIXZ91DE0L9, last access: ~~10 September 2019~~28

July 2020), CS2 data (https://doi.org/10.5067/96JO0KIFDAS8, last access: 10 September 2019), and SIC data (https://doi.org/10.5067/7Q8HCCWS4I0R, last access: 12 September 2019).

Author contribution

HS and BJS conceptualized and developed the methodology and HS conducted data analysis and visualization. GD and RTT gave important feedback for the algorithm development and result interpretation. GD provided AASTI data. All of the authors participated in writing the manuscript; HS prepared the original draft under the supervision of BJS and GD, and BJS critically revised the manuscript.

Competing interests

The authors declare that they have no conflict of interest.

Acknowledgments

This study has been supported by the Space Core Technology Development Program (NRF-2018M1A3A3A02065661) of the National Research Foundation of Korea. Authors also acknowledge that this study is also supported by the International Network Programme of the Ministry of Higher Education and Science, Denmark (Grant ref. no. 8073-00079B). We appreciate NSIDC for producing and providing the OIB, CS2, and SIC dataset. We also give thanks to CRREL and NCAR/EOL under the sponsorship of the National Science Foundation for providing IMB and SHEBA buoy data. The authors express their sincere thanks to an anonymous reviewer and to Dr. Isobel R. Lawrence for their valuable comments that led to improve the paper.

References

Alexandrov, V., Sandven, S., Wahlin, J., and Johannessen, O. M.: The relation between sea ice thickness and freeboard in the Arctic, The Cryosphere, 4, 373-380, doi: 10.5194/tc-4-373-2010, 2010.

Armitage, T. W. K., and Ridout, A. L.: Arctic sea ice freeboard from AltiKa and comparison with CryoSat-2 and Operation IceBridge, Geophys. Res. Lett., 42, 6724–6731, doi: 10.1002/2015GL064823, 2015.

Berg, W., Kroodsma, R., Kummerow, C. D., and McKague, D. S.: Fundamental Climate Data Records of Microwave Brightness Temperatures, Remote Sens., 10(8), 1306, doi: 10.3390/rs10081306, 2018.

Braakmann-Folgmann, A., and Donlon, C.: Estimating snow depth on Arctic sea ice using satellite microwave radiometry and a neural network, The Cryosphere, 13, 2421–2438, doi: 10.5194/tc-13-2421-2019, 2019.

Brucker, L., and Markus, T.: Arctic-scale assessment of satellite passive microwave-derived snow depth on sea ice using Operation IceBridge airborne data, J. Geophys. Res.-Oceans, 118(6), 2892–2905, doi: 10.1002/jgrc.20228, 2013.

Comiso, J. C.: Bootstrap Sea Ice Concentrations from Nimbus-7 SMMR and DMSP SSM/I-SSMIS, Version 3, Boulder, Colorado USA. NASA National Snow and Ice Data Center, doi: 10.5067/7Q8HCCWS4I0R, 2017.

Comiso, J. C., Cavalieri, D. J., and Markus, T.: Sea ice concentration, ice temperature, and snow depth using AMSR-E data, IEEE Trans. Geosci. Remote Sens., 41(2), 243–252, doi: 10.1109/TGRS.2002.808317, 2003.

Cox, G. F. N., and Weeks, W. F.: Salinity variations in sea ice, J. Glaciol., 13(67), 109–120, doi: 10.3189/S0022143000023418, 1974.

Dybkjær, G., and Eastwood, S.: Validation Report for the OSI SAF High Latitude L2 Sea and Sea Ice Surface Temperature, OSI-205, Version 1.1, OSI SAF, 30 pp., 2016.

Dybkjær, G., Eastwood, S., Borg, A. L., Højer, J., and Tonboe, R.: Algorithm theoretical basis document for the OSI SAF Sea and Sea Ice Surface Temperature L2 processing chain, OSI-205-a and OSI-205-b, Version 1.4, OSI SAF, 40 pp., 2018.

Dybkjær, G., Tonboe, R., Højer, J., and Eastwood, S.: Arctic and Antarctic snow and ice Surface Temperatures from AVHRR thermal Infrared satellite sensors, 1982-2015, 2020. (Manuscript in preparation)

Guerreiro, K., Fleury, S., Zakharova, E., Rémy, F., and Kouraev, A.: Potential for estimation of snow depth on Arctic sea ice from CryoSat-2 and SARAL/AltiKa missions, Remote Sens. Environ., 186, 339–349, doi: 10.1016/j.rse.2016.07.013, 2016.

Guerreiro, K., Fleury, S., Zakharova, E., Kouraev, A., Rémy, F., and Maisongrande, P.: Comparison of CryoSat-2 and ENVISAT radar freeboard over Arctic sea ice: toward an improved Envisat freeboard retrieval, The Cryosphere, 11, 2059–2073, doi: 10.5194/tc-11-2059-2017, 2017.

Hendricks, S., Ricker, R., and Helm, V.: User Guide – AWI CryoSat-2 sea Ice thickness data product (v1.2), doi: 10013/epic.48201, 2016.

Karlsson, K.-G., Anttila, K., Trentmann, J., Stengel, M., Meirink, J. F., Devasthale, A., Hanschmann, T., Kothe, S., Jääskeläinen, E., Sedlar, J., Benas, N., van Zadelhoff, G.-J., Schlundt, C., Stein, D., Finkensieper, S., Håkansson, N., Hollmann, R., Fuchs, P., and Werscheck, M.: CLARA-A2: CM SAF cLoud, Albedo and surface RAdiation dataset from AVHRR data - Edition 2, Satellite Application Facility on Climate Monitoring (CM SAF), doi: 10.5676/EUM_SAF_CM/CLARA_AVHRR/V002, 2017.

Kern, S., and Spreen, G.: Uncertainties in Antarctic sea-ice thickness retrieval from ICESat, Ann. Glaciol., 56(69), 107–119, doi: 10.3189/2015AoG69A736, 2015.

Kern, S., Khvorostovsky, K., Skourup, H., Rinne, E., Parsakhoo, Z. S., Djepa, V., Wadhams, P., and Sandven S.: The impact of snow depth, snow density and ice density on sea ice thickness retrieval from satellite radar altimetry: results from the ESA-CCI Sea Ice ECV Project Round Robin Exercise, The Cryosphere, 9, 37–52, doi: 10.5194/tc-9-37-2015, 2015.

Kilic, L., Tonboe, R. T., Prigent, C., and Heygster, G.: Estimating the snow depth, the snow-ice interface temperature, and the effective temperature of Arctic sea ice using Advanced Microwave Scanning Radiometer 2 and ice mass balance buoy data, The Cryosphere, 13, 1283–1296, doi: 10.5194/tc-13-1283-2019, 2019.

Kurtz, N. T., and Farrell, S. L.: Large-scale surveys of snow depth on Arctic sea ice from Operation IceBridge, Geophys. Res. Lett., 38, L20505, doi:10.1029/2011GL049216, 2011.

Kurtz, N. T., Farrell, S. L., Studinger, M., Galin, N., Harbeck, J. P., Lindsay, R., Onana, V. D., Panzer, B., and Sonntag, J. G.: Sea ice thickness, freeboard, and snow depth products from Operation IceBridge airborne data, The Cryosphere, 7, 1035–1056., doi: 10.5194/tc-7-1035-2013, 2013.

Kurtz, N. T., Galin, N., and Studinger, M.: An improved CryoSat-2 sea ice freeboard retrieval algorithm through the use of waveform fitting, The Cryosphere, 8, 1217–1237, doi: 10.5194/tc-8-1217-2014, 2014.

Kurtz, N. and Harbeck, J.: CryoSat-2 Level-4 Sea Ice Elevation, Freeboard, and Thickness, Version 1, Boulder, Colorado USA. NASA National Snow and Ice Data Center Distributed Active Archive Center, doi: 10.5067/96JO0KIFDAS8, 2017.

Kurtz, N., M. Studinger, J. Harbeck, V. Onana, and D. Yi.: IceBridge L4 Sea Ice Freeboard, Snow Depth, and Thickness, Version 1, Boulder, Colorado USA. NASA National Snow and Ice Data Center, doi: 10.5067/G519SHCKWQV6, 2015.

Kwok, R., and Cunningham, G. F.: Variability of Arctic sea ice thickness and volume from CryoSat-2, Phil. Trans. R. Soc. A, 373(2045), 20140157, doi: 10.1098/rsta.2014.0157, 2015.

Kwok, R., and Markus, T.: Potential basin-scale estimates of Arctic snow depth with sea ice freeboards from CryoSat-2 and ICESat-2: An exploratory analysis, Adv. Space Res., 62(6), 1243–1250, doi: 10.1016/j.asr.2017.09.007, 2018.

Kwok, R., Cunningham, G. F., Wensnahan, M., Rigor, I., Zwally, H. J., and Yi, D.: Thinning and volume loss of the Arctic Ocean sea ice cover: 2003–2008, J. Geophys. Res.-Oceans, 114(C7), C07005, doi: 10.1029/2009JC005312, 2009.

Lawrence, I. R., Tsamados, M. C., Stroeve, J. C., Armitage, T. W. K., and Ridout, A. L.: Estimating snow depth over Arctic sea ice from calibrated dual-frequency radar freeboards, The Cryosphere, 12, 3551–3564, doi:10.5194/tc-12-3551-2018, 2018.

Laxon, S., Peacock, N., and Smith, D.: High interannual variablility of sea ice thickness in the Arctic region, Nature, 425, 947–950, doi: 10.1038/nature02050, 2003.

Laxon, S. W., Giles, K. A., Ridout, A. L., Wingham, D. J., Willatt, R., Cullen, R., Kwok, R., Schweiger, A., Zhang, J., Haas, C., Hendricks, S., Krishfield, R., Kurtz, N., Farrell, S., and Davidson, M.: CryoSat-2 estimates of Arctic sea ice thickness and volume, Geophys. Res. Lett., 40, 732– 737, doi: 10.1002/grl.50193, 2013.

Lee, S.-M., Sohn, B.-J., and Kummerow, C. D.: Long-term Arctic snow/ice interface temperature from special sensor for Microwave imager measurements, Remote Sens., 10(11), 1795, doi: 10.3390/rs10111795, 2018.

Maaß, N., Kaleschke, L., Tian-Kunze, X., and Drusch, M.: Snow thickness retrieval over thick Arctic sea ice using SMOS satellite data, The Cryosphere, 7(6), 1971–1989, doi: 10.5194/tc-7-1971-2013, 2013.

Mallett, R. D. C., Lawrence, I. R., Stroeve, J. C., Landy, J. C., and Tsamados, M.: Brief communication: Conventional assumptions involving the speed of radar waves in snow introduce systematic underestimates to sea ice thickness and seasonal growth rate estimates, The Cryosphere, 14, 251-260, doi: 10.5194/tc-14-251-2020, 2020.

Markus, T. and Cavalieri, D. J.: Snow depth distribution over sea ice in the Southern Ocean from satellite passive microwave data, Antarct. Res. Ser., 74, 19–39, 1998.

Markus, T., Neumann, T., Martino, A., Abdalati, W., Brunt, K., Csatho, B., Farrell, S., Fricker, H., Gardner, A., Harding, D., Jasinski, M., Kwok, R., Magruder, L., Lubin, D., Luthcke, S., Morison, J., Nelson, R., Neuenschwander, A., Stephen, P., Popescu, S., Shum, CK, Schutz, B. E., Smith, B., Yang. Y., Zwally, J.: The Ice, Cloud, and land Elevation Satellite-2 (ICESat-2): Science requirements, concept, and implementation, Remote Sens. Environ, 190, 260–273, doi: 10.1016/j.rse.2016.12.029, 2017.

Maykut, G. A., and Untersteiner, N.: Some results from a time-dependent thermodynamic model of sea ice, J. Geophys. Res., 76(6), 1550–1575, doi: 10.1029/JC076i006p01550, 1971.

Nandan, V., Geldsetzer, T., Yackel, J., Mahmud, M., Scharien, R., Howell, S., King, J., Ricker, R., and Else, B.: Effect of Snow Salinity on CryoSat-2 Arctic First-Year Sea Ice Freeboard Measurements, Geophys. Res. Lett., 44(20), 10,419–10,426, doi:10.1002/2017GL074506, 2017.

Perovich, D., Richter-Menge, J., and Polashenski, C.: Observing and understanding climate change: Monitoring the mass balance, motion, and thickness of Arctic sea ice, CRREL-Dartmouth mass balance buoy program, http://imb-crrel-dartmouth.org, 2019.

Perovich, D., Richter-Menge, J., Tucker, W., Elder, B., and Bosworth, B.: Snow and Ice Temperature Profiles. Version 1.0. UCAR/NCAR - Earth Observing Laboratory, doi:10.5065/D6KS6PZ7, 2007.

Pringle, D. J., Trodahl, H. J., and Haskell, T. G.: Direct measurement of sea ice thermal conductivity: no surface reduction, J. Geophys. Res.-Oceans, 111(C5), C05020, doi: 10.1029/2005JC002990, 2006.

Ricker, R., Hendricks, S., Helm, V., Skourup, H., and Davidson, M.: Sensitivity of CryoSat-2 Arctic sea-ice freeboard and thickness on radar-waveform interpretation, The Cryosphere, 8, 1607–1622, doi: 10.5194/tc-8-1607-2014, 2014.

Rostosky, P., Spreen, G., Farrell, S. L., Frost, T., Heygster, G., and Melsheimer, C.: Snow depth retrieval on Arctic sea ice from passive microwave radiometers – improvements and extensions to multiyear ice using lower frequencies, J. Geophys. Res.-Oceans, 123(10), 7120–7138, doi: 10.1029/2018JC014028, 2018.

Sturm, M., Holmgren, J., König, M., and Morris, K.: The thermal conductivity of seasonal snow, J. Glaciol., 43(143), 26–41, doi: 10.3189/S0022143000002781, 1997.

Sturm, M., Perovich, D. K., and Holmgren, J.: Thermal conductivity and heat transfer through the snow on the ice of the Beaufort Sea, J. Geophys. Res., 107(C21), 8043, doi: 10.1029/2000JC000409, 2002.

Tilling, R. L., Ridout, A., and Shepherd, A.: Estimating Arctic sea ice thickness and volume using CryoSat-2 radar altimeter data, Adv. Space Res., 62, 1203–1225, doi: 10.1016/j.asr.2017.10.051, 2018.

Tiuri, M., A. Sihvola, E. Nyfors, and M. Hallikainen, The complex dielectric constant of snow at microwave frequencies, IEEE J. Ocean. Eng., 9, 377–382, 1984.

Tonboe, R. T., Pedersen, L. T., Haas, C.: Simulation of the CryoSat-2 satellite radar altimeter sea ice thickness retrieval uncertainty, Can. J. Remote Sens., 36(1), 55–67, doi: 10.5589/m10-027, 2010.

Trodahl, H. J., Wilkinson, S. O. F., McGuinness, M. J., and Haskell, T. G.: Thermal conductivity of sea ice; dependence on temperature and depth, Geophys. Res. Lett., 28(7), 1279–1282, doi: 10.1029/2000GL012088, 2001.

Ulaby, F. T., Moore, R. K., and Fung, A. K.: Microwave remote sensing: Active and passive, Volume 3 - From theory to applications, 1986.

Warren, S. G., Rigor, I. G., Untersteiner, N., Radionov, V. F., Bryazgin, N. N., Aleksandrov, Y. I., and Colony, R.: Snow depth on Arctic sea ice, J. Climate, 12(6), 1814–1829, doi: 10.1175/1520-0442(1999)012<1814:SDOASI>2.0.CO;2, 1999.

Webster, M. A., Rigor, I. G., Nghiem, S. V., Kurtz, N. T., Farrell, S. L., Perovich, D. K., and Sturm, M.: Interdecadal changes in snow depth on Arctic sea ice, J. Geophys. Res.-Oceans, 119(8), 5395–5406, doi: 10.1002/2014JC009985, 2014.

Wingham, D. J., Francis, C. R., Baker, S., Bouzinac, C., Brockley, D., Cullen, R., Chateau-Thierry, P., Laxon, S. W., Mallow, U., Mavrocordatos, C., Phalippou, L., Ratier, G., Rey, L., Rostan, F., Viau, P., and Wallis, D. W.: CryoSat: a mission to determine the fluctuations in Earth's land and marine ice fields, Adv. Space Res., 37(4), 841–871, doi: 10.1016/j.asr.2005.07.027, 2006.

Willatt, R., Laxon, S., Giles, K., Cullen, R., Haas, C., and Helm, V.: Ku-band radar penetration into snow cover on Arctic sea ice using airborne data, Ann. Glaciol., 52, 197–205, doi:10.3189/172756411795931589, 2011.

Zhou, L., Xu, S., Liu, J., and Wang, B.: On the retrieval of sea ice thickness and snow depth using concurrent laser altimetry and L-band remote sensing data, The Cryosphere, 12(3), 993–1012, doi: 10.5194/tc-12-993-2018, 2018.

Zwally, H. J., Schutz, B., Abdalati, W., Abshire, J., Bentley, C., Brenner, A., Bufton, J., Dezio, J., Hancock, D., Harding, D., Herring, T., Minster, B., Quinn, K., Palm, S., Spinhirne, J., and Thomas, R.: ICESat's laser measurements of polar ice, atmosphere, ocean, and land, J. Geodyn., 34, 405–445, doi: 10.1016/S0264-3707(02)00042-X, 2002.

Zygmuntowska, M., Rampal, P., Ivanova, N., and Smedsrud, L. H.: Uncertainties in Arctic sea ice thickness and volume: new estimates and implications for trends, The Cryosphere, 8(2), 705–720, doi: 10.5194/tc-8-705-2014, 2014.

Table 1. Information on the measurement sites of buoys whose observations were used in this study.

Name		Deployment Location	Ice Type	Initial Snow Depth [m]	Initial Ice Thickness [m]
CRREL	2010F	Beaufort Sea	Multi-Year	0.25	1.97
	2011M	Central Arctic	Multi-Year	0.07	1.67
	2012G	Central Arctic	First-Year	0.16	1.41
	2013F	Beaufort Sea	Multi-Year	0.00	1.40
	2013G	Beaufort Sea	Multi-Year	0.00	1.40
	2014G	Beaufort Sea	Multi-Year	0.10	1.08
	2014I	Beaufort Sea	Multi-Year	0.23	1.32
SHEBA	Q2	Beaufort Sea	Multi-Year	0.06*	1.75*
	PIT	Beaufort Sea	Multi-Year	0.12*	2.01*
	BALT	Beaufort Sea	First Year	0.07*	1.40*
	R4	Beaufort Sea	Second-Year Ridge	0.09*	4.23*
	SEA	Beaufort Sea	Ponded Area	0.10*	1.54*

*The initial snow depth and ice thickness of the SHEBA sites are average values of all thickness gauge measurements in the corresponding site because there was one thermistor string but several thickness gauges in each measurement site

695

Table 2. Coefficients of the regression equation for averaging periods of 1, 7, 15, and 30 days. a_1, b_1, a_2, b_2, and x_0 are given in Eq. (15).

Averaging Periods	a_1	b_1	a_2	b_2	x_0
1 day	0.166	0.047	0.050	0.263	1.864
7 days	0.179	0.028	0.053	0.254	1.796
15 days	0.180	0.034	0.029	0.339	2.022
30 days	0.185	0.022	0.076	0.214	1.769

700

705

Table B1. The physical state of typical cases of points A, B, and C.

Type	H_i [m]	h_s [m]	α	F_t [m]	F_r [m]
A	3.961	0.332	0.084	0.65	0.30
B	1.646	0.123	0.075	0.26	0.13
C	0.616	0.152	0.246	0.17	0.01

710

Table B2. Errors of snow depth (Δh_s) and ice thickness (ΔH_i) for snow depth to ice thickness ratio error ($\Delta\alpha$) of ±0.~~03~~05.

	Total Freeboard Method		Radar Freeboard Method	
$\Delta\alpha$	-0.~~03~~05	0.~~03~~05	-0.~~03~~05	0.~~03~~05
		Δh_s (cm)		
A	-~~4.070~~7.502	~~3.161~~4.903	-~~14.59~~22.417	~~19.54~~36.719
B	-~~1.913~~3.543	~~1.471~~2.277	-~~5.840~~9.002	~~7.730~~14.437
C	-0.~~045~~080	0.~~039~~062	-~~7.230~~9.499	~~37.62~~Retrieval Fail*
		ΔH_i (m)		
A	0.~~263~~485	-0.~~204~~317	-0.~~502~~771	~~0.672~~1.264
B	0.~~124~~229	-0.~~095~~147	-0.~~201~~310	0.~~266~~497
C	0.~~003~~005	-0.~~003~~004	-0.~~249~~327	~~1.294~~Retrieval Fail*

715 *Retrieval fail occurs if $\alpha + \Delta\alpha > \alpha_{crit}$ (α_{crit} = 0.291 for ρ_s = 320 kg m^{-3}, ρ_l = 915 kg m^{-3}, ρ_w = 1024 kg m^{-3}, and f = 0.84).

Table B3. Statistics of success/fail ratio α retrieval for 2011-2015 winter.

Year Month	Total Pixels (SIC > 95%)	Success		Fail ($T_{as} > T_{si}$)		Fail ($\alpha > \alpha_{crit}$)	
2010 12	13879	12080	(87.04%)	1799	(12.96%)	0	(0.00%)
2011 01	16246	14004	(86.20%)	2242	(13.80%)	0	(0.00%)
2011 02	17986	14779	(82.17%)	3206	(17.82%)	1	(0.01%)
2011 03	17610	12871	(73.09%)	4738	(26.91%)	1	(0.01%)
2011 12	13915	11405	(81.96%)	2510	(18.04%)	0	(0.00%)
2012 01	16812	13765	(81.88%)	3047	(18.12%)	0	(0.00%)
2012 02	17528	14131	(80.62%)	3397	(19.38%)	0	(0.00%)
2012 03	18741	13586	(72.49%)	5155	(27.51%)	0	(0.00%)
2012 12	14059	11144	(79.27%)	2915	(20.73%)	0	(0.00%)
2013 01	16413	13510	(82.31%)	2903	(17.69%)	0	(0.00%)
2013 02	18640	15526	(83.29%)	3114	(16.71%)	0	(0.00%)
2013 03	19078	14134	(74.09%)	4944	(25.91%)	0	(0.00%)
2013 12	14515	12071	(83.16%)	2444	(16.84%)	0	(0.00%)
2014 01	16880	14201	(84.13%)	2678	(15.86%)	1	(0.01%)
2014 02	16987	14731	(86.72%)	2247	(13.23%)	9	(0.05%)
2014 03	17699	13300	(75.15%)	4391	(24.81%)	8	(0.05%)
2014 12	14071	11119	(79.02%)	2952	(20.98%)	0	(0.00%)
2015 01	17008	15095	(88.75%)	1913	(11.25%)	0	(0.00%)
2015 02	18076	15907	(88.00%)	2169	(12.00%)	0	(0.00%)
2015 03	17618	14042	(79.70%)	3576	(20.30%)	0	(0.00%)
December	70439	57819	(82.08%)	12620	(17.92%)	0	(0.00%)
January	83359	70575	(84.66%)	12783	(15.33%)	1	(0.00%)
February	89217	75074	(84.15%)	14133	(15.84%)	10	(0.01%)
March	90746	67933	(74.86%)	22804	(25.13%)	9	(0.01%)

α_{crit}=0.291 for ρ_s=320 kg m^{-3}, ρ_i=915 kg m^{-3}, ρ_w=1024 kg m^{-3}, and f=0.84.

Table C1. Values and uncertainties of input variables for uncertainty estimation.

	α	F_r [m]	ρ_i [kg m^{-3}]	ρ_s [kg m^{-3}]	f
Value	α^{sat}	F_r^{CS2}	915	320	0.84
Uncertainty	0.05	0.065	20	50	0.04

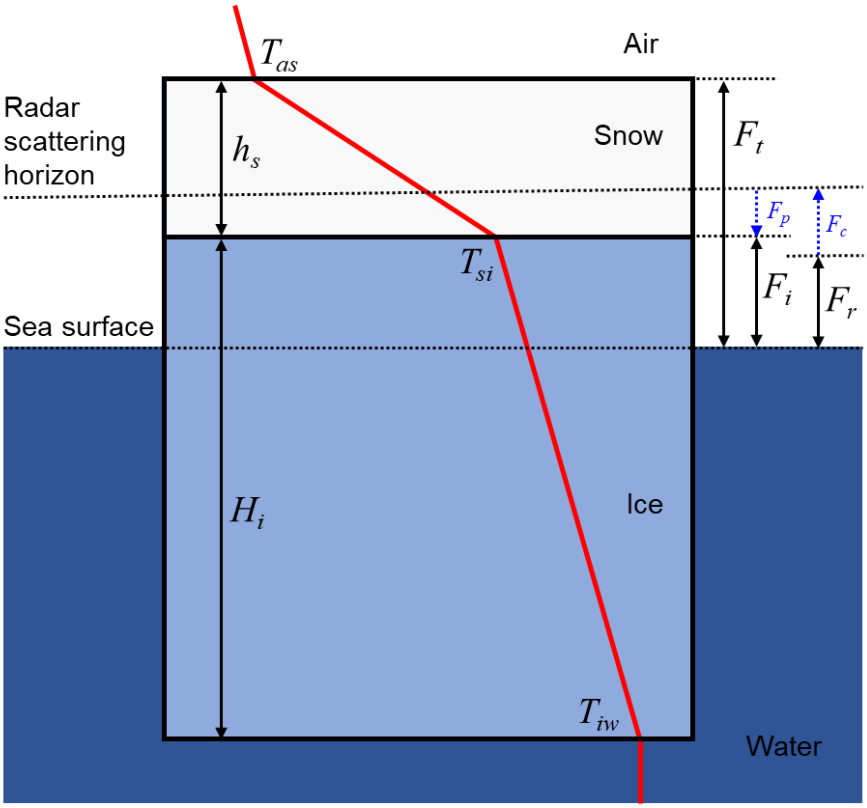

Figure 1. Schematic diagram of a typical snow–ice system during the winter. Snow depth (h_s), ice thickness (H_i), total freeboard (F_t), radar freeboard (F_r), and ice freeboard (F_i) are indicated. Correction terms regarding the wave propagation speed change in snow layer (F_c) and the displacement of the scattering horizon from the ice surface (F_p) are indicated by blue arrows. The red line denotes a typical temperature profile with air–snow interface temperature (T_{as}), snow–ice interface temperature (T_{si}), and ice–water interface temperature (T_{iw}).

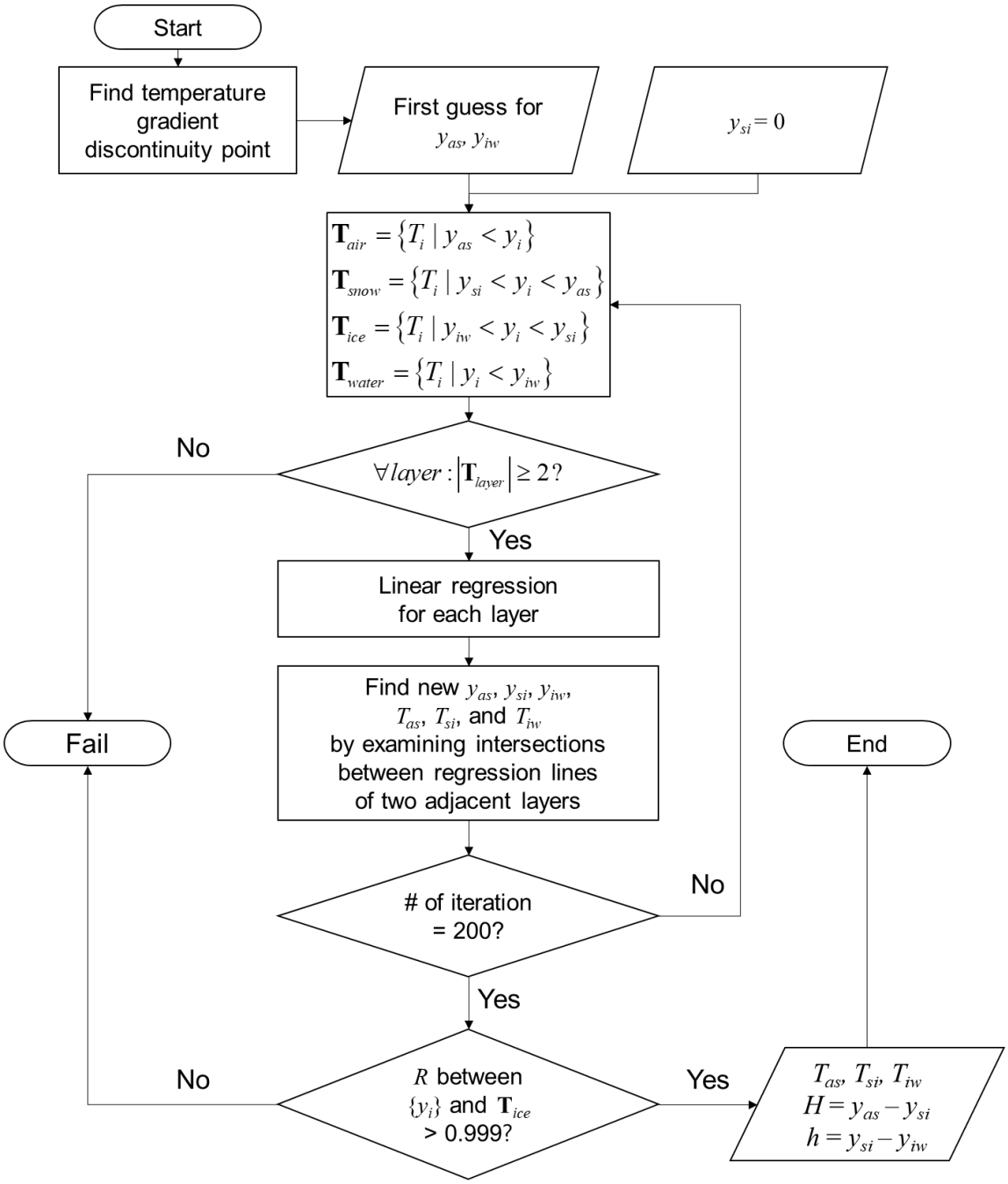

730 **Figure 2.** The flow chart of the interface searching algorithm. y_i and T_i denote the position and temperature of a data point in the temperature profile. y_{as}, y_{si}, and y_{iw} denote the position of the interfaces, and $\mathbf{T}_{layer}$ denotes a set of temperature data points.

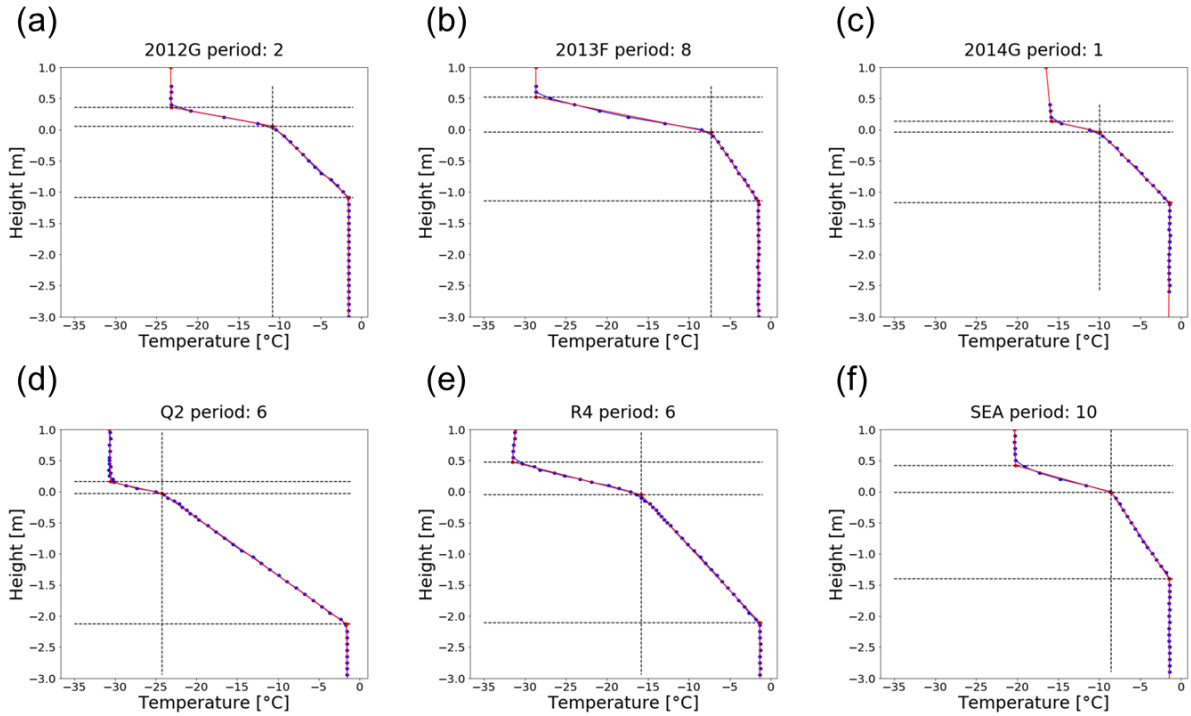

Figure 3. Examples of interface searching results with an averaging period of 15 days: (a) 2012G period 2, (b) 2013F period 8, (c) 2014G period 1, (d) Q2 period 6, (e) R4 period 6, and (f) SEA period 10. The period number ~~is equivalent to~~ indicates the ~~number of~~ sequential 15-day period from November 1 (e.g. 'period: 2' denotes a time-averaging ~~bin.~~period of November 16th to November 30th). Blue dots are buoy-measured temperature profiles and red lines are regression lines. Black dashed lines indicate the intersections between adjacent regression lines.

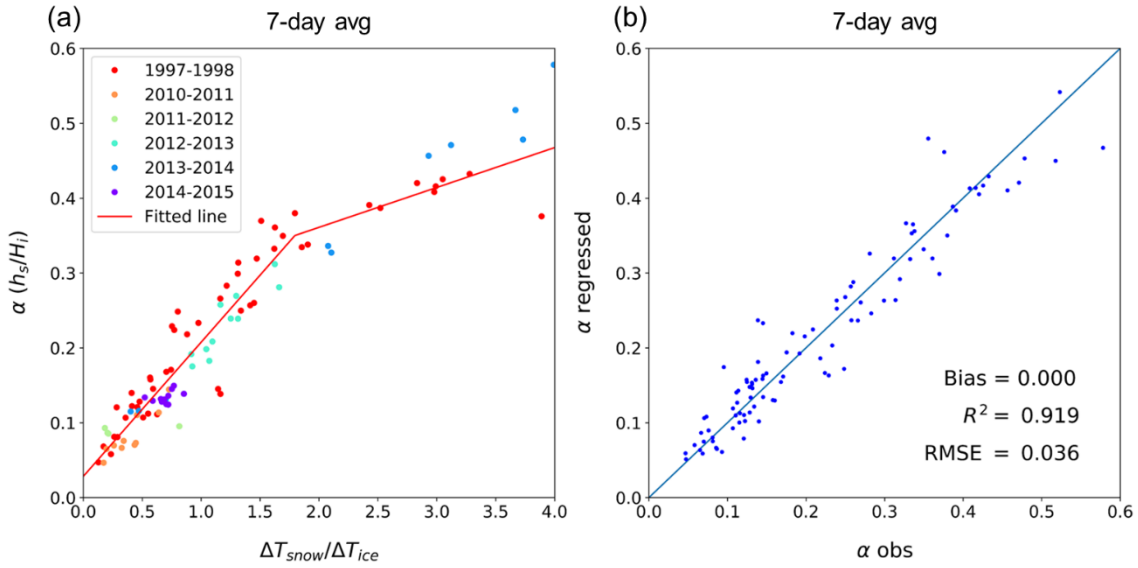

740

Figure 4. (a) Scatterplots of the temperature difference ratio of the snow and ice layer ($\Delta T_{snow}/\Delta T_{ice}$) and the snow–ice thickness ratio (α). Color denotes the collected year of buoy data. The red lines are the regression lines (defined in Eq. (15)). (b) The scatter plot of observed and regressed α.

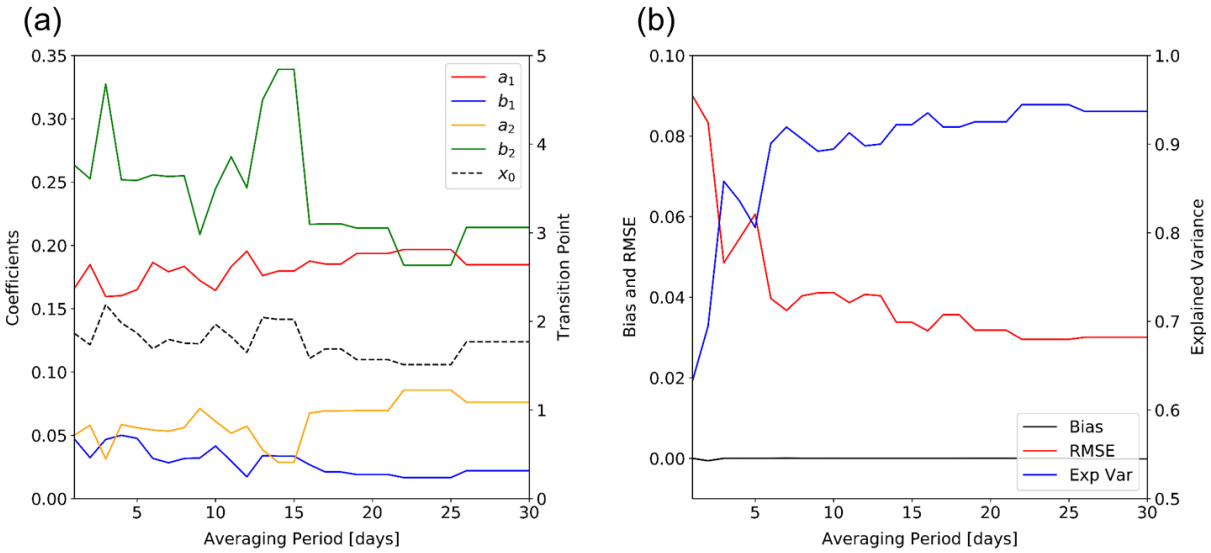

745

Figure 5. (a) The regression coefficients (a_1, b_1, a_2, b_2) in Eq. (15) and (b) the error statistics of the regression with averaging periods from 1 to 30 days.

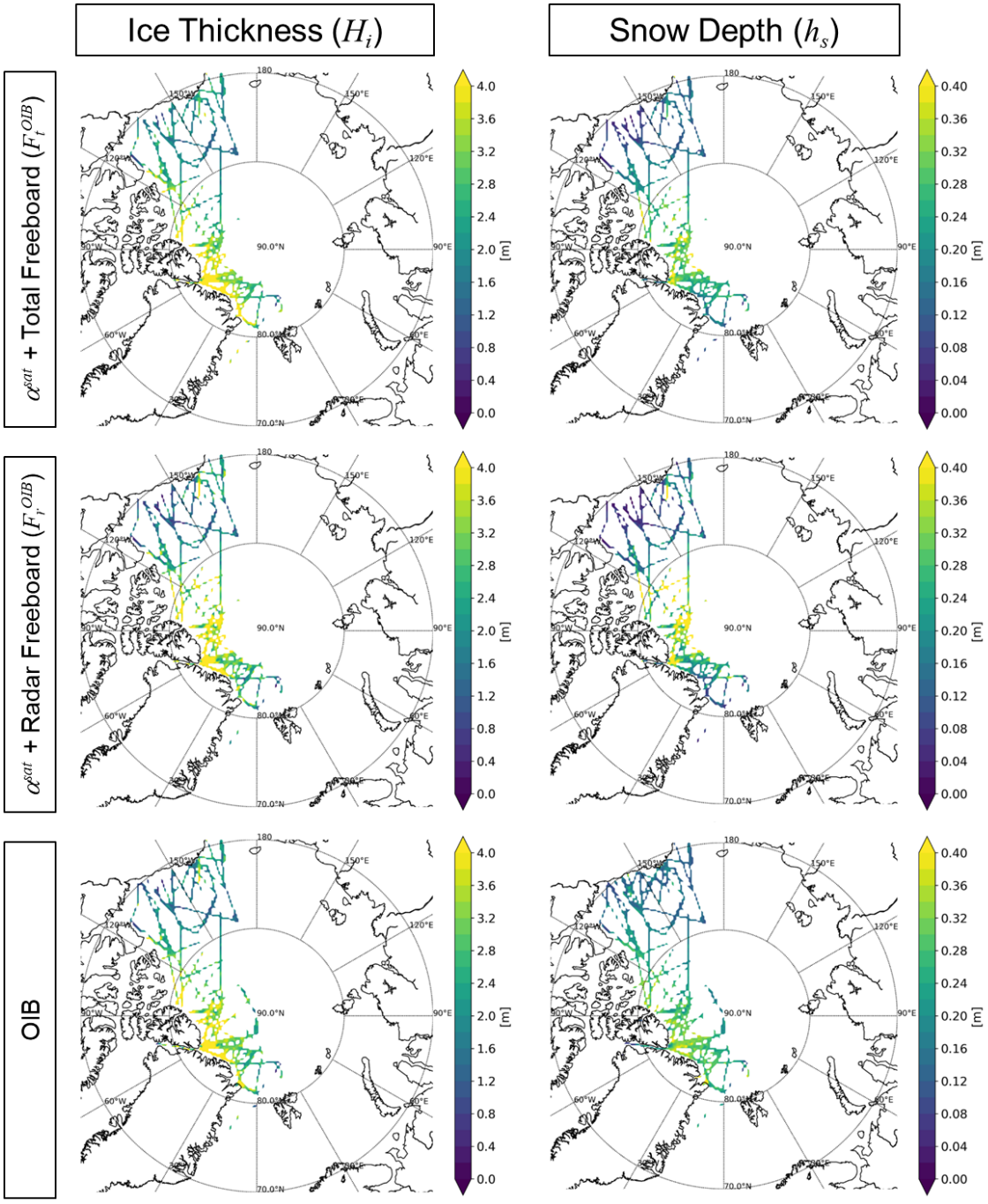

750 **Figure 6.** Simultaneously retrieved ice thickness and snow depth from OIB total/radar freeboard in March of the 2011–2015 period. Corresponding OIB products are at the bottom.

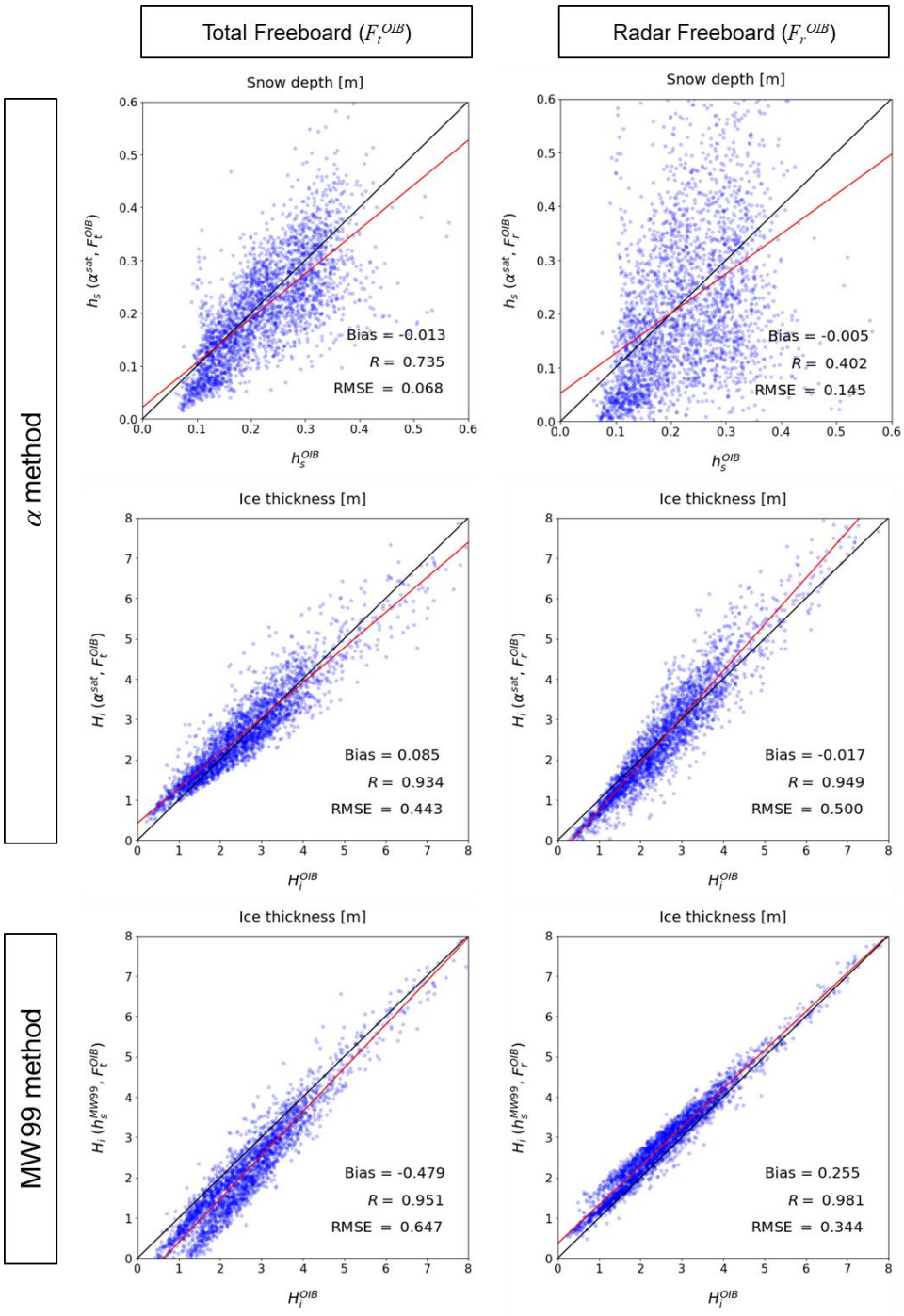

Figure 7. Scatter plots between OIB products and the simultaneously retrieved snow depth and ice thickness from OIB total/radar freeboards during the March 2011–2015 period. Corresponding ice thicknesses estimated from MW99 are in the third row. The red lines are linear regression lines.

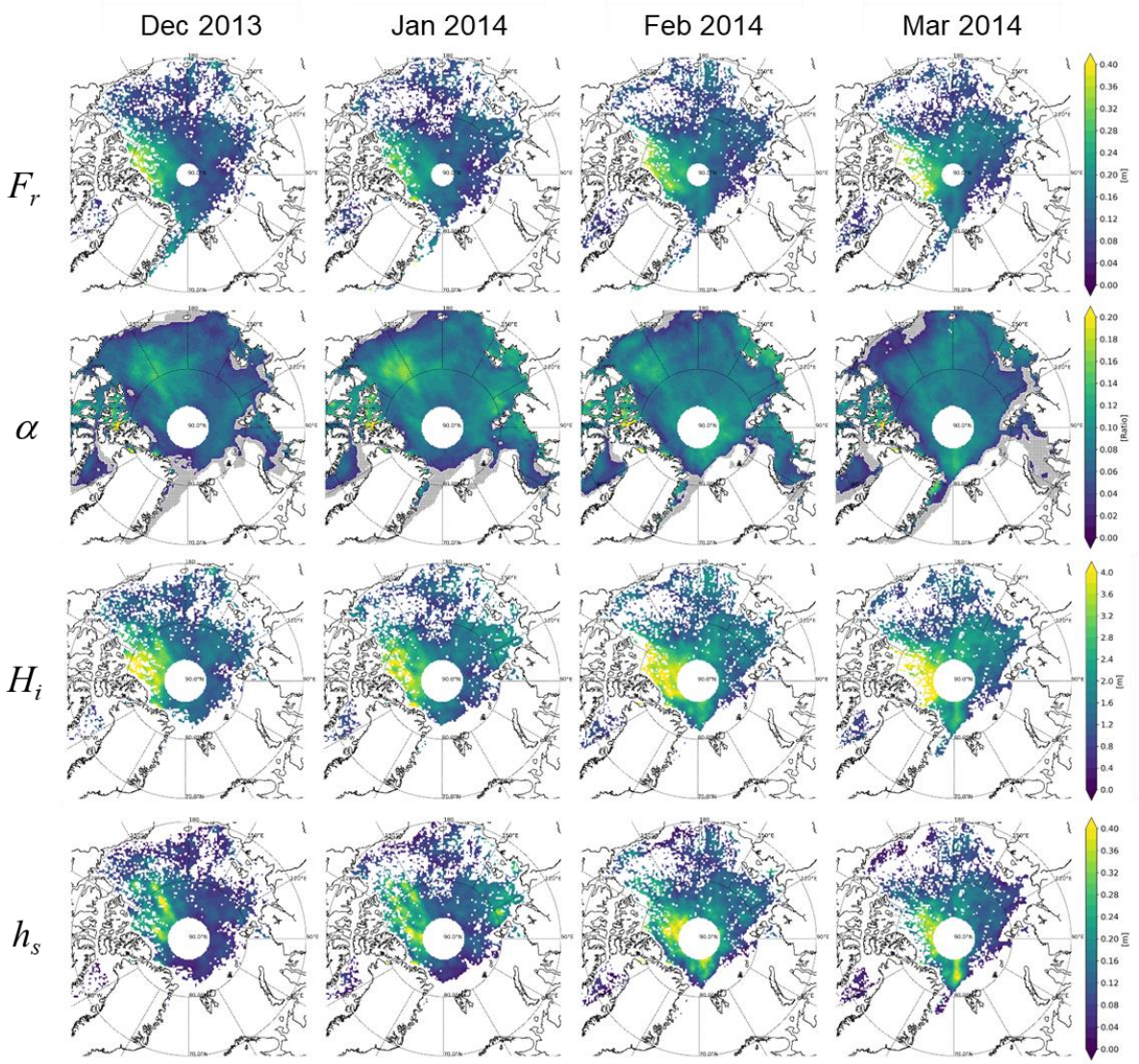

Figure 8. Geographical distributions of observed CS2 radar freeboard (F_r) and estimated snow–ice thickness ratio (α), ice thickness (H_i), and snow depth (h_s) from December 2013 to March 2014. Grey areas in the second row denote where α retrieval ~~is~~ failed because T_{as} is warmer than ~~T_{as}~~T_{si}.

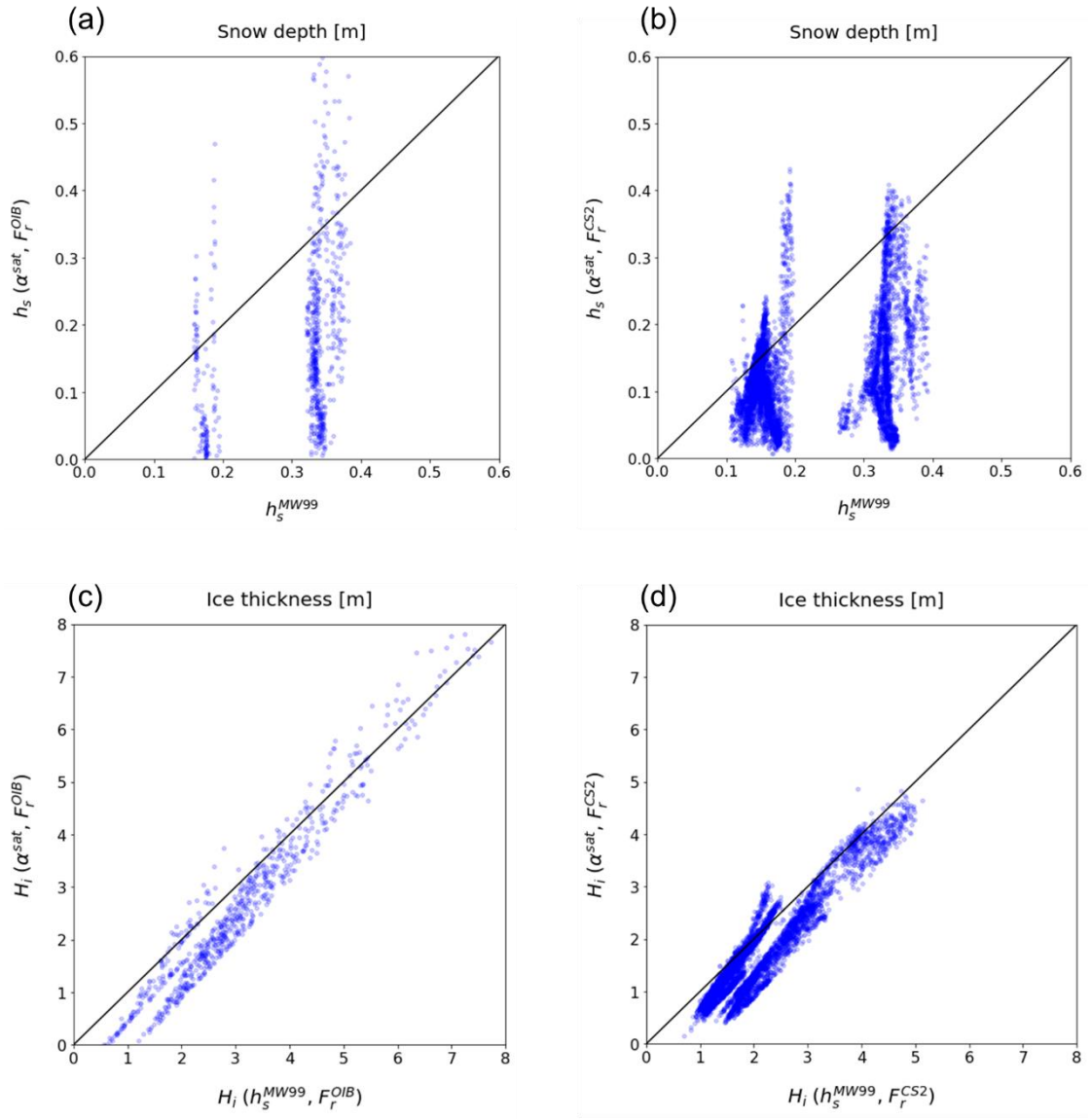

Figure 9. Comparison of simultaneous retrieved snow depth and ice thickness to those from the MW99 method. (a) Snow depth from OIB radar freeboard, (b) snow depth from CS2 radar freeboard, (c) ice thickness from OIB radar freeboard, and (d) ice thickness from CS2 radar freeboard.

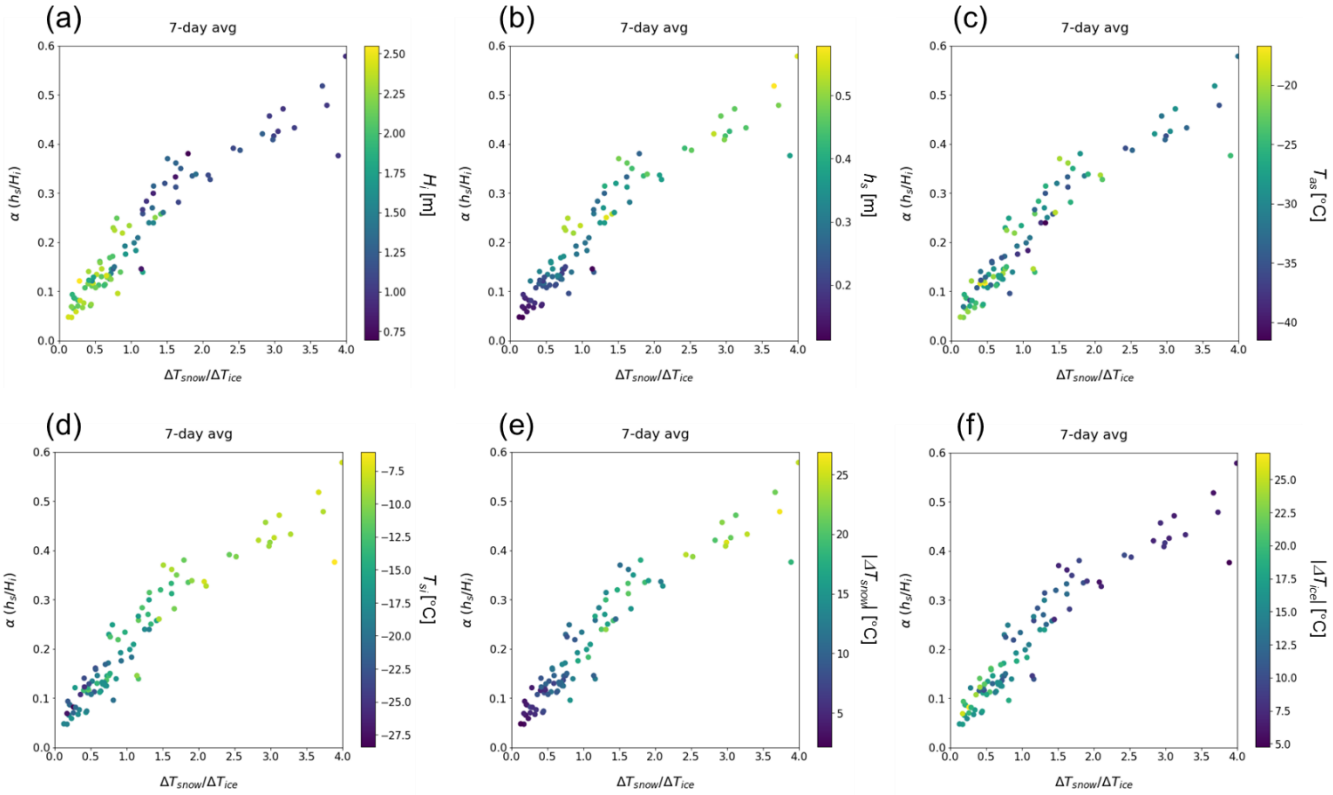

Figure A1. Distribution of physical variables on scatterplots of the temperature difference ratio of snow and ice layer ($\Delta T_{snow}/\Delta T_{ice}$) and the snow–ice thickness ratio (α). Color denotes the value of physical variables: (a) ice thickness (~~H~~H_i), (b) snow depth (~~h~~h_s), (c) air–snow interface temperature (T_{as}), (d) snow–ice interface temperature (T_{si}), (e) temperature difference within snow layer ($|\Delta T_{snow}|$), and (f) temperature difference within ice layer ($|\Delta T_{ice}|$).

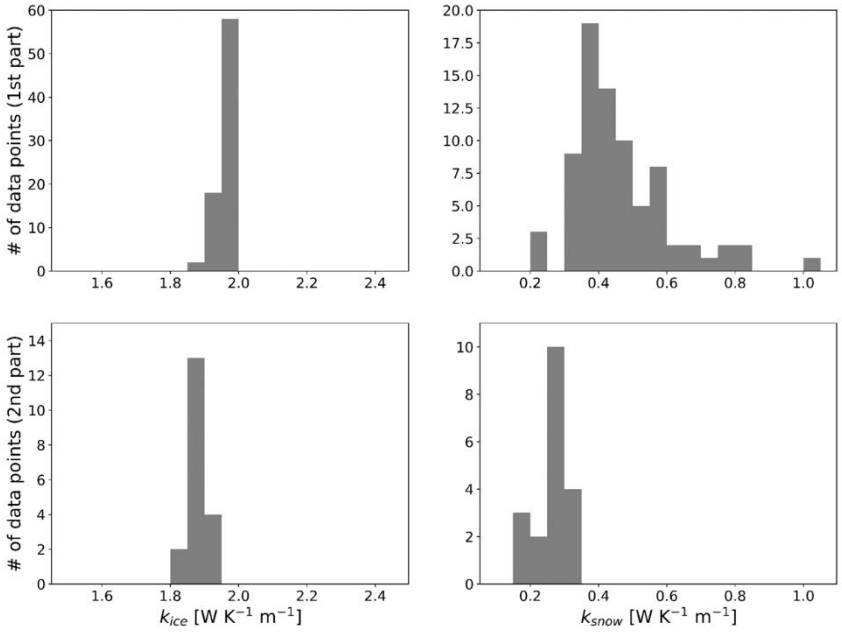

775

Figure A2. Histogram of estimated (left column) k_{ice} and (right column) k_{snow}. The top and bottom row denote the first and the second part, respectively. The size of the bins is 0.05 W K^{-1} m^{-1}.

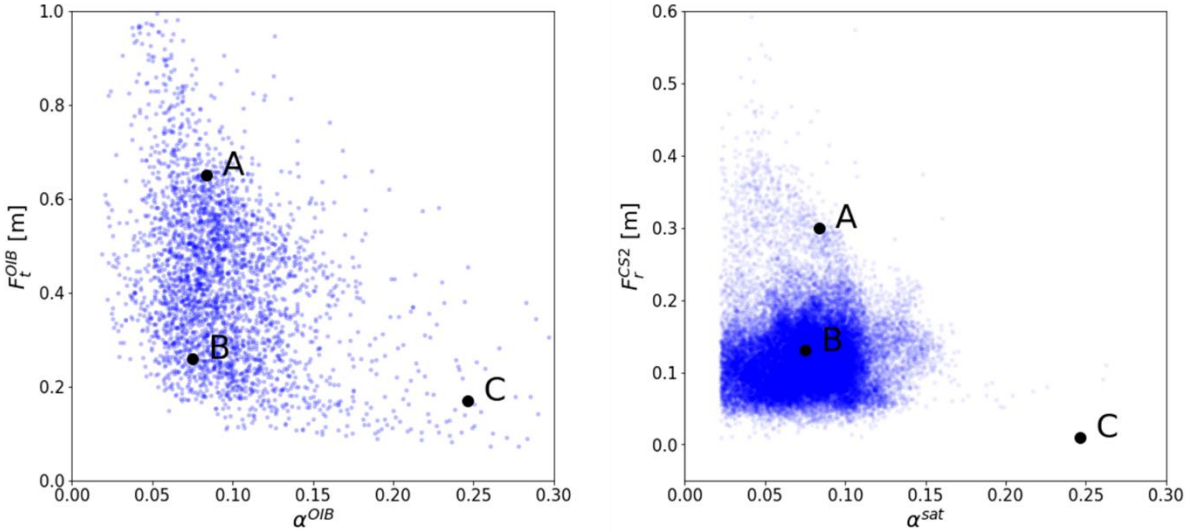

780 **Figure B1.** Locations of physical states for typical types (A, B, C) on the freeboard-thickness ratio space. Blue dots are from (left) OIB data and (right) retrieved thickness ratio and CS2 radar freeboard.

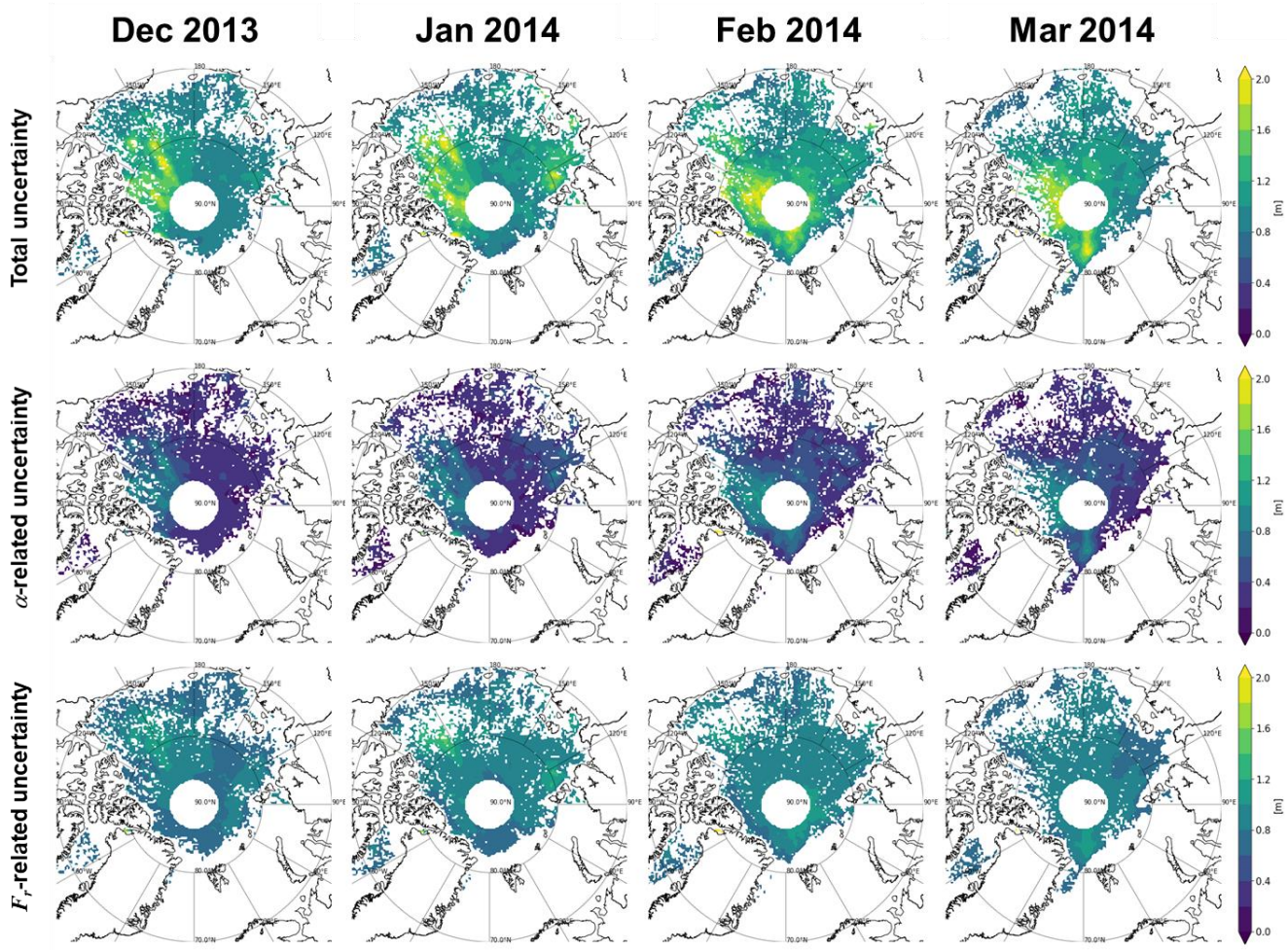

Figure C1. Geographical distributions of sea ice thickness uncertainty: (first row) total uncertainty, (second row) α-related uncertainty, and (third row) F_r-related uncertainty for the period from December 2013 to March 2014.

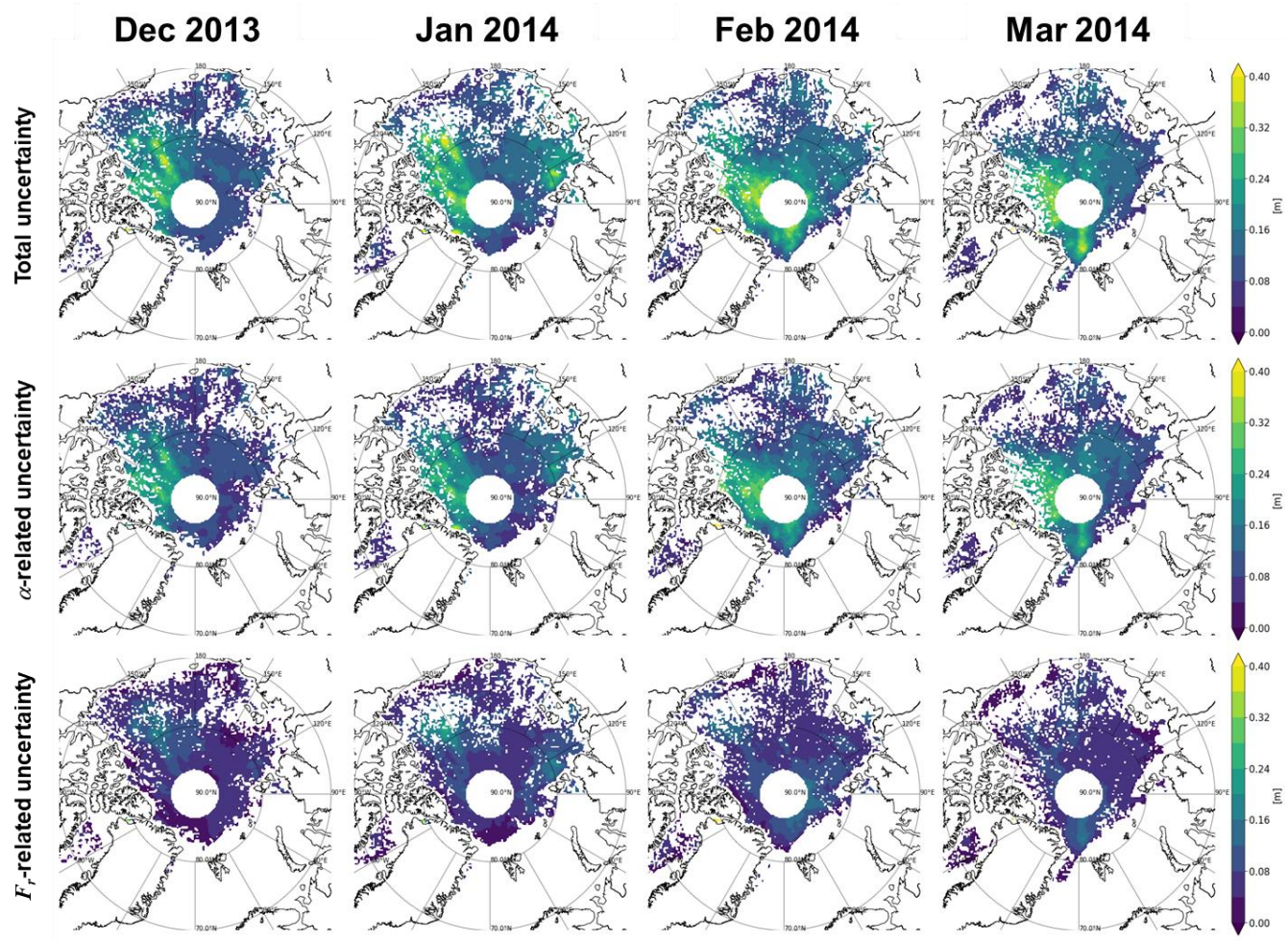

Figure C2. Geographical distributions of snow depth uncertainty: (first row) total uncertainty, (second row) α-related uncertainty, and (third row) F_r-related uncertainty for the period from December 2013 to March 2014.